Neuronal connectome of a visual eye circuit in *Platynereis dumerilii*

Dissertation
der Mathematisch-Naturwissenschaftlichen Fakultät
der Eberhard Karls Universität Tübingen
zur Erlangung des Grades eines
Doktors der Naturwissenschaften
(Dr. rer. nat.)

vorgelegt von
Dipl. Biol. Nadine Randel
aus Magdeburg

Tübingen
2014

Gedruckt mit Genehmigung der Mathematisch-Naturwissenschaftlichen Fakultät der Eberhard Karl Universität Tübingen.

Tag der mündlichen Qualifikation:	05.03.2015
Dekan:	Prof. Dr. Wolfgang Rosenstiel
1. Berichterstatter:	Dr. Gáspár Jékely
2. Berichterstatter:	Prof. Dr. Oliver Betz

Acknowledgement

First I would like to thank my supervisor Gáspár Jékely for his support and for the opportunity to work on this great connectome project. I could always develop and realize my own ideas, which kept the work exciting and interesting during my PhD.

I would also like to thank all of my former and current lab members, especially those who collaborated with me or helped me in every sense. Special thanks to Albina Asadulina for her support with data and image analysis, Martin Gühmann for his help with analyzing data and also Elizabeth A. Williams for proofreading my scripts. I'm also thankful for the collaboration with Luis A. Bezares-Calderón, Réza Shahidi, Csaba Veraszto, Markus Conzelmann and Aurora Panzera.

I would also like to acknowledge the people who introduced me to electron microscopy techniques, including Heinz Schwarz, Matthias Flötenmeyer, Dan Bumbarger and Metta Riebesell and also Jürgen Berger, who provided the SEM images. Finally I thank my family and friends for their support during my study.

Table of Contents

Zusammenfassung

Die Funktionsweise des Sehens ist von großem wissenschaftlichem Interesse und eine Vielzahl von Studien beschäftigt sich mit den Augen und den primären Verarbeitungszentren in *Drosophila* und Vertebraten. Allerdings gab es bis jetzt keine Beschreibung der synaptischen Verbindungen kompletter neuronaler Schaltkreise. Während meiner Dissertation studierte ich den für die Phototaxis verantwortlichen neuronalen Schaltkreis in *Platynereis dumerilii*. Mit Hilfe von Serienschnitten konnte ich den ersten kompletten neuronale Augen-Schaltkreis in der drei Tage alten Larve rekonstruieren. Die vier sich entwickelnden adulten Augen sind für die Phototaxis verantwortlich. Sie bestehen aus Photorezeptorzellen unterschiedlichen Alters, die über mehrere Interneurone die Muskeln und Wimpernzellen innervieren. Mit zunehmendem Alter der Photorezeptorzellen vergrößert sich das Rhabdomvolumen, die Axonlänge und die Anzahl der Synapsen. Die Photorezeptorzellen sind auf dem Level der Interneurone vernetzt und ermöglichen den Vergleich des einfallenden Lichtes zwischen beiden Körperseiten. Die Larve reagiert auf ein Ungleichgewicht der Lichtintensität mit einseitiger Muskelkontraktion und ändert so ihre Schwimmrichtung. Die Analyse der räumlichen Lichtverhältnisse durch den Vergleich des einfallenden Lichtes auf beiden Körperseiten ist das Merkmal 'echten' Sehens. Es unterscheidet sich von der Phototaxis im frühen Larvenstadium, bei dem die räumliche Auflösung durch fortwährendes scannen der Umgebung erreicht wird. Meine Daten zeigen ebenfalls, dass ein Auge die Muskulatur auf beiden Körperseiten innerviert. Dadurch kann die Larve entweder zum Licht oder vom Licht weg schwimmen. Zudem ist die Effektivität der Phototaxis vom Kontrast, aber nicht von der Lichtintensität abhängig. Ich konnte ein Interneuron-Motiv identifizieren, welches für die Erhöhung der Kontrastwahrnehmung verantwortlich ist. Zusätzlich beschrieb ich das Expressionsmuster zweier rhabdomerer Opsine in verschiedenen Larvenstadien. Basierend auf der Opsinexpression und der Rekonstruktion des Larvenauges, konnte ich eine zweite Photorezeptorzelle beschreiben, die wahrscheinlich auch im adulten Wurm eine Funktion hat.

Summary

Visually guided behavior is widespread in the animal kingdom. Despite this, most studies focused on the eyes and visual processing centers of vertebrates and *Drosophila*. We therefore have detailed understanding of the neuronal bases of visually-guided behavior in these organisms. However, a complete synaptic-level connectivity-map (connectome) of a visual circuit has not yet been described in any animal. In this thesis I studied the neural circuit mediating phototaxis in the marine annelid *Platynereis dumerilii*. Using serial section electron microscopy (ssEM), I was able to reconstruct the first complete eye circuit in a 3 dpf old *Platynereis* larva, from photoreceptor cells, via several interneurons and motorneurons to the motor organs (muscles and cilia). Phototaxis is mediated by four visual eyes, which grow during the whole life by adding new cells throughout the animal's life. Older photoreceptor cells had larger rhabdomes, longer axon and a greater number of synapses. The four eyes of the larva are connected at the level of the interneurons and allow the comparison of light levels on either side of the body. An imbalance in light intensity evokes a unilateral muscle contraction, leading to body bending and a change in swimming direction. The comparison of light inputs on either side of the body in order to achieve spatial resolution is a hallmark of vision and represents a navigation strategy completely different from the scanning non-visual phototaxis found in *Platynereis* larvae younger than three days. My connectome data also demonstrate that signals from one eye can reach the longitudinal muscles on either side of the body. This allows the larva to switch between positive and negative phototaxis. I also showed that the efficiency of phototaxis depends on light contrast and not total light intensity. I identified a reciprocal inhibitory interneuron motif between the crosswise eyes that enhances contrast detection.

I also describe in detail in this thesis the expression patterns of two rhabdomeric opsin genes in the visual eyes and larval eyes of *Platynereis* at different developmental stages. These gen expression patterns led me to identify a second photoreceptor cell in the larval eye that, based on its opsin expression and connectivity, likely still has a function in the adult worm.

List of publications in the thesis

N. Randel, A. Asadulina, L.A. Bezares-Calderón, C. Verasztó, E.A. Williams, M. Conzelmann, R. Shahidi, G. Jékely. **Neuronal connectome of a sensory-motor circuit for visual navigation**. eLife 2014; 10.7554/eLife.02730

N. Randel, L.A. Bezares-Calderón, M. Gühmann, R. Shahidi and G. Jékely. **Expression dynamics and protein localization of rhabdomeric opsins in *Platynereis* larvae**. Integrative and Comparative Biology 2013, 53 (1).

Own contribution to the publications

N. Randel, A. Asadulina, L.A. Bezares-Calderón, C. Verasztó, E.A. Williams, M. Conzelmann, R. Shahidi, G. Jékely. **Neuronal connectome of a sensory-motor circuit for visual navigation.**

I prepared the animal for sectioning and did the sectioning, using self-made formvar grids. I sectioned, contrasted and carbon coated 78% and imaged 25% of the sections. I montaged and aligned the complete stack. I traced all neurons. I reviewed most of the neurons (>95%), but was helped with the reconstruction of landmarks by L.A. Bezares-Calderón and C. Verasztó. I performed the ablation and swimming assays. Some of the bending assays were performed by G. Jékely. The figures and movies were prepared together with G. Jékely and A. Asadulina. Drafting and revision were done by G. Jékely with contributions from me.

N. Randel, L.A. Bezares-Calderón, M. Gühmann, R. Shahidi and G. Jékely. **Expression dynamics and protein localization of rhabdomeric opsins in *Platynereis* larvae.**

I performed antibody purification, immunostaining, in-situ hybridization and confocal microscopy. I prepared the animal for sectioning and did the sectioning, using self-made formvar grids. I sectioned, contrasted and carbon coated all sections and imaged 80% of the sections. I montaged and aligned the complete stack. I traced all neurons. The figures and movies were prepared together with G. Jékely and A. Asadulina. Drafting and revision were done by G. Jékely with contributions from me.

Introduction

Visual navigation requires the detection of spatial differences in environmental light levels at the level of the neuronal circuit without body movement (Nilsson 2009). Understanding how visual navigation works would require the ultrastructural mapping of the structure and function of neuronal circuits at single cell resolution and the identification of all synapses. Recent efforts on the connectomic reconstruction of the visual system in *Drosophila* provided detailed insights into the mechanisms of motion detection (Takemura et al. 2013) (Meier et al. 2014) (Maisak et al. 2014) (Shinomiya et al. 2014) and color vision (Gao et al. 2008) (Morante & Desplan 2008). In vertebrates, the synaptic connectivity of the retina was studied in great detail (Anderson et al. 2011) (Marc et al. 2012), leading to the identification of direction sensitive neurons (Helmstaedter et al. 2013) (Briggman et al. 2011). However, in flies and mice, the description of the eye connectome is still restricted to the retina or the first visual processing center (optic lobe) and we lack the complete synaptic connectivity maps of visual systems encompassing the photoreceptor cells and all downstream neurons until the motor organs. During my thesis work I reconstructed the first complete eye circuit, downstream of the adult eyes in the three day post fertilization (dpf) old larva of *Platynereis dumerilii*.

For the reconstruction I fixed and sectioned the head and first segment of a 3 dpf old *Platynereis* larva for serial section transmission electron microscopy (ssTEM). Each section was imaged at high resolution and stitched and aligned into a series encompassing 1600 sections. The adult eyes could be identified in the EM sections by the pigment cup, the lens and the rhabdome of the photoreceptor cells (Figure 1A, 3C). Using TrakEM (Cardona et al. 2012), I reconstructed the full neuronal circuitry postsynaptic to the eye photoreceptors. First I segmented the photoreceptor cells and annotated their synapses and postsynaptic targets (Figure 1A-C). Synapses were identified as accumulations of vesicles close to the cell membrane (Figure 1D-F). Then I identified and reconstructed all neurons postsynaptic to the eyes, reaching the motor targets of the eye circuit, the longitudinal trunk muscles and prototroch

cells. The complete reconstruction of the eye circuit gives detailed information about morphological arrangement of cells and synapses and their connectivity. The connectivity map of the eye circuit together with behavioral experiments provided detailed insights into the neuronal mechanisms of phototaxis in 3 dpf old *Platynereis* larvae.

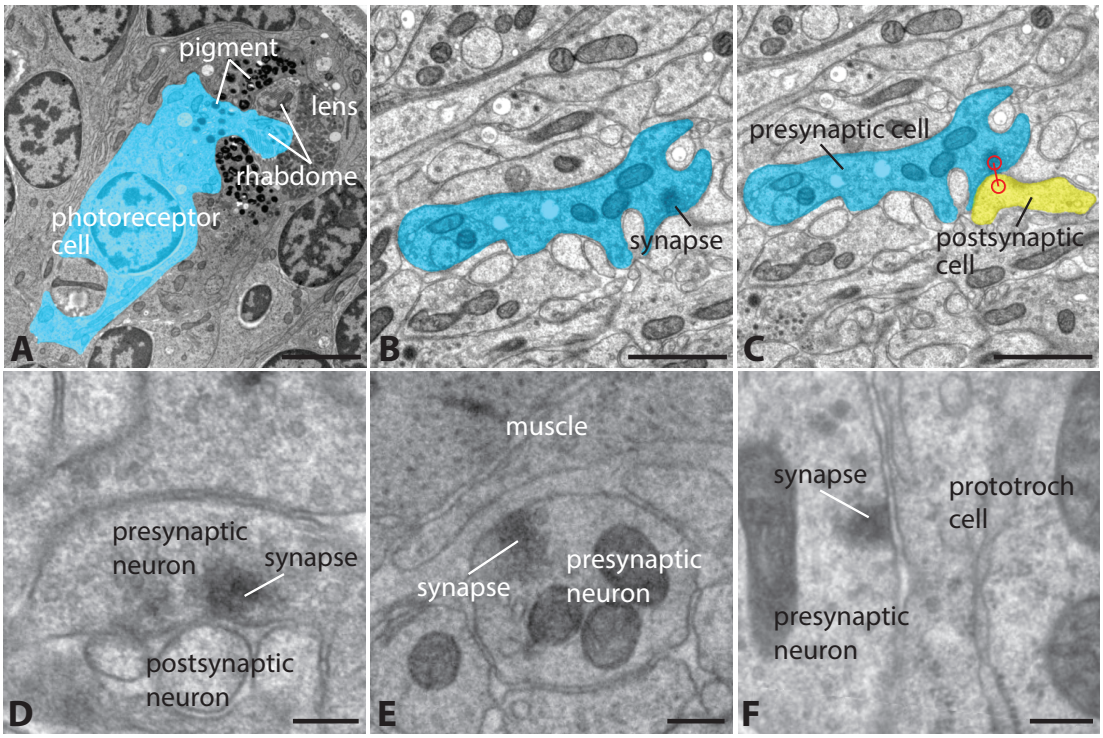

Figure 1. Transmission electron microscopy images of the visual eye circuit from a 3 dpf old *Platynereis* larva. (**A**-**C**) Reconstruction of a photoreceptor cell and its postsynaptic target. (**A**) Right anterior adult eye with one segmented photoreceptor cell (cyan). (**B**) TEM of the nerve plexus with a segmented axon (cyan) of the photoreceptor cell and its synapse. (**C**) Linkage of the photoreceptor cell (cyan) with its postsynaptic neuron (yellow) by a 'connector' (red). (**D**-**F**) Examples of different synapses. (**D**) Synapse between two neurons. (**E**) Neuromuscular synapse between a motorneuron and a muscle cell. (**F**) Synapse between motorneuron and a prototroch cell. Scale bars: (**A**) 3 µm; (**B**, **C**) 1 µm; (**D**, **E**, **F**) 0,2 µm.

Platynereis is a marine annelid with a biphasic life-cycle consisting of a tube-dwelling adult phase and a free-swimming phototactic larval phase (Fischer et al. 2010) (Figure 2). It has two different types of eyes, the larval eyes (eyespots) and the adult eyes. The two small larval eyes mediate positive phototaxis in the trochophora larva (up to 2 dpf). Each of the larval eyes

consist of a single rhabdomeric photoreceptor cell and a pigment cell (Rhode 1992). Upon a light stimulus, the photoreceptor cell releases acetylcholine onto a prototroch cell and decreases the ciliary beating frequency, which leads to a re-orientation of the body axis during phototaxis (Jékely et al. 2008). The larva gains spatial light information by constantly scanning the environment during rotation around the body axis (Jékely et al. 2008), a hallmark of non-visual phototaxis (Nilsson 2009).

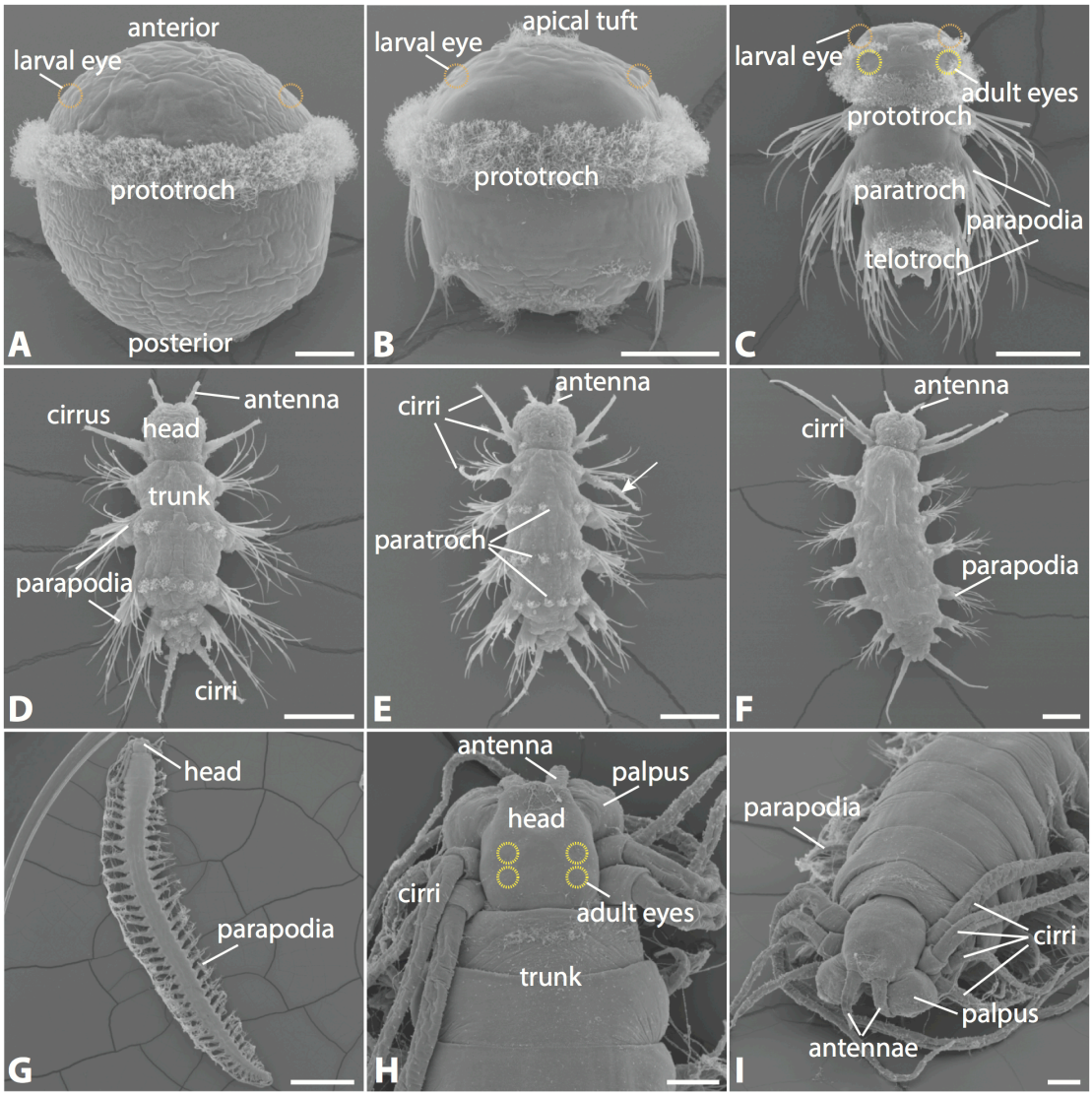

Figure 2. Scanning electron micrographs of different developmental stages of *Platynereis*: (**A**) Early trochophora larva (1 dpf) with the ciliary band and the larval eyes. (**B**) In the late trochophora larva (2 dpf) the parapodia starts to develop. (**C**) Dorsal view of a three segmented nectochaete larva (3 dpf) with three ciliary bands. The adult eyes develop on the dorsal side of the head. (**D**, **E**) Addition of a fourth (**D**) and fifth (**E**) segment in a juvenile. In (**E**) cephalic metamorphosis is initiated, visible

by the replacement of the first parapodia with a pair of dorsal cirrus (indicated by the arrow). (**F**) Metamorphosed juvenile *Platynereis*. (**G**-**I**) Tube-dwelling four month old adult, which grows by constant addition of segments. (**H**, **I**) Close-up of the head in a four month old adult *Platynereis* with the antennae, cirri and palpae. Scale bars: (**A**, **B**, **C**) 50 µm; (**D**, **E**, **F**, **H**, **I**) 100 µm; (**G**) 1 mm.

The nectochaete larval stage (>3 dpf) of *Platynereis* is also phototactic. At this stage the larva has two larval eyes (Figure 3A, B) and additionally four dorsal eyes, the developmental precursors to the adult's visual eyes (Figure 3A-C). The adult eye precursors appear during the third day of development as simple structures composed of a few photoreceptor and pigment cells with a lens (3dpf). These eyes later develop into the large visual eyes of the adult comprised of several hundred photoreceptors and pigment cells (Rhode 1992).

The eyes of *Platynereis* consist of rhabdomeric photoreceptor cells. In rhabdomeric photoreceptors the phototransduction cascade is initiated in specialized apical microvilli, the rhabdoms. Rhabdomeric photoreceptors use rhabdomeric-type opsins, seven transmembrane G-protein coupled receptors coupled to retinal chromophore. Light triggers the conformational change of 11-cis-retinal to all-trans-retinal and initiates a transduction cascade via a Gq-protein (Yau & Hardie 2009) (Terakita 2005).

Platynereis larvae also have ciliary photoreceptors with specialized sensory cilia containing a ciliary opsin, however, these cells are not associated with pigment cells (Arendt et al. 2004) (Figure 3A, D). Although the distinction of ciliary versus rhabdomeric-type opsins and photoreceptors is clear for visual eyes, members of other opsin families, including peropsins and retinochrome, are sometimes coexpressed with ciliary or rhabdomeric-type opsins in the same cell. Often multiple opsins of the same family are coexpressed in the same eye or photoreceptor cell, providing broader coverage of the visual spectrum (Lukáts et al. 2005) (Porter et al. 2009) (Katti et al. 2010). The co-expression of two kinds of opsin, which differ in their absorption spectra, can act as a depth gauge, where the water-depth is determined according to the spectral profile of the water.

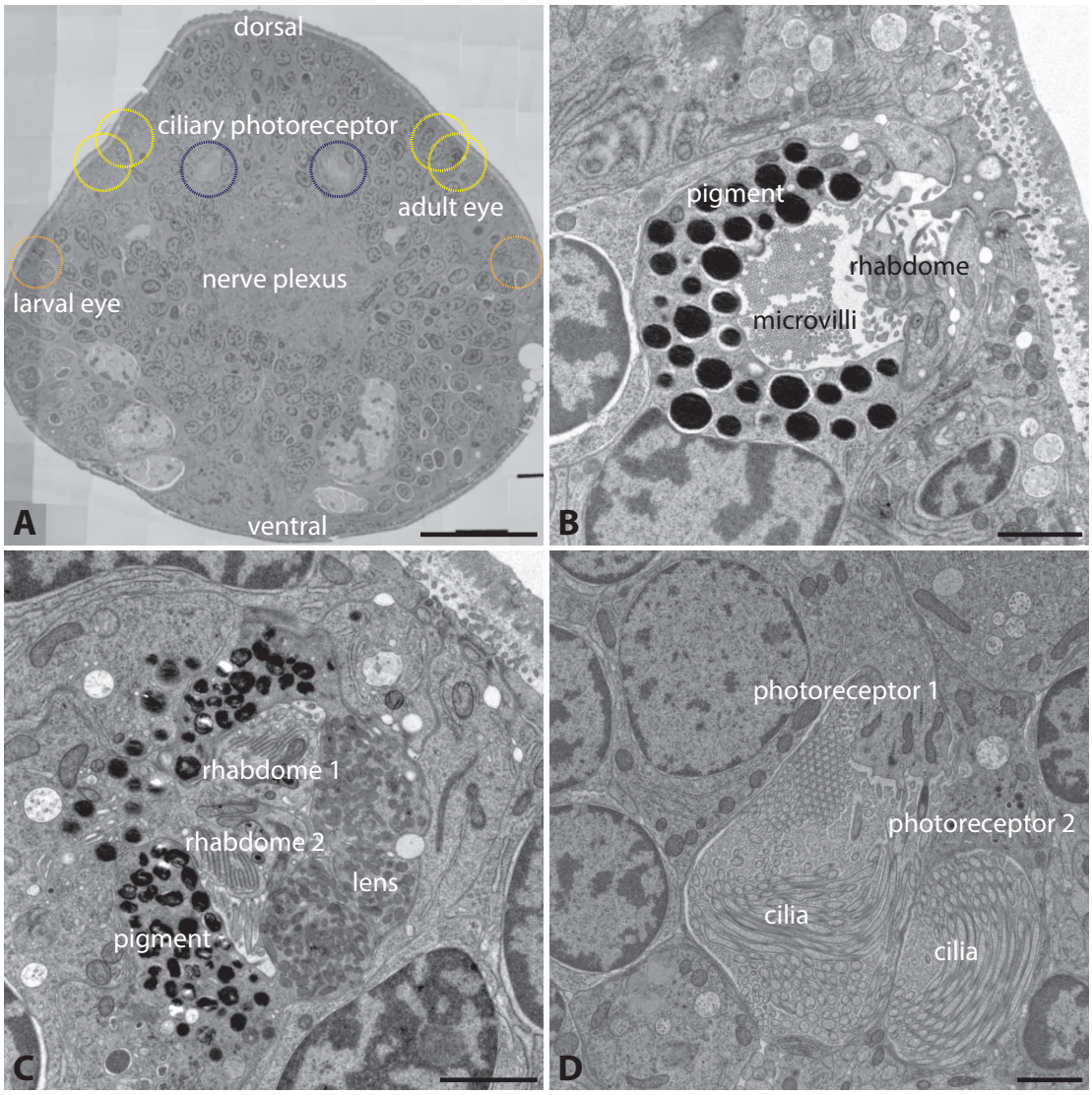

Figure 3. Serial section transmission electron microscopy images in a 3 dpf old *Platynereis* larva: (**A**) A representative cross-section from the head. The position of the larval and adult eyes and the ciliary photoreceptor cells are indicated by the circles. (**B**-**D**) Ultrastructure of the different types of eye: The rhabdomeric photoreceptor cells of the larval (**B**) and adult eye (**C**) are associated with pigment cells. In contrast the cilia of the ciliary photoreceptor cells (**D**) are not shaded by pigment granules. Scale bars: (**A**) 25 µm; (**B**-**D**) 1,5 µm.

During their planktonic free-swimming stage (1-6 dpf), *Platynereis* larvae perform phototaxis. Phototaxis is a widely distributed behavior amongst planktonic organisms, including copepodes (Cohen & Forward 2002), (Chae & Nishida 2004), (Bollens & Frost 1990), (Stearns & Forward 1984) (Swift & Forward 1983) and larvae of sponges ((Collin et al. 2010), (Leys et al. 2002), cirrepedia (Barnes & Klepal 1972), (Lang et al. 1979), (Visscher 1928)

mollusks (Barile et al. 1994) (Miller & Hadfield 1986), bryozoan (Pires & Woollacott 1997), polychaetes (Marsden 1986) (Marsden 1988), (Marsden 1990), (Young & Chia 1982) (Jékely et al. 2008), flatworms (Johnson & Forward 2003) and ascidian (McHenry & Strother 2003) (Kajiwara & Yoshida 1985).

The mechanism of phototaxis in the early stage is well understood, but phototaxis in the late larval stages has not yet been studied. Phototaxis represents directional movement along a light vector either towards (positive) or away (negative) from the light source. The minimal requirements for phototaxis are a partly shaded photoreceptor cell to detect the light direction, which is able to transmit the signal to the motor organ. Phototaxis also requires the ability to gain spatial resolution (Jékely 2009). This can be achieved either by a consistent scanning of the light field by axial body rotation and the fast adaption of the photoreceptor cells (non-visual phototaxis) as in the trochophora larvae of *Platynereis* (Jékely et al. 2008) or by vision where spatial resolution is achieved by comparison of the light input on both body sides without body movement (Nilsson 2009), as in *Danio rerio* (zebrafish) larvae (Burgess et al. 2010) or in the lamprey (Ullén et al. 1997). *Drosophila* larvae seem to use a non-directional mechanism allowing the larvae to move along a light gradient, but not a light vector (Kane et al. 2013).

In this thesis, I describe the neural connectome of the *Platynereis* visual eyes and how this neural circuit mediates visual phototaxis in the late larval stage.

Aim of the thesis

It has long been known that planktonic organisms perform vertical migration, which is often triggered by light. Many studies describe the behavioral response of zooplankton upon a light stimulus, but the underlying mechanism is mostly unknown. In the early larval stage of *Platynereis* (1-2 dpf) a direct sensory-motor system mediates non-visual positive phototaxis. However, older *Platynereis* larvae are able to switch between positive and negative phototaxis, which indicates a change in the neuronal processing. A description of the mechanisms in late larval stage are still missing. Moreover, information about opsin expression in different larval stages is important for understanding the functional diversity of eyes.

The main goal of my thesis is to understand the function of the eye circuit, driving phototaxis in late *Platynereis* larvae. I mainly focused on the following questions: Do 3 dpf old *Platynereis* perform visual or non-visual phototaxis? How is the phototactic sign-switch regulated? How is the light stimulus transmitted to the motor organ? How does the opsin expression change during development?

To address those questions, I used ssTEM to reconstruct the complete eye circuit in a 3 dpf old larva, including photoreceptor cells, several classes of interneuron, motorneurons and the motor organs. The reconstruction reveals the morphology and connectivity of single neurons and provided insights into the function of the neural circuit. This connectome data enables me to formulate several hypotheses on the mechanism of phototaxis in *Platynereis*. I tested these hypotheses using behavioral experiments combined with laser ablations. I also characterized in detail the expression and localization of two rhabdomeric opsins in the eyes, which gave insights into their photoreceptor complement and ontogenetic changes.

The combination of different approaches, including ssTEM, laser ablation, swimming assays and molecular markers, allows me to gain unprecedented insights into a visually guided behavior, and represents the first integrative description of the structure and function of a complete visual circuit and visually-guided behavior in any animal.

Results

N. Randel, A. Asadulina, L.A. Bezares-Calderón, C. Verasztó, E.A. Williams, M. Conzelmann, R. Shahidi, G. Jékely. **Neuronal connectome of a sensory-motor circuit for visual navigation**. eLife 2014; 10.7554/eLife.02730.

The understanding of how environmental stimuli result in distinct motor outputs requires the study of the neuronal connectivity of behaviorally relevant circuits. Here I reconstructed the first complete connectivity map of all neurons lying on synaptic pathways from visual eye photoreceptors to locomotor organs (muscles and ciliary bands) in order to understand the mechanism of phototaxis in the 3 dpf old larva of *Platynereis dumerilii.*

The larva has six eyes, two eyespots and four visual eyes (adult eyes). Using laser ablation experiments, I investigated the involvement of the different types of eyes in phototaxis. At 3 dpf the larval eyes are no longer able to mediate phototaxis, it is the adult eyes that are responsible for directional light responses. In order to understand how the swimming direction is changed during phototaxis, I mounted larvae between a coverslip and a slide and selectively illuminated the eyes on one side. These experiments revealed that unilateral illumination provokes tail bending by unilateral muscle contraction. In free-swimming larvae, such muscle contractions lead to a change in the swimming direction.

The eye ablation experiments also showed that at least one adult eye on each side of the body has to be functional in order to generate a phototactic response. If the larva is completely blinded on one side, it reacts to a light stimulus by constant tail bending and circular swimming, and is unable to swim straight towards or away from a directional light source. These experiments showed that larvae compare the light input from both sides of the body and an imbalance in left-right illumination leads to the unilateral contraction of muscles and the re-orientation of the larva in relation to the light. The response is therefore visual, because the larvae are able to detect spatial differences in light levels without body movement (axial rotation). Hence the larva uses visual navigation to orient itself in the light beam, and

this response is mediated by visual eyes.

To map the neural circuitry of the visual eyes, I performed ssTEM and reconstructed the neuronal circuit of the eyes. The head and part of the first trunk segment was sectioned in 40-50 nm steps in one larva. I registered and aligned the image stacks and reconstructed the neural circuitry manually using TrakEM2. To visualize the cell complement of the eye network and to analyze its connectivity I used 3Dviewer, Imaris, Blender and Gephi.

The visual eye circuit is composed of 21 photoreceptor cells, 42 interneurons and 11 motorneurons. I classified 6 classes of interneurons based on the position of the cell bodies and connectivity. The photoreceptor cells have a dendrite (rhabdome) but all other neurons are unipolar and are connected by axo-axonal contacts.

All four visual eyes are connected at the level of the interneurons and this wiring allows the comparison of light input from the left and the right side of the body. The motorneurons innervate the ventro- and dorsolateral longitudinal muscles and the cells of the ciliary bands (prototroch and metatroch). I also used calcium imaging to show directly that the longitudinal muscles in the trunk are contracted during unilateral illumination of the eyes, in agreement with the wiring diagram. Although during this project I only reconstructed the circuit of one individual, I was able to assess the stereotypy of synaptic connection by comparing the connectivity matrix of neurons from the left and right side of the body. I also compared the spatial arrangement of pre- and postsynapses from left and right neurons of the same classes of neurons. The number and the spatial arrangement of synapses are very similar between the left and right sides of the body, indicating that the neuronal connectome is stereotypic.

All synaptic contacts in the visual circuit are axo-axonal and the synapses are concentrated in two defined optic neuropils in the larval brain. I also identified and reconstructed three giant multilamellate glial cells that tightly surround the optic neuropils. Several of the neurons are intrinsic to either the primary or the secondary optic neuropil, with connections between the two neuropils provided by two distinct classes of interneurons, the trans-optic neuropil interneurons and the Schnörkel-interneurons.

The eye circuit is a feed-forward circuit and the signal flows from the

photoreceptor cells of one eye to a single primary interneuron. There are four primary interneurons, one per eye, and the main targets of these cells are the trans-optic neuropil interneurons, which innervate the motorneurons via the Schnörkel-interneurons. The neurons in the circuit are mostly connected in a cross-wise manner, with cells synapsing on neurons on the contra-lateral side. The Schörkel-interneurons are an exception, because they innervate both the ipsi- and the contralateral motorneurons. The motorneurons always project to the muscles and ciliated cells on the contra-lateral side. The signal from the eye diverges at the level of the Schörkel-interneurons and can reach both sides of the body. This may explain the ability of the larvae to perform both positive and negative phototaxis.

The analysis of the connectivity matrix shows a sparse overall connectivity, with approximately 6% of all possible connections realized. By analyzing the connectivity and network centrality of neurons in the eye network we could identify two distinct modules, corresponding to the neurons intrinsic to the two neuropils.

We also analyzed reciprocal connections, and identified a motif of strong reciprocal contacts between the crosswise positioned primary interneurons. Two crosswise interneurons form a pair with several reciprocal synaptic contacts. We think that these synapses are inhibitory and this motif represents a mutual inhibitory connectivity, where the interneurons of one reciprocal pair are able to inhibit each other. This could increase the contrast perception and therefore improve the phototactic efficiency.

We tested this hypothesis by quantifying the efficiency of phototaxis by measuring the magnitude of larval tail bending upon unilateral illumination. We performed eye ablation experiments, ablating the eyes in different combinations. The connectome data indicated that if one eye is eliminated, one particular primary interneuron will not receive a signal. We therefore anticipated different behavioral outcomes from the ablation of a bilateral pair of eyes versus a crosswise pair of eyes. These experiments showed that larvae with pairwise eye ablations, where all input to both reciprocal interneuron motifs was eliminated, had reduced bending efficiency compared to crosswise eye-ablated larvae. These experiments supported the model that the reciprocal connections between the crosswise interneurons enhance the

magnitude of the motor response, thereby leading to more efficient phototaxis. I also analyzed the connectivity of photoreceptor cells at different stages of developmental maturation in the same individual. We found that different photoreceptors from the same eye had different rhabdome volumes and axon lengths, indicating that the photoreceptor cells were at different stages of maturation at the time of larval fixation. We found that more mature neurons, characterized by larger rhabdomes and longer axons, had established more connections to the primary interneurons and that younger photoreceptors only formed few probably transient synapses with neurons that were not connected by the mature neurons.

To understand the neurotransmitter content of the different neuron types of the visual eye circuit, we characterized the gene expression patterns of markers for classical neurotransmitters and monoamines. We found that the photoreceptor cells of the adult eyes are glutamatergic, the interneurons express a variety of monoaminergic markers, and the motorneurons are cholinergic and partly GABAergic.

To conclude, my reconstruction of the 3 dpf old *Platynereis* connectome represents the first complete sensory-motor-circuit reconstructed in any animal. I identified a simple visual system which mediates phototaxis. The *Platynereis* visual eye circuit has the capacity to compare light inputs from different sides of the body, enhance contrast by reciprocal inhibition and guide visual phototaxis. Phototaxis can be either positive or negative, indicating that the circuit can be modulated by other sensory inputs. From an evolutionary point of view, the simplest visual eyes may have mediated phototaxis, and allowed animals to distinguish between a light and a dark field in the ocean.

N. Randel, L.A. Bezares-Calderón, M. Gühmann, R. Shahidi and G. Jékely. **Expression dynamics and protein localization of rhabdomeric opsins in *Platynereis* larvae**. Integrative and Comparative Biology 2013, 53 (1).

Opsins, light sensitive seven-transmembrane G-protein coupled receptors, are present in photoreceptor cells across Eumetazoa (Terakita 2005). The diversity and subcellular localization of different classes of opsins helps us to understand the functional diversity of animal eyes.

I investigated the localization and expression of two rhabdomeric-type opsins in *Platynereis*. One of the opsins, r-opsin1, has already been described in late larval stage of *Platynereis*, the other, r-opsin3, was described in this study. In r-opsin3 I could identify conserved residues characteristic of opsins, including the lysine residue in the 7th transmembrane segment and a tripeptide motif (HPR) characteristic of rhabdomeric opsins. Phylogenetic analysis of r-opsins suggested one gene duplication event at the base of mollusks/annelids and one before the split of errant and sedentary annelids.

Both r-opsins are expressed in the larval and adult eye during *Platynereis* development. After hatching, the larva has two larval eyes, which consist of a rhabdomeric photoreceptor cell and a pigment cell. Until 3 dpf the eyespot only expresses r-opsin3 in a single photoreceptor cell. At 3 dpf expression of r-opsin1 can also be detected in the eyespot. To determine a possible coexpression of the two opsins, we performed double RNA *in situ* hybridization. This revealed that the two opsins are expressed in two adjacent cells, indicating the presence of a second photoreceptor cell in the eyespot. The r-opsin1-expressing cell is likely present until adulthood, whereas the expression of r-opsin3 cannot be detected in the eyespot after 3 dpf. To characterize the second eyespot photoreceptor, I performed ssTEM on a 3 dpf larva. The reconstruction of the larval eye confirmed the presence of a second rhabdomeric photoreceptor cell in the eyespot, with a defined rhabdome within the pigment cup. Interestingly, the axonal projections of the two photoreceptors are different. The r-opsin3-expressing cell, which represents the photoreceptor cell in the early larval stage, innervates the ipsilateral prototroch and projects towards the neuropil. In contrast, the newly

developed r-opsin1-expressing rhabdomeric photoreceptor cell directly projects towards the neuropil, to a distinct area.

After 2 dpf, *Platynereis* larvae develop additional four adult eyes. All rhabdomeric photoreceptor cells in the adult eyes co-express r-opsin1 and r-opsin3. This expression pattern could be observed in all stages examined, from 2 dpf until adulthood.

I also developed antibodies against r-opsin1 and r-opsin3 to characterize their localization within the photoreceptor cells. I could detect the opsins in the rhabdome of the larval and adult eye photoreceptors. Additionally, I could detect r-opsin1 in the axonal projection of the adult eyes in the primary optic neuropil.

This study revealed a change in the opsin expression in the eyespots during development and identified a second photoreceptor cell in the larval eyespot with a different projection pattern from its neighbouring photoreceptor cell. This eyespot photoreceptor may be maintained until adulthood. In contrast to the eyespots, the adult eye photoreceptors express both opsins during larval and adult stages.

Discussion and Conclusion

Visual navigation with the capability of phototactic sign switch and contrast enhancement

The mechanism of phototaxis in the 3 dpf old larva of *Platynereis* differs from the previously described non-visual phototaxis in younger larvae (Jékely et al. 2008). With the development of the adult eyes, the larva is able to compare and contrast spatial differences in light during phototaxis. The ability to compare light input from both sides of the body without body movement is the hallmark of vision (Nilsson 2009). Spatial resolution is not achieved by single photoreceptor cells, but by all photoreceptor cells within one eye, because the signal from all photoreceptors in one eye converge on a single primary interneuron. This means that the larva is able to distinguish between four different light/dark areas, each area detected by one eye. This kind of a four-pixel eye circuit represents the simplest form of vision, able to detect only four pixels, sufficient only to mediate visual phototaxis.

The *Platynereis* larval visual eye circuit also has implications for eye evolution. It might represent a precursor to low resolution image-forming eyes, as an intermediate stage between non-directional light response mediated by a sensory-motor eyespot and an eye able to mediate low resolution vision (Nilsson 2009).

The progression from non-visual to visual phototaxis in the life cycle of a pelagic larva may be necessary because of changes in locomotion pattern during development (Chia & Buckland-Nicks 1984). Late-stage *Platynereis* larvae have a mixed pelagic-benthic life style and in addition to rotational swimming with cilia, they can also crawl or glide on the substrate. Such a bilateral crawling motion would not be compatible with helical phototaxis, but is compatible with visual phototaxis, where constant body rotation is not necessary.

Phototaxis is widely distributed among planktonic marine larvae (Thorson 1964). Larval phototaxis is always mediated by simple eyes. Such eyes have been described in many invertebrate larvae, including sponges (Leys &

Degnan 2001), cnidarians (Nordstrom et al. 2003), annelids (Bartolomaeus 1992a), mollusks (Bartolomaeus 1992b), nemerteans (Döhren & Bartolomaeus 2007), flatworms (Eakin & Brandenburger 1981), brachiopods (Passamaneck et al. 2011), crustaceans (Lacalli 2009), hemichordates (Brandenburger et al. 1973) and cephalochordates (Lacalli 1996). Sometimes the simple larval eyes develop into the adult's visual eyes, like in gastropods (Blumer 1996), (Blumer 1994), (Chia & Koss 1983). Larval eyes can also be reduced as in some annelids (Blumer 1997) (Eakin & Westfall 1964) or coexist with the adult eyes, like in *Platynereis*, or the late larvae of other polychaetes (Heffernan & Keegan 1988), (Irvine et al. 1999). With the exception of *Platynereis*, the function and neural circuitry of simple eyes is poorly understood. It would be interesting to investigate how phototaxis changes during development and how it correlates with changes in behavior in other taxa.

Phototactic sign switching is also very common among planktonic larvae (Thorson 1964). The mechanism of sign switching is not fully understood in *Platynereis*. However, the connectome reconstruction suggests that the signal from the eyes diverges at the level of the Schörkel-interneurons which innervate both the ipsi- and the contralateral motorneurons. We have observed that other external sensory stimuli, including temperature and mechanical stimulation, can switch the sign of *Platynereis* phototaxis. The mechanism of such cross-modal integration will be an interesting subject for further studies.

In *Platynereis* the larval and visual eyes express distinct neurotransmitters. The larval eye releases acetylcholine (Jékely et al. 2008), whereas the visual adult eyes use glutamate. Glutamate is also expressed in vertebrate photoreceptor cells, where a light stimulus induces a hyperpolarization of the photoreceptor and inhibits the release of the neurotransmitter. This triggers the hyperpolarization of postsynaptic OFF-bipolar cells or the depolarization of ON-bipolar cells (Sanes & Zipursky 2010). In arthropods, histamine is commonly used as a neurotransmitter in the eye (Stuart et al. 2007), while in *Drosophila* larvae the Bolwig organ uses acetylcholine (Yasuyama et al. 1995). In other taxa the information about eye neurotransmitters is limited, but

studies identified glutamate in the mollusks *Aplysia* and *Bulla* (Michel et al. 2000) and acetylcholine in *Hermissenda* (Heldman et al. 1979).

The morphology and connectivity of photoreceptor cells at different stages of maturation in *Platynereis* revealed how neuronal connectivity may develop in annelids. Shaping of the connectivity by spontaneous activity (Yamamoto & López-Bendito 2012) or by glia cells (Corty & Freeman 2013) is known from other taxa. Glia cells also play an important role in neuronal development, regeneration, activity and the establishment of synaptic connectivity (Stout et al. 2014) (Mashanov et al. 2013) (Edwards & Meinertzhagen 2010) (Freeman & Doherty 2006). Myelinated axons have also been identified in annelids (Hartline & Kong 2009) but their function in this group is unknown. In *Platynereis*, the organization of the glia cells is different and no myelin sheath is formed. The glial cells in *Platynereis* surround the primary and secondary optic neuropils from the anterior side forming a boundary between these neuropils and adjacent tissues. Further investigations about the organization and function of glia cells in annelids are necessary to quantify their influence on neuronal development.

Functional and sensitivity of the larval and adult eyes in *Platynereis*

The larval and adult eyes of *Platynereis* undergo different spectral and functional maturation. At the onset of phototaxis the photoreceptor cell of the larval eye expresses only r-opsin3. It has been shown that the larval eye mediates phototaxis by a direct projection to the lateral prototroch cells (Jékely et al. 2008). The larval eyes may retain their function in mediating phototaxis until r-opsin3 is expressed. The later function of the eyespot in older *Platynereis* is unknown, but the r-opsin1 expression is maintained until adulthood in the second photoreceptor cell, as shown by an r-opsin1-GFP transgenic line (Backfisch et al. 2013). The projection of the second eyespot photoreceptor to the neuropil indicates that further functions may develop e.g. the entrainment of circadian rhythms or spectral light avoidance in the larval and adult worm.

The photoreceptor cells of the adult eyes co-expressed both rhabdomeric opsins, which probably broadens their spectral sensitivity. Opsin co-expression is known from different arthropods (Katti et al. 2010) (Mazzoni et al. 2008) (Porter et al. 2009) and vertebrates (Lukáts et al. 2002) (Lukáts et al. 2005). A possible function of the two r-opsins as a depth gauge is unlikely, since r-opsins are known to depolarize photoreceptor cells, likely excluding the possibility of antagonistic interactions between them.

The localization of both rhabdomeric opsins in the rhabdome within the pigment cup agrees well with their phototactic function, which requires a restricted view angle. The axonal localization of *r-opsin1* mRNA and r-opsin1 protein in the visual eye photoreceptors may indicate further regulatory functions for r-opsin1 (Martin & Ephrussi 2009). In vertebrates, melanopsin of the retinal ganglion cells is localized in the cell body, the dendrite and the axon and is involved in circadian clock regulation and pupillary light reflex (Hattar 2002).

Conclusion

The detailed anatomical and functional studies of the visual eyes in the late-stage *Platynereis* larva presented in this thesis led to an in-depth understanding of the neuronal mechanisms of visual phototaxis in a marine larva. From an evolutionary point of view, the visual eye circuit of *Platynereis* is a model for the simplest visual eyes that only allow an animal to distinguish between a light and a dark field in order to perform phototaxis. Contrast enhancement and spectral broadening of the response by the use of multiple opsins increase the efficiency of phototaxis and allow the larvae to navigate in a wider depth range and in different water qualities.

Bibliography

Anderson, J.R. et al., 2011. Exploring the retinal connectome. *Molecular Vision*, 75(2), pp.209–217.

Arendt, D., Tessmar-Raible, K. & Snyman, H., 2004. Ciliary photoreceptors with a vertebrate-type opsin in an invertebrate brain. *Science*, 309, pp.869–871.

Backfisch, B., Rajan, V. & Fischer, R.M., 2013. Stable transgenesis in the marine annelid Platynereis dumerilii sheds new light on photoreceptor evolution. In Proceedings of the National Academy of Sciences. pp. 193–198.

Barile, P.J., Stoner, A.W. & Young, C.M., 1994. Phototaxis and vertical migration of the queen conch (< i> Strombus gigas</i> linne) veliger larvae. *Journal of Experimental Marine Biology and Ecology*, 183(2), pp.147–162.

Barnes, H. & Klepal, W., 1972. Phototaxis in stage I nauplius larvae of two cirripedes. *Journal of Experimental Marine Biology and Ecology*.

Bartolomaeus, T., 1992a. *Ultrastructure of the photoreceptors in certain larvae of the Annelida*, Microfauna Marina.

Bartolomaeus, T., 1992b. *Ultrastructure of the photoreceptors in the larvae of Lepidochiton cinereus (Mollusca, Polyplacophora) and Lacuna divaricata (Mollusca, Gastropoda)*, Microfauna Marina.

Blumer, M., 1996. Alterations of the eyes during ontogenesis inAporrhais pespelecani (Mollusca, Caenogastropoda). *Zoomorphology*, 116, pp.123–131.

Blumer, M., 1997. The larval ocelli of Golfingia misakiana (Sipuncula, Golfingiidae) and of a pelagosphera of another unidentified species. *Zoomorphology*, 117(2), pp.115–120.

Blumer, M., 1994. The ultrastructure of the eyes in the veliger-larvae of Aporrhais sp. and Bittium reticulatum (Mollusca, Caenogastropoda). *Zoomorphology*, 114, pp.149–159.

Bollens, S.M. & Frost, B.W., 1990. UV light and vertical distribution of the marine planktonic copepod Acartia hudsonica Pinhey. *Journal of Experimental Marine Biology and Ecology*, 137, pp.89–93.

Brandenburger, J.L., Woolacott, R.M. & Eakin, R.M., 1973. Fine structure of eyespots in tornarian larvae (Phylum: Hemichordata). *Zeitschrift für Zellforschung und Mikroskopische Anatomie*, 142, pp.89–102.

Briggman, K.L., Helmstaedter, M. & Denk, W., 2011. Wiring specificity in the

direction-selectivity circuit of the retina. *Nature*, 471(7337), pp.183–188.

Burgess, H.A., Schoch, H. & Granato, M., 2010. Distinct retinal pathways drive spatial orientation behaviors in zebrafish navigation. *Current Biology*, 20, pp.381–386.

Cardona, A. et al., 2012. TrakEM2 Software for Neural Circuit Reconstruction. *PLoS ONE*, 7(6), p.e38011.

Chae, J. & Nishida, S., 2004. Swimming behaviour and photoresponses of the iridescent copepods, Sapphirina gastrica and Sapphirina opalina (Copepoda: Poecilostomatoida). *J. Mar. Biol. Ass. U.K.*, 84, pp.727–731.

Chia, F.S. & Buckland-Nicks, J., 1984. Locomotion of marine invertebrate larvae: a review. *Canadian Journal of Zoology*, 62(7), pp.1205–1222.

Chia, F.S. & Koss, R., 1983. Fine structure of the larval eyes of Rostanga pulchra (Mollusca, Opisthobranchia, Nudibranchia). *Zoomorphology*, 102(1), pp.1–10.

Cohen, J.H. & Forward, R.B., 2002. Spectral sensitivity of vertically migrating marine copepods. *The Biological Bulletin*, 203, pp.307–314.

Collin, R. et al., 2010. Phototactic responses of larvae from the marine sponges Neopetrosia proxima and Xestospongia bocatorensis (Haplosclerida: Petrosiidae). *Invertebrate Biology*, 129(2), pp.121–128.

Corty, M.M. & Freeman, M.R., 2013. Cell biology in neuroscience: Architects in neural circuit design: Glia control neuron numbers and connectivity. *The Journal of Cell Biology*, 203(3), pp.395–405.

Döhren, von, J. & Bartolomaeus, T., 2007. Ultrastructure and development of the rhabdomeric eyes in Lineus viridis (Heteronemertea, Nemertea). *Zoology*, 110(5), pp.430–438.

Eakin, R.M. & Brandenburger, J.L., 1981. Fine structure of the eyes of Pseudoceros canadensis (Turbellaria, Polycladida). *Zoomorphology*, 98(1), pp.1–16.

Eakin, R.M. & Westfall, J.A., 1964. Further observations on the fine structure of some invertebrate eyes. *Zeitschrift für Zellforschung und Mikroskopische Anatomie*, 62(3), pp.310–332.

Edwards, T.N. & Meinertzhagen, I.A., 2010. The functional organisation of glia in the adult brain of Drosophila and other insects. *Progress in Neurobiology*, 90(4), pp.471–497.

Fischer, A., Henrich, T. & Arendt, D., 2010. The normal development of Platynereis dumerilii (Nereididae, Annelida). *Frontiers in Zoology*, 7, pp.1–31.

Freeman, M.R. & Doherty, J., 2006. Glial cell biology in Drosophila and

vertebrates. *Trends in Neurosciences*, 29(2), pp.82–90.

Gao, S. et al., 2008. The Neural Substrate of Spectral Preference in Drosophila. *Neuron*, 60(2), pp.328–342.

Hartline, D.K. & Kong, J.H., 2009. Axonal sheaths in two reportedly myelinated polychaete nervous systems: Asychis elongata and Capitella sp. I., pp.1–2.

Hattar, S., 2002. Melanopsin-Containing Retinal Ganglion Cells: Architecture, Projections, and Intrinsic Photosensitivity. *Science*, 295(5557), pp.1065–1070.

Heffernan, P. & Keegan, B.F., 1988. The larval development of Pholoe minuta (Polychaeta: Sigalionidae) in Galway Bay, Ireland. *J. Mar. Biol. Ass. U.K.*, 68, pp.339–350.

Heldman, E., Grossman, Y. & Jerussi, T.P., 1979. Cholinergic features of photoreceptor synapses in Hermissenda. *Journal of Neurophysiology*, 42(1), pp.153–165.

Helmstaedter, M. et al., 2013. Connectomic reconstruction of the inner plexiform layer in the mouse retina. *Nature*, 500(7461), pp.168–174.

Irvine, S.Q., Chaga, O. & Martindale, M.Q., 1999. Larval Ontogenetic Stages of Chaetopterus: Developmental Heterochrony in the Evolution of Chaetopterid Polychaetes. *The Biological Bulletin*, 197(3), pp.319–331.

Jékely, G., 2009. Evolution of phototaxis. *Philosophical Transactions of the Royal Society B: Biological Sciences*, 364(1531), pp.2795–2808.

Jékely, G. et al., 2008. Mechanism of phototaxis in marine zooplankton. *Nature*, 456, pp.395–400.

Johnson, K.B. & Forward, R.B., Jr, 2003. Larval photoresponses of the polyclad flatworm< i> Maritigrella crozieri</i>(Platyhelminthes, Polycladida)(Hyman). *Journal of Experimental Marine Biology and Ecology*, 282, pp.103–112.

Kajiwara, S. & Yoshida, M., 1985. Changes in behavior and ocellar structure during the larval life of solitary ascidians. *The Biological Bulletin*, 169, pp.565–577.

Kane, E.A., Gershow, M. & Afonso, B., 2013. Sensorimotor structure of Drosophila larva phototaxis. In Proceedings of the National Academy of Sciences. pp. E3868–E3877.

Katti, C. et al., 2010. Opsin co-expression in Limulus photoreceptors: differential regulation by light and a circadian clock. *Journal of Experimental Biology*, 213(15), pp.2589–2601.

Lacalli, T.C., 1996. Frontal Eye Circuitry, Rostral Sensory Pathways and Brain

Organization in Amphioxus Larvae: Evidence from 3D Reconstructions. *Philosophical Transactions of the Royal Society B: Biological Sciences*, 351(1337), pp.243–263.

Lacalli, T.C., 2009. Serial EM analysis of a copepod larval nervous system: Naupliar eye, optic circuitry, and prospects for full CNS reconstruction. *Arthropod Structure and Development*, 38(5), pp.361–375.

Lang, W.H., Forward, R.B. & Miller, D.C., 1979. Behavioral responses of Balanus improvisus nauplii to light intensity and spectrum. *The Biological Bulletin*, 157(1), pp.166–181.

Leys, S.P. & Degnan, B.M., 2001. Cytological basis of photoresponsive behavior in a sponge larva. *The Biological Bulletin*, 201, pp.323–338.

Leys, S.P. et al., 2002. Spectral sensitivity in a sponge larva. *Journal of Comparative Physiology A*, 188(3), pp.199–202.

Lukáts, Á. et al., 2005. Photopigment coexpression in mammals: comparative and developmental aspects. *Histology and Histopathology*, 20, pp.551–574.

Lukáts, Á., Dkhissi-Benyahya, O. & Szepessy, Z., 2002. Visual pigment coexpression in all cones of two rodents, the Siberian hamster, and the pouched mouse. *Investigative Ophthalmology & Visual Science*, 43(7), pp.2468–2473.

Maisak, M.S. et al., 2014. A directional tuning map of Drosophila elementary motion detectors. *Nature*, 500(7461), pp.212–216.

Marc, R.E. et al., 2012. Building retinal connectomes. *Current Opinion in Neurobiology*, 22(4), pp.568–574.

Marsden, J.R., 1990. Light response of the planktotrophic larva of the serpulid polychaete *Spirobranchus polycerus*. *Marine Ecology Progress Series*, 58, pp.225–233.

Marsden, J.R., 1988. Light responses of the larva of the serpulid polychaeteGaleolaria caespitosa. *Marine Biology*, 99(3), pp.397–407.

Marsden, J.R., 1986. Response to light by trochophore larvae of Spirobranchus giganteus. *Marine Biology*, 93, pp.13–16.

Martin, K.C. & Ephrussi, A., 2009. mRNA Localization: Gene Expression in the Spatial Dimension. *Cell*, 136(4), pp.719–730.

Mashanov, V.S., Zueva, O.R. & García-Arrarás, J.E., 2013. Radial glial cells play a key role in echinoderm neural regeneration. *BMC Biology*, 11(1), p.49.

Mazzoni, E.O. et al., 2008. Iroquois Complex Genes Induce Co-Expression of rhodopsins in Drosophila. *PLoS Biology*, 6(4), p.e97.

McHenry, M. & Strother, J., 2003. The kinematics of phototaxis in larvae of the ascidian Aplidium constellatum. *Marine Biology*, 142(173-184).

Meier, M. et al., 2014. Neural Circuit Components of the Drosophila OFF Motion Vision Pathway. *Current Biology*, 24(4), pp.385–392.

Michel, S., Schoch, K. & Stevenson, P.A., 2000. Amine and amino acid transmitters in the eye of the mollusc Bulla gouldiana: An immunocytochemical study. *Journal of Comparative Neurology*, 425(2), pp.244–256.

Miller, S.E. & Hadfield, M.G., 1986. Ontogeny of phototaxis and metamorphic competence in larvae of the nudibranch< i> Phestilla sibogae</i> Bergh (Gastropoda: Opisthobranchia). *Journal of Experimental Marine Biology and Ecology*, 97(1), pp.95–112.

Morante, J. & Desplan, C., 2008. The Color-Vision Circuit in the Medulla of Drosophila. *Current Biology*, 18(8), pp.553–565.

Nilsson, D.E., 2009. The evolution of eyes and visually guided behaviour. *Philosophical Transactions of the Royal Society B: Biological Sciences*, 364(1531), pp.2833–2847.

Nordstrom, K. et al., 2003. A simple visual system without neurons in jellyfish larvae. *Proceedings of the Royal Society B: Biological Sciences*, 270(1531), pp.2349–2354.

Passamaneck, Y.J. et al., 2011. Ciliary photoreceptors in the cerebral eyes of a protostome larva. *EvoDevo*, 2(1), p.6.

Pires, A. & Woollacott, R.M., 1997. Serotonin and dopamine have opposite effects on phototaxis in larvae of the bryozoan Bugula neritina. *The Biological Bulletin*, 192, pp.399–409.

Porter, M.L., Bok, M.J. & Robinson, P.R., 2009. Molecular diversity of visual pigments in Stomatopoda (Crustacea). *Visual Neuroscience*, 26, pp.255–265.

Rhode, B., 1992. Development and differentiation of the eye in Platynereis dumerilii (Annelida, Polychaeta). *Journal of Morphology*, 212, pp.71–85.

Sanes, J.R. & Zipursky, S.L., 2010. Design principles of insect and vertebrate visual systems. *Neuron*, 66, pp.15–36.

Shinomiya, K. et al., 2014. Candidate Neural Substrates for Off-Edge Motion Detection in Drosophila. *Current Biology*, pp.1–9.

Stearns, D.E. & Forward, R.B., Jr, 1984. Photosensitivity of the calanoid copepod Acartia tonsa. *Marine Biology*, 82(1), pp.85–89.

Stout, R.F., Jr, Verkhratsky, A. & Parpura, V., 2014. Caenorhabditis elegans glia modulate neuronal activity and behavior. *Frontiers in Cellular*

Neuroscience, 8(67), pp.1–9.

Stuart, A.E., Borycz, J. & Meinertzhagen, I.A., 2007. The dynamics of signaling at the histaminergic photoreceptor synapse of arthropods. *Progress in Neurobiology*, 82(4), pp.202–227.

Swift, M.C. & Forward, R.B., 1983. Photoresponses of the copepod Mesocyclops edax. *Journal of Plankton Research*.

Takemura, S. et al., 2013. A visual motion detection circuit suggested by Drosophila connectomics. *Nature*, 500(7461), pp.175–181.

Terakita, A., 2005. The opsins. *Genome biology*, 6, p.213.

Thorson, G., 1964. Light as an ecological factor in the dispersal and settlement of larvae of marine bottom invertebrates. *Ophelia*, 1(1), pp.167–208.

Ullén, F., Deliagina, T.G. & Orlovsky, G.N., 1997. Visual pathways for postural control and negative phototaxis in lamprey. *Journal of Neurophysiology*, 78, pp.960–976.

Visscher, J.P., 1928. Reactions of the cyprid larvae of barnacles at the time of attachment. *The Biological Bulletin*, 54(4), pp.327–335.

Yamamoto, N. & López-Bendito, G., 2012. Shaping brain connections through spontaneous neural activity. *European Journal of Neuroscience*, 35(10), pp.1595–1604.

Yasuyama, K., Kitamoto, T. & Salvaterra, P.M., 1995. Localization of choline acetyltransferase-expresing neurons in the larval vissual system of Drosophila melanogaster. *Cell and Tissue Research*, 282(2), pp.193–202.

Yau, K.-W. & Hardie, R.C., 2009. Phototransduction Motifs and Variations. *Cell*, 139(2), pp.246–264.

Young, C.M. & Chia, F.S., 1982. Ontogeny of phototaxis during larval development of the sedentary polychaete, Serpula vermicularis (L.). *The Biological Bulletin*, 163, pp.457–468.

Neuronal connectome of a sensory-motor circuit for visual navigation

eLIFE elifesciences.org

RESEARCH ARTICLE

Neuronal connectome of a sensory-motor circuit for visual navigation

Nadine Randel, Albina Asadulina, Luis A Bezares-Calderón, Csaba Verasztó, Elizabeth A Williams, Markus Conzelmann, Réza Shahidi, Gáspár Jékely*

Max Planck Institute for Developmental Biology, Tübingen, Germany

Abstract Animals use spatial differences in environmental light levels for visual navigation; however, how light inputs are translated into coordinated motor outputs remains poorly understood. Here we reconstruct the neuronal connectome of a four-eye visual circuit in the larva of the annelid *Platynereis* using serial-section transmission electron microscopy. In this 71-neuron circuit, photoreceptors connect via three layers of interneurons to motorneurons, which innervate trunk muscles. By combining eye ablations with behavioral experiments, we show that the circuit compares light on either side of the body and stimulates body bending upon left-right light imbalance during visual phototaxis. We also identified an interneuron motif that enhances sensitivity to different light intensity contrasts. The *Platynereis* eye circuit has the hallmarks of a visual system, including spatial light detection and contrast modulation, illustrating how image-forming eyes may have evolved via intermediate stages contrasting only a light and a dark field during a simple visual task.

DOI: 10.7554/eLife.02730.001

Introduction

Visually guided behavior is widespread in animals (***Ullén et al., 1997***; ***Garm et al., 2007***; ***Orger et al., 2008***; ***Burgess et al., 2010***; ***Huang et al., 2013***), yet the underlying neuronal circuits and their evolutionary origins remain poorly understood. Spatial vision requires at least two photoreceptors and a neural circuitry capable of making a comparison between the photoreceptor inputs without body movement (***Land and Nilsson, 2002***; ***Nilsson, 2009***). The spatial information obtained must then translate to a coordinated motor output.

A comprehensive description of the sensory-motor visual circuitry, including all neurons and their synaptic connectivity, is required for a plausible explanation of how visual inputs drive motor output during animal behavior. This can only be achieved using electron microscopic imaging to construct connectomes, comprehensive synaptic-level connectivity maps for large blocks of neural tissue containing behaviorally relevant circuits (***Bock et al., 2011***; ***Briggman et al., 2011***; ***Jarrell et al., 2012***; ***Bumbarger et al., 2013***; ***Helmstaedter et al., 2013***). However, despite recent advances in the connectomics of visual systems (***Briggman et al., 2011***; ***Rivera-Alba et al., 2011***; ***Sprecher et al., 2011***; ***Takemura et al., 2011***, ***2013***), a complete synaptic-level connectivity-map of a visual circuit, including sensory-, inter-, and motorneurons, has not yet been described.

Here we reconstruct the neural connectome of the visual eyes in a larva of the marine annelid *Platynereis dumerilii* using serial-section transmission electron microscopy (ssTEM). *Platynereis* larvae develop four visual eyes, the 'adult eyes' (henceforth 'eyes'), that are the precursors of the adult's visual pigment-cup eyes, and are distinct from the more ventrally located 'eyespots' (***Jékely et al., 2008***). These eyes consist of only 2–7 photoreceptors, a few shading pigment cells, and a lens, representing the simplest visual eyes described to date (***Rhode, 1992***; ***Arendt et al., 2002***; ***Randel et al., 2013***). The *Platynereis* larval visual connectome consists of 71 neurons and 1106 synapses, and was reconstructed from a tissue block containing the larval head and trunk. Using behavioral experiments combined with eye ablations we demonstrate that the eyes mediate spatial vision, whereby light

***For correspondence:** gaspar.jekely@tuebingen.mpg.de

Competing interests: The authors declare that no competing interests exist.

Funding: See page 20

Received: 11 March 2014
Accepted: 25 May 2014
Published: 27 May 2014

Reviewing editor: Eve Marder, Brandeis University, United States

eLife digest Many animals show automatic responses to light, from moths, which are attracted to light sources, to cockroaches, which are repelled by them. This phenomenon, known as phototaxis, is thought to help animals navigate through their environment. It is an evolutionarily ancient behavior, as revealed by its widespread presence in the animal kingdom. One animal with a simple visual system for phototactic behavior is the marine worm *Platynereis dumerilii*.

Platynereis is a segmented worm (annelid) with four eyes on the top of its head, two on the right and two on the left. Exposure to light triggers the contraction of muscles that run along the length of the body, causing the worm to bend and thus change the direction it is swimming in. Now, using a combination of high-resolution microscopy and behavioral experiments in larvae, Randel et al. have mapped the neural circuits underlying the worm's phototactic behavior.

A 3-day-old Platynereis larva was sectioned to produce almost 1700 slices, each less than 50 nanometers thick, which were then viewed under a transmission electron microscope. By tracing individual neurons from one slice to the next, it was possible to reconstruct the entire visual system and all of its connections. This 'visual connectome' consisted of 71 neurons—21 light-sensitive cells, 42 interneurons, and 8 muscle-controlling motorneurons—organized into a circuit with 1106 connections.

Shining light onto living larvae triggered phototaxis, with some larvae consistently swimming towards the light and others away from it. Using a laser to destroy all four eyes abolished this behavior, as did the removal of both eyes on either side of the head. By contrast, removing one eye from each side had no effect. This was because these larvae were still able to simultaneously compare the amounts of light reaching the left and right sides of their body, and to use any difference in these levels as a directional cue to guide swimming.

By revealing the circuitry underlying phototaxis in a marine worm, Randel et al. have provided clues to the mechanisms that support this behavior in other species. The data could also provide insights into the processes that contributed to the evolution of more complex visual systems.

DOI: 10.7554/eLife.02730.002

intensities at the left and right eyes are compared to mediate tail bending during phototactic turns. This combination of connectomics and behavioral analysis provides a circuit-level and mechanistic explanation for the regulation of phototactic behavior by spatial vision. The *Platynereis* visual connectome also provides insights into the origin of visual eyes, and suggests that phototaxis may have been the first visual task in evolution performed by animals.

Results

Eye-circuit connectome reconstruction

To reconstruct the full chemical synaptic connectivity map of the visual eyes in the *Platynereis* larva we used ssTEM. Following high-pressure freezing and cryosubstitution, we collected 1690 thin sections (40–50 nm) from a single Epon-embedded 3-day-old larva, encompassing the entire head and part of the first trunk segment. Following contrasting, we imaged the sections at 3.7 nm/pixel resolution, in a 140 µm × 140 µm × 80 µm volume (***Figure 1A–C***; ***Video 1***).

We identified the eyes based on the presence of pigment-filled vesicles in the pigment cells, the presence of a lens formed by the apical extensions of the pigment cells, and the presence of the apical microvillar extensions (rhabdoms) of the photoreceptors (***Rhode, 1992***; ***Randel et al., 2013***; ***Figure 1D***; ***Video 2***). We then manually traced all neurons lying on synaptic pathways from photoreceptors to locomotor organs (muscles and ciliary bands). We identified 21 photoreceptor cells (PRC), 42 interneurons (IN) and 8 motorneurons (MN) (***Figure 1—figure supplement 1–4***), forming a 'minimal eye circuit' from sensors to effectors. We identified 1106 chemical synapses between these cells and their motor targets. We found further sensory neurons other than the photoreceptors providing direct or indirect input to the minimal eye circuit. These upstream circuits will be described in detail elsewhere. In this paper we focus on the analysis of the 71 neurons constituting the minimal eye circuit.

First, we describe the anatomy and synaptic contacts of the eyes and the main neuron types identified as part of the eye circuit. To provide an easily accessible representation of the data we generated

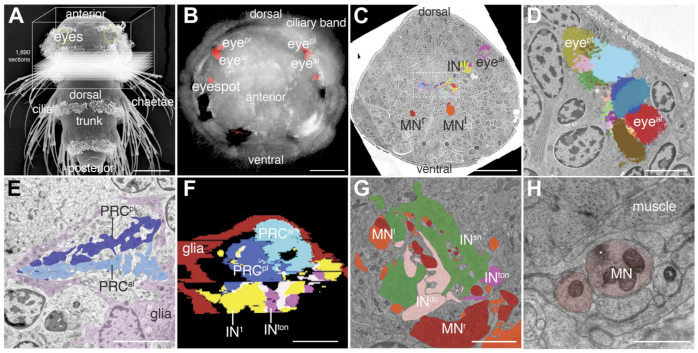

Figure 1. Serial-section electron microscopy imaging of the visual eye circuit in a *Platynereis* larva. (**A**) Scanning electron micrograph of a 72 hr-post-fertilization larva, dorsal view. The boxed volume was sectioned and imaged. (**B**) Anterior view of a 72 hr-post-fertilization larva visualized with differential interference contrast (DIC) optics (grey) showing the position of the eyes visualized by the reflection of the pigments (red). (**C**) A representative electron micrograph from the series with traced neurons. The boxed area contains the primary optic neuropil. (**D**) Reconstruction of the pigment cup of the left anterior and posterior eyes. Pigment granules from the different pigment cells and photoreceptors are colored differently. (**E**) TEM image of the left primary optic neuropil surrounded by glia (pink), with the photoreceptor projections from the anterior and posterior eye colored differently. (**F**) A virtual cross-section of the primary optic neuropil based on ssTEM shows the anterior-posterior layering of glia, photoreceptor, primary interneuron (IN^{1}) and trans-optic-neuropil interneuron (IN^{ton}) processes, anterior is up. (**G**) TEM image of the secondary optic neuropil, with segmented IN^{ton}, IN^{sn} , IN^{dc} and ipsi- and contralateral motorneuron projections. (**H**) TEM image of a neuromuscular synapse from a motorneuron to the ventral longitudinal muscle. Asterisk marks a cluster of synaptic vesicles. Eye^{al}, anterior-left eye; eye^{ar}, anterior-right eye; eye^{pl}, posterior-left eye; eye^{pr}, posterior-right eye; PRC, photoreceptor; IN, interneuron; MN, motorneuron. Scale bars, 50 μm (**A**), 30 μm (**B** and **C**), 5 μm (**D**, **E**, **G**), 1 μm (**F**), 0.5 μm (**H**).

DOI: 10.7554/eLife.02730.003

The following figure supplements are available for figure 1:

Figure supplement 1. Morphology of photoreceptor cells reconstructed from serial TEM sections.

DOI: 10.7554/eLife.02730.004

Figure supplement 2. Morphology of IN1, IN^{ton}, IN^{sn}, and IN^{dc} cells reconstructed from serial TEM sections.

DOI: 10.7554/eLife.02730.005

Figure supplement 3. Morphology of IN^{int} and IN^{vc} cells reconstructed from serial TEM sections.

DOI: 10.7554/eLife.02730.006

Figure supplement 4. Morphology of motorneurons reconstructed from serial TEM sections.

DOI: 10.7554/eLife.02730.007

Figure supplement 5. Axon diameter and synapse size in the *Platynereis* larval connectome.

DOI: 10.7554/eLife.02730.008

Figure supplement 6. Synapses of photoreceptors and IN^{1} cells.

DOI: 10.7554/eLife.02730.009

Figure supplement 7. Synapses of IN^{1} cells.

DOI: 10.7554/eLife.02730.010

Figure supplement 8. Synapses of IN^{ton} cells and IN^{sn} cells.

DOI: 10.7554/eLife.02730.011

Figure supplement 9. Synapses of motorneurons.

DOI: 10.7554/eLife.02730.012

a comprehensive 3D anatomical atlas of all neurons, synapses, muscles and ciliated cells using Blender (http://www.blender.org/) (***Randel et al., 2014***; ***Video 3***). Neuron morphologies were reconstructed based on the raw traces (***Figure 1—figure supplement 1–4***) and represented in the atlas with a simplified

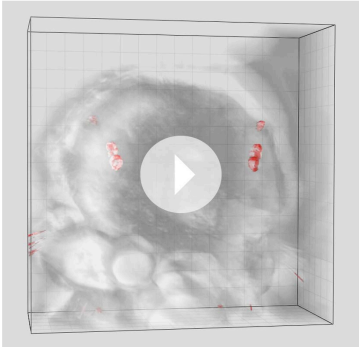

Video 1. Head and first trunk segment of a 3-day-old Platynereis larva. DIC and reflection imaging of the head and first trunk segment of a 73 hr-post-fertilization *Platynereis* larva, corresponding to the volume analyzed by ssTEM. The four eyes and the eyespots are visualized based on the reflection of the pigment (red). The frame contains a volume of 151 × 151 × 61 µm. The larva is squeezed dorso-ventrally with the coverslip. Grid spacing is 10 µm.
DOI: 10.7554/eLife.02730.013

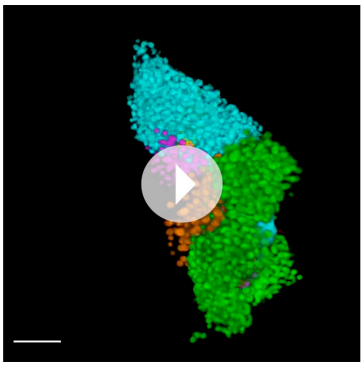

Video 2. Volume reconstruction of the two left eyecups. The pigment vesicles of the pigment cells and the rhabdoms of the photoreceptors were reconstructed by ssTEM. The pigment of the photoreceptors is on the convex surface of the pigment cup, shown in different colors. The photoreceptor rhabdoms are inside the pigment cup. Scale bar, 2 µm.
DOI: 10.7554/eLife.02730.014

morphology (***Figure 2***). Users can display groups of neurons, query for pre- and post-synaptic partners of neurons, and display synapses.

Morphology of neurons and synapses

The neurons of the eye circuit only contain axo-axonal synapses. With the exception of the photoreceptors, all neurons lack dendrites. Axons have a median diameter of 160 nm (***Figure 1—figure supplement 5***), allowing reliable tracing of most processes. The morphology of all neurons is very simple, with one primary branch giving rise to several very short secondary branches in the synaptic regions of the optic neuropils (***Figure 1—figure supplement 1–4***). These short branches often contain pre- or postsynaptic sites (***Video 4***). Only two neurons have a branched main axon (MN^{r3}, MN^{l1}, see 'Materials and methods' for nomenclature).

Synapses were identified as electron dense accumulations of several vesicles close to the presynaptic membrane (no T-bars as in *Drosophila*). Prominent postsynaptic structures were not detected, in agreement with previous ultrastructural studies in annelids (***Wells et al., 1972***). 69% of the synapses could be identified in at least two and up to five consecutive sections (***Figure 1—figure supplement 5***). To further characterize the ultrastructure of synapses we created high-resolution images (0.2 nm/pixel) of 60 randomly chosen synapses belonging to the different neuron types (***Figure 1—figure supplement 6–9***). In all cases we observed a cluster of vesicles adjacent to the plasmamembrane, but no pre- or post-synaptic specializations.

We could not identify gap junctions in the eye circuit. Gap junctions exist in annelids, and we could find several innexin genes, encoding gap junction proteins of invertebrates (***Kandarian et al., 2012***), in the *Platynereis* transcriptome (data not shown). However, we did not see structures similar to ultrastructurally characterized annelid gap junctions (***Muller and Carbonetto, 1979***; ***Shen et al., 2002***), even in a stack of high-resolution (1.13 nm/pixel) images of the primary optic neuropil (***Randel et al., 2014***). If gap junctions are present in the larval stage they may be too small to be distinguished from obliquely cut membranes even at high resolution.

Synaptic contacts in the eye circuit

The photoreceptors of the four eyes (3–7 per eye) project to a primary optic neuropil area at the center of the larval brain (***Figure 1C,E***, ***Figure 2B***), consistent with results obtained by the genetic

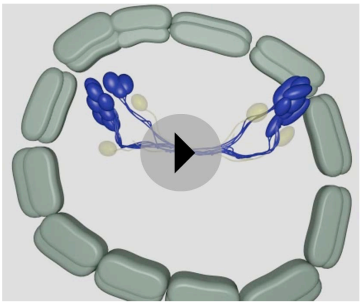

Video 3. Cellular complement of the Platynereis larval visual circuit. 3D reconstruction of the cellular complement of the *Platynereis* larval visual circuit. The different cell types appear in the following order: photoreceptors, IN^{1}, IN^{int}, IN^{ton}, IN^{sn}, IN^{dc}, IN^{vc}, motorneurons, synapses, glia, muscles.
DOI: 10.7554/eLife.02730.015

labeling of the photoreceptors (***Backfisch et al., 2013***). All photoreceptors from the same eye project along the same axon bundle, forming four separate eye nerves (***Figure 2A,B***).

The eye nerves from the anterior and posterior eyes from the same side innervate distinct anterior and posterior areas in the primary optic neuropil (***Figure 1E,F***). Some photoreceptor axons cross the midline and project to the contralateral primary optic neuropil. The primary optic neuropil is surrounded by three giant glia cells. These cells form lamellae that tightly surround the primary and secondary optic neuropils from the dorsal but not the ventral side (***Figure 1F***, ***Figure 2C***; ***Video 4***). The main targets of the photoreceptors of the four eyes are four primary interneurons (IN^{1}), with photoreceptors from one eye forming several (up to 30) synaptic contacts to one primary interneuron with a contralateral cell body (e.g., PRC^{al} to IN^{1pr}; ***Video 4***). The four eyes and the four primary interneurons show a crosswise arrangement (***Figure 2D***). Primary interneurons have mutual synaptic contacts (see below) and also form synapses on two other interneuron types (***Figure 2E,H***; ***Video 3***; ***Randel et al., 2014***). One type of interneuron is intrinsic to the optic neuropil (IN^{int}) with both ipsilateral and contralateral cell bodies and axons crossing the midline. Another target of the primary interneurons are interneurons that project out of the primary optic neuropil into a secondary optic neuropil area (***Figure 1G***). The major targets of these trans-optic-neuropil interneurons (IN^{ton}) are a group of contralateral interneurons, which we named Schnörkel interneurons (IN^{sn}). Schnörkel interneurons project a curved axon to the ipsilateral secondary optic neuropil (***Figure 2H***, ***Figure 2—figure supplement 1***). The Schnörkel interneurons are presynaptic to a bilateral group of ventral motorneurons (MN; ***Figure 2—figure supplement 1***). Two groups of dorsal and ventral interneurons (IN^{dc}, IN^{vc}) also form synapses on the Schnörkel interneurons and motorneurons (***Figure 2H***; ***Video 3***).

We identified two distinct motorneuron types. The first type sends a contralateral projection to both the ciliary band and the dorsal longitudinal muscle, and branches to send a descending projection to the trunk (***Figure 2G***, ***Figure 2—figure supplement 1***). The second type only projects posteriorly along the circumesophageal nerve after crossing the midline. Both motorneuron types form neuromuscular and neurociliary synapses (***Figure 1H***, ***Figure 2—figure supplement 1***; ***Video 3***, ***Video 5***). Due to the lack of further trunk sections we did not trace descending motorneuron axons along their entire length, therefore we cannot exclude the possibility that motorneurons have other synaptic partners in the trunk. Nevertheless, these data represent, to our knowledge, the most complete connectomic reconstruction of a visual circuit to date, from photoreceptors to effector muscles and ciliated cells.

Synapse types in the eye circuitry

To gain insights into the nature of synapses in the eye circuit we measured vesicle diameter in the high-resolution images of synapses (***Figure 3—figure supplement 1***). The mean diameter of synaptic vesicles in interneurons was significantly larger than in photoreceptors and motorneurons. Photoreceptor synaptic vesicles were not significantly different from neuromuscular synaptic vesicles in motorneurons. However, neurociliary synaptic vesicles in motorneurons were significantly smaller than photoreceptor or neuromuscular synaptic vesicles. These observations indicate the use of different neurotransmitters in the eye circuitry and also suggest that the dual-function muscle- and cilio-motor neurons (MN^{r2}, MN^{l1}) may have mixed neurotransmitter content.

To identify possible neurotransmitters in the eye circuit we performed whole-mount RNA in situ hybridizations with marker genes for various neurotransmitters (***Randel et al., 2014***) and compared the expression domains to cell body positions in the TEM series (***Figure 3***). In *Platynereis* larvae the colocalization of distinct gene expression patterns can be determined with near cellular resolution

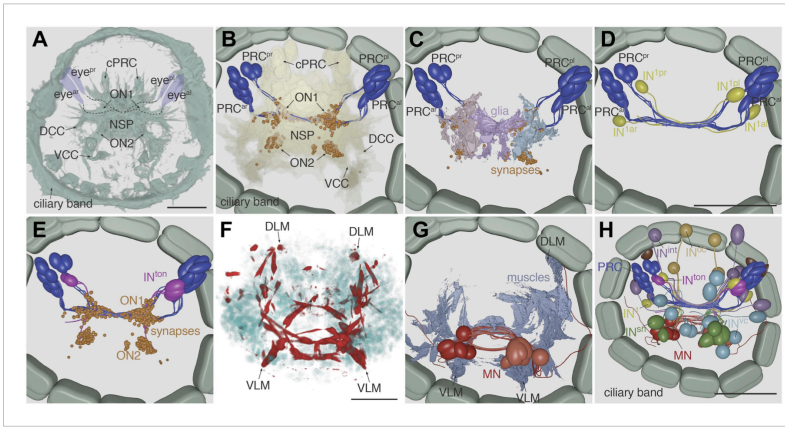

Figure 2. Cell complement of the visual circuit. (**A**) Confocal microscopic image of a 3-day-old larva stained with an anti-acetylated tubulin antibody to label neurites and cilia. Anatomical landmarks are labeled. (**B**) Blender visualization of all photoreceptor cells and all synapses of the minimal eye circuit shown in relation to the outline of neuropil, reconstructed by ssTEM. The position of synapses in the visual circuit reveals the primary and secondary optic neuropils. The schematized ciliary band cells are also shown. (**C**) ssTEM reconstruction of photoreceptors, glia cells and synapses. (**D**) ssTEM reconstruction of photoreceptors and primary interneurons (IN^{1}). (**E**) ssTEM reconstrucion showing the trans-optic-neuropil interneurons (IN^{ton}) connecting the two optic neuropils. (**F**) Confocal microscopic image of a 3-day-old larva stained with phalloidin to label the musculature (red) and with DAPI to label nuclei (cyan). (**G**) ssTEM reconstruction of muscles and motorneurons (MN). (**H**) ssTEM reconstruction of the complete cell complement of the minimal visual circuit. Neurons are colored by type. Pigment cups are shown in brown. All images show anterior views. PRC, photoreceptor; IN, interneuron; MN, motorneuron; eye^{al}, anterior-left eye; eye^{ar}, anterior-right eye; eye^{pl}, posterior-left eye; eye^{pr}, posterior-right eye; ON, optic neuropil; cPRC, ciliary photoreceptor; DCC, dorsal branch of the circumesophageal connectives; VCC, ventral branch of the circumesophageal connectives; NSP, neurosecretory plexus; DLM, dorsal longitudinal muscle; VLM, ventral longitudinal muscle. The coloring of cell types is consistent throughout the paper (PRC, blue; IN^{1}, yellow; IN^{int}, lilac; IN^{ton} , magenta; IN^{dc}, light brown; IN^{vc}, cian; IN^{sn}, green; MN, red). Scale bars, 30 μm. The Blender atlas with the volume rendering of all cells and synapses is available in ***Randel et al. (2014)***.

DOI: 10.7554/eLife.02730.016

The following figure supplements are available for figure 2:

Figure supplement 1. Muscles and ciliary bands in 3-day old larvae.

DOI: 10.7554/eLife.02730.017

using whole-mount RNA in situ hybridizations and image registration, allowing the molecular profiling of cell types (***Tomer et al., 2010***; ***Asadulina et al., 2012***). Although expression patterns for several of these genes have already been reported in *Platynereis* (***Denes et al., 2007***; ***Jékely et al., 2008***; ***Tomer et al., 2010***), we acquired new whole-body expression data to analyze patterns in the 3-day-old brain in more detail. We found that *vesicular glutamate transporter* (*VgluT*), a marker of glutamatergic neurons, colocalized with *r-opsin1*, a marker of eye photoreceptors (***Arendt et al., 2002***; ***Randel et al., 2013***; ***Figure 3—figure supplement 2***, ***Figure 3—figure supplement 3***), indicating that the photoreceptors are glutamatergic. In contrast, *histidine decarboxylase* (*hdc*), an enzyme catalyzing the synthesis of histamine, the transmitter in arthropod rhabdomeric photoreceptors (***Stuart, 1999***), does not localize to the eyes, as shown by image registration and double RNA in situ hybridization (***Figure 3—figure supplement 3***).

In the cell body regions of the interneurons we found expression of several monoaminergic markers in single cells or small cell clusters. These include *tryptophan hydroxylase* (*TrpH*), *tyrosine hydoxylase* (*TyrH*), *hdc*, *dopa-beta-hydoxylase* (*dbh*), markers for serotonergic, dopaminergic, histaminergic, and noradrenergic neurons, respectively (***Figure 3B***, ***Figure 3—figure supplement 2***, ***Figure 3—figure supplement 3***). This indicates that the interneurons of the eye circuit use several distinct monoamine neurotransmitters.

Choline acetyltransferase (*ChAT*) and *vesicular acetylcholine transporter* (*VAChT*), two markers of cholinergic neurons, are localized in the cell body region of the ventral motorneurons (***Figure 3C***,

Video 4. Volume rendering of the left primary optic neuropil. The reconstructed volume shows parts of two glia cells (pink and light blue), one IN^1 axon (yellow) and the photoreceptor axons (different hues of blue) forming synapses on the IN^1 axon. The position of the individual synapses to the IN^1 axon are indicated in different colors for the different photoreceptors.
DOI: 10.7554/eLife.02730.018

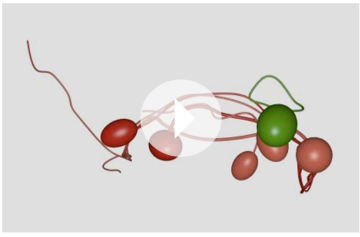

Video 5. Volume reconstruction of a Schnörkel interneuron and motorneurons. 3D reconstruction of one Schnörkel interneuron and its postsynaptic motorneuron targets. One Schnörkel interneuron is shown with its five postsynaptic motorneurons. The synapses are indicated. The Schnörkel interneuron connects to both ipsilateral and contralateral motorneurons either at a cell body proximal or a cell body distal position along the motorneuron axon.
DOI: 10.7554/eLife.02730.019

Figure 3—figure supplement 2). This is consistent with earlier observations showing that the longitudinal trunk muscles, targets of the ventral motorneurons, are influenced by acetylcholine (***Denes et al., 2007***). A marker for GABAergic cells, *glutamate decarboxlase* (*gad*), partly colocalizes with the ventral cholinergic domain, in the area of the motorneuron cell bodies (***Figure 3C***, ***Figure 3—figure supplement 2***, ***Figure 3—figure supplement 3***). This suggests that some motorneurons may have mixed GABAergic and cholinergic identity. The difference in mean vesicle size at neuromuscular and neurociliary synapses in motorneurons (***Figure 3—figure supplement 1***) also supports a mixed neurotransmitter identity. Further cellular resolution mapping will be needed to confirm this and to establish the neurotransmitter identities of individual interneurons and motorneurons.

Network analysis of the eye connectome

For a detailed analysis of synaptic contacts in the eye circuit, we represented the connectome as a directed graph and as an all-against-all synaptic connectivity matrix (***Figure 4A***, ***Figure 4—figure supplement 1***, ***Figure 4—source data 1***). In the graph, the nodes correspond to neurons and the directed edges to synaptic contacts, weighted by synapse number. We displayed the full cell complement (79 nodes; ***Figure 4A***) and a trimmed graph (61 nodes) where all cells with <3 pre- and post-synaptic sites were omitted and only edges of three or more synapses were shown (***Figure 4—figure supplement 2***). Manual or force-field-based clustering was used for graph layout. We also constructed a merged graph where the same neuron types from the left and right body sides were grouped. In this graph the weight of connections is represented as the maximum number of synapses between any individual cell pair of the distinct groups (***Figure 4B***, ***Figure 4—source data 2***).

To analyze information flow we calculated the maximum distance of all nodes to any other node within the directed graph (eccentricity; ***Figure 4A***). The eye circuit is a feed-forward circuit where information flows from the eyes to the muscles and ciliary bands. We also calculated centrality measures to identify strongly connected nodes in the network (***Figure 4—figure supplement 2***). With three different centrality measures (eigenvector centrality, weighted-degree centrality and authority) the four primary interneurons (IN^1) ranked among the top five nodes (***Randel et al., 2014***). These four cells receive several synapses from the photoreceptors, with the highest number of each IN^1 received from the crosswise eyes (***Figure 4B***, ***Figure 4—figure supplement 2***). The four IN^1 cells also have strong mutual connections (see below).

A search for highly interconnected nodes or communities (***Blondel et al., 2008***) subdivided the eye network into four modules (***Figure 4—figure supplement 3***). The four IN^1 cells belong to two different

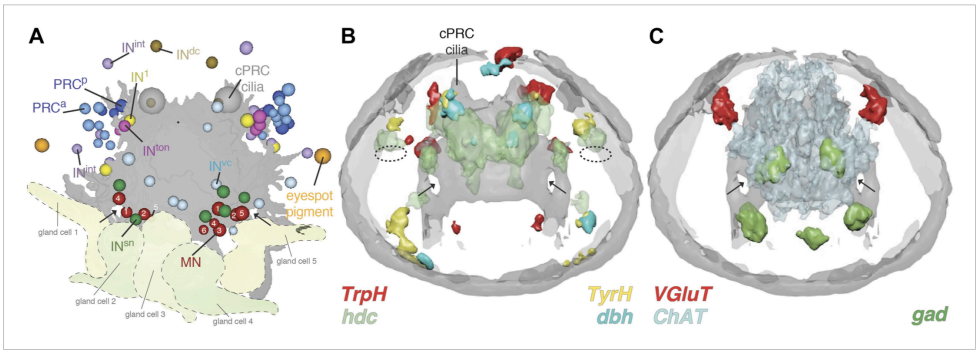

Figure 3. Neurotransmitters of the eye circuit. (**A**) Cell body positions of eye circuit neurons relative to the larval axonal scaffold and five large gland cells. Motorneurons are numbered according to the cell identifiers. (**B** and **C**) Surface representation of the average expression domains of neurotransmitter marker genes relative to the larval axonal scaffold. The following genes are shown: (**B**) histaminergic marker *histidine decarboxylase* (*hdc*; green), serotonergic marker *tryptophan hydroxylase* (*TrpH*; red), dopaminergic marker *tyrosine hydroxylase* (*TyrH*; yellow), adrenergic marker *dopamine beta hydroxylase* (*dbh*; cyan), (**C**) glutamatergic marker *vesicular glutamate transporter* (*VGluT*; red), cholinergic marker *choline acetyltransferase* (*ChAT*; grey), GABAergic marker *glutamate decarboxylase* (*gad*; green). The axonal scaffold, based on average acetylated-tubulin signal, is shown in grey. PRC, photoreceptor; cPRC, ciliary photoreceptor; IN, interneuron; MN, motorneuron. In (**B**) dashed ovals mark the position of the eyespots. Black arrows show the ring formed by the circumesophageal connectives.

DOI: 10.7554/eLife.02730.020

The following figure supplements are available for figure 3:

Figure supplement 1. Synaptic vesicle diameter for different synapse types.

DOI: 10.7554/eLife.02730.021

Figure supplement 2. Expression of neurotransmitter markers in the head of *Platynereis* larva.

DOI: 10.7554/eLife.02730.022

Figure supplement 3. Neurotransmitter marker gene expression profiling.

DOI: 10.7554/eLife.02730.023

modules in the eye circuit (***Figure 4—figure supplement 3***), which together contain all neurons with projections intrinsic to the primary optic neuropil. Both modules consist of a crosswise pair of eyes and the associated IN^{1} cells and trans-optic-neuropil interneurons (IN^{ton}). The anatomy of the circuitry in the primary optic neuropil thus displays point symmetry rather than bilateral symmetry (***Figure 4—figure supplement 3***).

The other two modules, the motor modules, contain all neurons intrinsic to the secondary optic neuropil, including Schnörkel interneurons and motorneurons and associated effector organs. A bilateral pair of IN^{ton} cells links the modules of the primary and secondary optic neuropils, reflecting the anatomy where IN^{ton} cells receive synapses in the primary and project to the secondary optic neuropil (***Figure 4—figure supplement 3***). One of the motor modules provides innervation to the prototroch and metatroch ciliary band cells. The other module contains motorneurons that connect to three out of four bundles of longitudinal muscles (we could not find neuromuscular synapses on the left dorsal longitudinal muscle) (***Figure 4A,B***, ***Figure 4—figure supplement 2***).

The connectome reveals that all four eyes can provide motor input to both body sides. The neuronal pathways from the eyes cross the midline multiple times throughout the circuit. The strongest synaptic connections are formed between photoreceptor—IN^{1}—IN^{ton}—Schnörkel interneuron, always to the contralateral side in a feed-forward circuit (***Figure 4B***). However, most Schnörkel interneurons form several synapses on both ipsilateral and contralateral motorneurons in the secondary optic neuropil, representing a bilateral divergence of the connections. Motorneuron axons receive cell-body-proximal synapses from the ipsilateral Schnörkel interneurons, cross the midline, and receive cell-body-distal synapses on the other side of the body from the contralateral Schnörkel interneurons (***Figure 4—figure supplement 6G,H***; ***Video 5***).

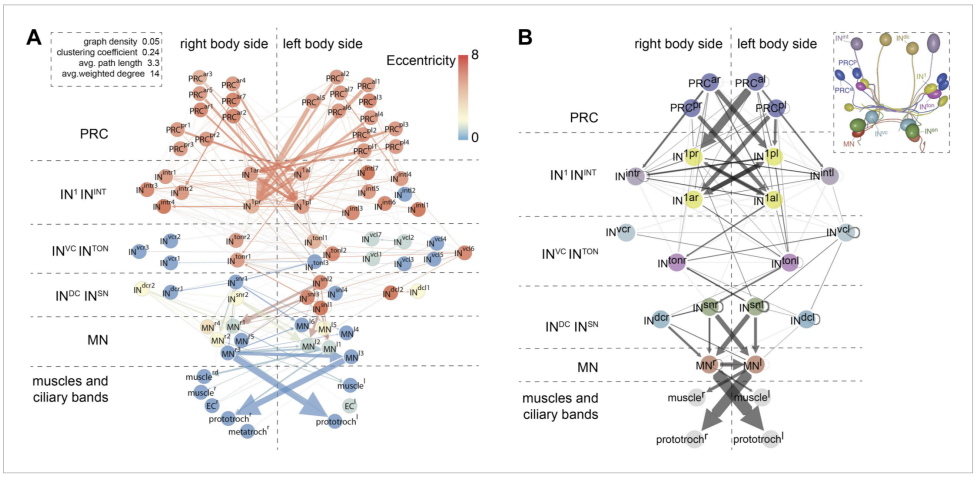

Figure 4. Network analysis of the visual eye circuitry. (**A**) Full connectomic graph of the visual eye circuit including 71 neurons and 8 effectors (muscles, ciliary band cells and epithelial cells). The edges are directed from presynaptic cell pointing to postsynaptic cells. Edges are weighted by the number of synapses. Inset shows selected network parameters. (**B**) Merged graph representation of the visual circuit. Nodes correspond to neuron classes, edges are weighted by the maximum number of synapses between two neuron types of each class. Nodes are colored following the color scheme used to label cell types. Inset shows the anatomical position of the cell types. PRC^{al}, anterior-left photoreceptors; PRC^{ar}, anterior-right photoreceptors; PRC^{pl}, posterior-left photoreceptors; PRC^{pr}, posterior-right photoreceptors; IN, interneuron; MN, motorneuron. Matrix files of the complete and the merged networks are available in ***Figure 4—source datas 1 and 2***.

DOI: 10.7554/eLife.02730.024

The following source data and figure supplements are available for figure 4:

Source data 1.

DOI: 10.7554/eLife.02730.025

Source data 2.

DOI: 10.7554/eLife.02730.026

Figure supplement 1. Synaptic connectivity matrix of the *Platynereis* larval visual circuit.

DOI: 10.7554/eLife.02730.027

Figure supplement 2. Connectivity graphs of the *Platynereis* larval visual circuit.

DOI: 10.7554/eLife.02730.028

Figure supplement 3. Modules in the eye connectivity graph.

DOI: 10.7554/eLife.02730.029

Figure supplement 4. Connectivity matrix of the left and right body sides.

DOI: 10.7554/eLife.02730.030

Figure supplement 5. Stereotypy of synapse distribution on IN^{1} cells.

DOI: 10.7554/eLife.02730.031

Figure supplement 6. Stereotypy of synapse distribution on IN^{ton}, IN^{sn} and MN cells.

DOI: 10.7554/eLife.02730.032

Stereotypy of synaptic connections

In order to estimate how stereotypic synaptic connectivity is within the circuit we compared the connectivity matrices of neurons with cell bodies on the left or right side of the body. We used the merged graph (***Figure 4B***) since not all neurons had a contralateral pair (e.g., we identified three IN^{ton} cells on the left and two on the right body side). We found a strong correlation between the left and right connectivity matrices (Spearman r = 0.67, p<0.0001; ***Figure 4—figure supplement 4***).

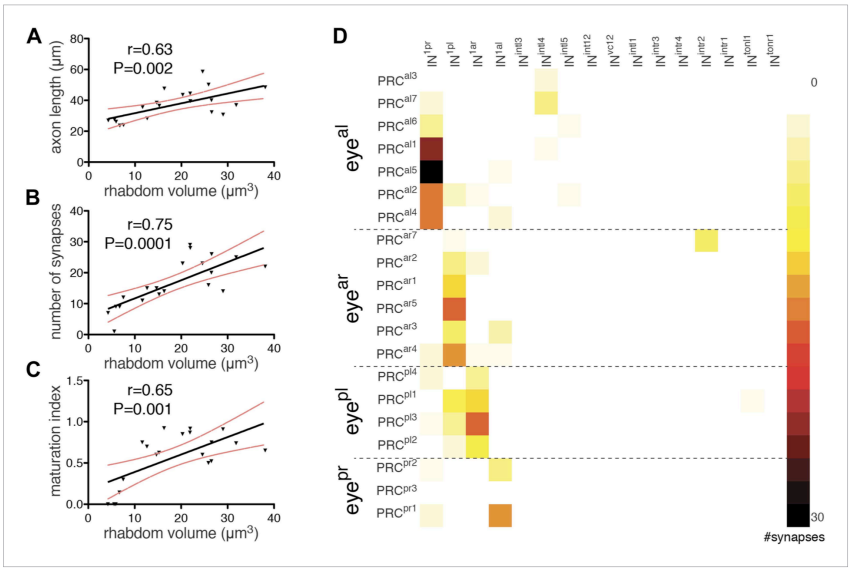

Figure 5. Maturation of photoreceptor connections. (**A**) Relationship of rhabdom volume to photoreceptor axon length. (**B**) Relationship of rhabdom volume to photoreceptor synapse number. (**C**) Relationship of photoreceptor connectivity-maturation index to rhabdom volume. In **A**–**C** the black line shows linear regression with 95% confidence interval (red dashed lines). Pearson r and p-value are shown. (**D**) Connectivity matrix of the photoreceptors. The matrix is ordered from top to bottom by eye and then for each eye by photoreceptor rhabdom size increasing from top to bottom. Eye^{al}, anterior-left eye; eye^{ar}, anterior-right eye; eye^{pl}, posterior-left eye; eye^{pr}, posterior-right eye.

DOI: 10.7554/eLife.02730.033

Video 6. Mixed positive and negative phototaxis in 3-day-old *Platynereis* larvae. Larvae were stimulated with alternating directional white light from the left or the right side of the phototaxis cuvette (shown by white bars on the side). Larvae display mixed phototaxis, some negatively phototactic larvae are tracked. Scale bar, 2 mm. Time increment: 0.07 s.

DOI: 10.7554/eLife.02730.034

We also analyzed the stereotypy of the spatial arrangement of pre-and postsynaptic sites among neurons of the same type. The four IN^{1} cells always receive photoreceptor input in a cluster at the most distal segment of their axon (***Figure 4—figure supplement 5***). Synapses onto the IN^{1} cells from the contralateral photoreceptors are intermingled with presynaptic sites of IN^{1} cells to IN^{ton} cells (***Figure 4—figure supplement 6***) and are not spatially segregated within the cluster. In contrast, IN^{1} cells receive axo-axonal synaptic input from the crosswise IN^{1} cell in a cluster positioned more proximal to the cell body (***Figure 4—figure supplement 5***). The spatial arrangement of synapses is also similar between the left and right sides for other neuron types (***Figure 4—figure supplement 6***). These observations show that both the number and the spatial arrangement of synapses are stereotypic between the left and right body sides. The reconstruction of further individuals will be needed to assess individual-to-individual variation.

Video 7. A single phototactic turn in 4-day-old larvae. The larvae were exposed to a 180-degree change in the direction of the white stimulus light, eliciting a phototactic turn. The stimulus direction is indicated by the white bars at the side of the video. During the turn the larvae are bending due to the contraction of the longitudinal muscles on one body side. Time increment: 0.066 s.
DOI: 10.7554/eLife.02730.035

Maturation of photoreceptor connectivity

During development of the *Platynereis* larva, photoreceptors are continuously added to the eyes at the periphery of the pigment cup (***Rhode, 1992***). Individual photoreceptors in an eye are thus at different stages of differentiation within the same individual. We noted that in our reconstructed specimen the photoreceptor rhabdoms have different sizes, and that rhabdom volumes positively correlate with axon length and synapse number (***Figure 5A,B***). Using rhabdom volume as a proxy to photoreceptor differentiation we then analyzed how photoreceptor connections change during neuron maturation (***Figure 5D***).

Photoreceptors with short axons connect weakly if at all to the primary interneurons (IN^1), while photoreceptors with longer axons form more synapses on IN^1 cells. Photoreceptors with the shortest axons have connections to other interneurons (e.g., IN^{int4}, IN^{intr2}) that are not observed in photoreceptors with longer axons (***Figure 5D***). We defined a photoreceptor connectivity-maturation index (number of crosswise IN^1 connections per all connections) and found that it correlates with rhabdom volume (***Figure 5C***). These data represent a snapshot during development in one individual, but suggest that during photoreceptor development connections to the IN^1 cells get stronger and initial contacts to other interneurons are eliminated.

The IN^{ton} cells also show variation in axon length and connectivity, possibly also reflecting developmental progression. The small number of these interneurons precluded similar analyses.

The eyes mediate visual phototaxis

The innervation of the longitudinal trunk muscles and ciliary bands by the eye circuit motorneurons suggested that the eyes could regulate tail bending and ciliary beating during larval swimming. To understand the function of the eye circuit we next analyzed larval photobehavior in detail, in conjunction with eye ablation experiments.

We first analyzed swimming trajectories of freely behaving 3- and 4-day-old larvae exposed to light stimuli of alternating directionality. 3- and 4-day-old larvae swim using their cilia while rotating around their anterior–posterior axis. When we used alternating illumination from the two opposite sides of an assay cuvette we observed directional swimming (phototaxis) of the larvae. Larvae showed mixed behavior, with some swimming towards and others away from the light source (***Video 6***). Such sign-switch in directional swimming responses is common for marine larvae and can be influenced by various environmental stimuli (***Thorson, 1964***; ***Young and Chia, 1982***; ***Marsden, 1990***). During reorientations we could observe prominent body bending in 4-day-old larvae and weaker bending in 3-day-old larvae, suggesting that larvae turn by contracting longitudinal muscles while swimming with cilia (***Video 7*** and data not shown). In agreement with the cholinergic identity of the motorneurons, treatment with mecamylamine, an acetylcholine receptor antagonist, blocked negative phototaxis. Mecamylamine treatment increased swimming speed, probably via influencing cilia (***Jékely et al., 2008***). The effects could be reversed by washout (***Figure 6—figure supplement 1***; ***Randel et al., 2014***).

Next we illuminated the cuvette constantly from both sides but with different left-right light intensities and measured the efficiency of phototaxis for a population of larvae using a phototaxis index. We found that phototactic efficiency increased with increasing contrast between the light intensity at each side of the cuvette, but was independent of total light intensity (***Figure 6—figure supplement 2***).

To test the contribution of the eyes and the two eyespots (independent ventral structures that develop in 1-day-old larvae, ***Figure 1B***) to directional swimming, we laser-ablated the eyes or eyespots and subsequently exposed the larvae to directional illumination. Ablation of the two eyespots required for non-visual phototaxis in 1-day-old larvae (***Jékely et al., 2008***) did not abolish phototaxis responses

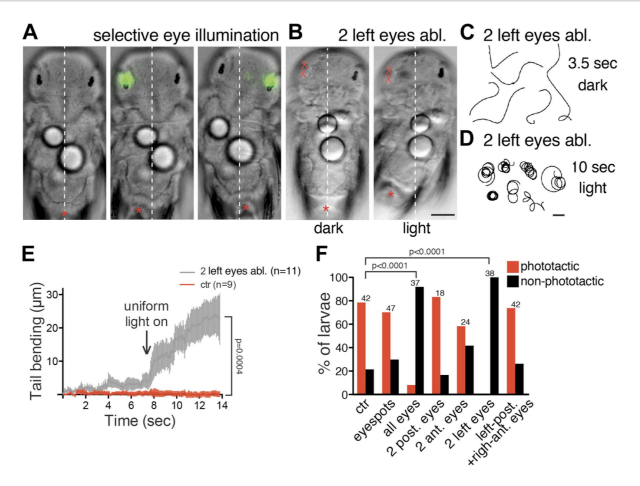

Figure 6. Eyes mediate body bending during visual phototaxis. (**A**) Selective eye illumination triggers body bending in an immobilized larva. (**B**) A larva with both left eyes ablated displays body bending upon uniform illumination with white light (light) but not with a red filter (dark). An asterisk marks the tip of the tail. (**C** and **D**) Trajectories of larvae with both left eyes ablated in the dark (red filter) (**C**) and upon uniform illumination with white light (**D**). (**E**) Tail bending upon uniform white light illumination of non-ablated control larvae and larvae lacking the two left eyes. Data are shown as mean ± SEM, n >9 for both condition. p-value of a *t* test calculated for the last time point is indicated. (**F**) Percentage of phototactic (red) and non-phototactic (black) larvae among non-ablated control and various eye-ablated larvae. p-values of a chi-square test are indicated relative to non-ablated controls. Only the 'all eyes' and 'two left eyes' ablated conditions are significantly different from non-ablated control. Number of larvae tested is shown above the columns for each condition. Scale bars, 40 µm (**A** and **B**), 1 mm (**C** and **D**).

DOI: 10.7554/eLife.02730.036

The following figure supplements are available for figure 6:

Figure supplement 1. Inhibition of phototaxis by a cholinergic antagonist.

DOI: 10.7554/eLife.02730.037

Figure supplement 2. Efficiency of phototaxis depends on contrast, not absolute light levels.

DOI: 10.7554/eLife.02730.038

in 3-day-old larvae. In contrast, ablation of all four eyes led to the loss of directional swimming (***Figure 6F***), demonstrating that only the eyes mediate this behavior.

To directly investigate if the eyes are able to mediate body bending we performed selective eye illumination experiments on larvae held between a slide and a coverslip. Unilateral illumination of the eyes triggered reproducible bending of the body in 3-day-old larvae (***Figure 6A***; ***Video 8***). When we used varying stimulus-light intensities for selective eye illumination we obtained graded bending responses with saturation kinetics (***Figure 7D***).

Unilateral laser ablation of both eyes (***Video 9***) followed by uniform illumination also triggered strong and persistent body bending (***Figure 6B,E***; ***Video 10***). Interestingly, in both experiments, the larvae either bent on or opposite to the illuminated side, with some larvae switching the response during repeated stimulation (***Video 8*** and data not shown). These results indicate that it is either the contra- or the ipsilateral motor pathway that dominates. Given that the Schnörkel interneurons synapse on both contra- and ipsilateral motorneurons (***Figure 4—figure supplement 6***), phototactic sign switching may take place at the level of the motorneurons.

To dissect the interplay of the four eyes during visual phototaxis, we ablated them in different combinations and tested phototactic ability. Larvae with unilateral ablation of both eyes were not

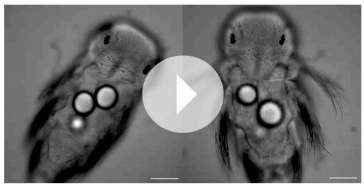

Video 8. Selective illumination of eyes triggers body bending. Illumination of the eyes on one body side in the area shown by the green signal triggers body bending on the opposite body side, corresponding to negative phototaxis (left), or the same body side, corresponding to positive phototaxis (right). Scale bar, 50 μm. Time increment: 0.43 s.
DOI: 10.7554/eLife.02730.039

phototactic and swam persistently in circles when illuminated (***Figure 6C,D,F***). The two anterior and two posterior eyes connect to distinct, though partly overlapping, circuits. To test if input to both the anterior and posterior eyes is necessary for directional swimming, we ablated either the anterior or the posterior eye pair. We also performed crosswise eye ablations. All of these ablated larvae showed phototactic responses similar to non-ablated controls (***Figure 6F***), hence the presence of at least one eye on both body sides is necessary and sufficient for directional turns.

To investigate if both dorsal and ventral longitudinal muscles are involved in body bending, we performed calcium-imaging experiments using ubiquitously expressed GCaMP6 (***Chen et al., 2013***). In immobilized larvae we repeatedly stimulated the eyes with 488 nm light on one body side. In agreement with the circuit diagram, upon selective eye stimulation we could observe corresponding calcium signals in both the ventral and dorsal longitudinal muscles on the opposing body side (***Videos 11 and 12***).

Overall, these experiments demonstrate that the eyes mediate visual turns by comparing simultaneous light inputs at each side of the body. This, together with the shading provided by the pigment cups (***Video 2***), allows the detection of the spatial distribution of light, without body movement. The visual contrast then leads to the graded contraction of the longitudinal muscles during turns. The modulation of ciliary beating, not investigated here, may also contribute to phototactic turns, as is known for younger larvae (***Jékely et al., 2008***). This sensorimotor structure is similar to visual phototaxis described in the lamprey (***Ullén et al., 1997***), but is very different from the non-visual phototactic responses in *Drosophila* larvae (***Kane et al., 2013***). Visual phototaxis is also fundamentally different from the helical phototaxis mediated by the eyespots during early *Platynereis* larval stages (1–2 days) (***Jékely et al., 2008***).

A contrast-enhancing circuit motif

When we analyzed mutual synaptic connections in the eye circuit we found that by far the strongest mutual connections are formed between the crosswise pairs of IN^1 cells (up to 18 synapses one way; ***Figure 7A,B***). These mutual, and thus likely inhibitory, connections are formed at the cell-body proximal segment of the IN^1 cells' axons, spatially segregated from the more distal sites of photoreceptor input (***Figure 4—figure supplement 5***). This reciprocal wiring may provide mutual inhibition and reinforce small differences in activation between the crosswise eyes, potentially representing a network motif for enhancing contrast-detection. Modularity analysis also revealed that the sub-networks of the crosswise eyes are more strongly connected than those of the pairwise eyes (***Figure 4—figure supplement 3***). This suggests that two reciprocally connected crosswise eyes are more efficient in visual information processing than a bilateral pair.

To test this, we performed various eye ablations and then subjected the larvae to selective eye illumination. We ablated a bilateral pair of eyes, thus eliminating inputs to one side of both crosswise mutual IN^1 motifs. We expect that these larvae would have a reduced bending response at the same level of contrast. We also performed crosswise eye ablations, leaving input to one of the crosswise IN^1 motifs intact. We then exposed larvae to a 488 nm background illumination and measured their tail bending following unilateral eye illumination with 488 nm stimulus light of varying intensity. Larvae with pairwise ablation of the anterior eyes showed significantly reduced bending relative to non-ablated controls with the average maximum tail displacement reduced to approximately half (***Figure 7C,D***). In contrast, larvae with crosswise eye ablation showed stronger bending that was not significantly different from non-ablated controls. Although both crosswise and pairwise ablated larvae have only two eyes and are phototactic (***Figure 6F***), these results show that pairwise ablated larvae have a markedly reduced motor response at the same level of contrast. We conclude that the strong mutual contacts between the crosswise IN^1 cells represent a circuit motif that enhances turning responses during phototaxis.

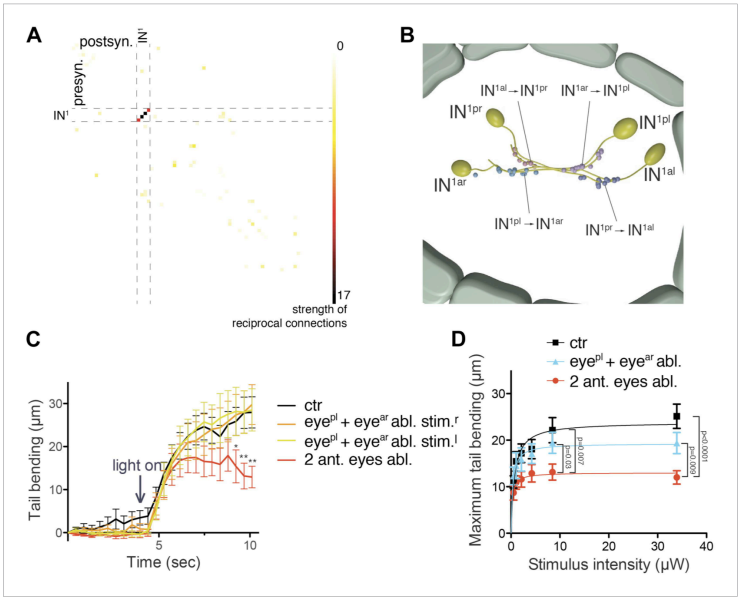

Figure 7. An interneuron motif for enhanced contrast detection. (**A**) Strength of reciprocal connections between all neuron pairs in the complete visual circuit. The strength of reciprocal connections was defined as the geometric mean of the number of reciprocal synapses between each neuron pair. The single neuron identifiers are not shown for simplicity. (**B**) The strongest reciprocal motif in the eye circuit is between the crosswise IN^1 pairs. The position and polarity of the synapses are indicated. (**C**) Quantification of tail bending in different eye ablated larvae under selective eye illumination with a 488-nm laser. Data are shown as mean ± SEM, n >17 for each condition. Larvae lacking two anterior eyes were compared to non-ablated control larvae at each time point (*p value<0.05, **p value<0.01, unpaired *t* test). (**D**) Signal-response curve of maximum tail bending upon selective eye illumination in immobilized larvae using 488-nm stimuli of different intensities. The data are fitted with a saturation-binding curve. Data are shown as mean ± SEM, n >24 larvae for each condition (independent from **C**). p-values of unpaired *t* tests comparing larvae lacking two anterior eyes to the other conditions are shown. Source bending data from (**C** and **D**) are shown in ***Figure 7—source data 1*** and ***Figure 7—source data 2***.

DOI: 10.7554/eLife.02730.040

The following source data are available for figure 7:

Source data 1.

DOI: 10.7554/eLife.02730.041

Source data 2.

DOI: 10.7554/eLife.02730.042

Discussion

Here we described the neural connectome of the visual system in the *Platynereis* larva. The four eyes mediate visual phototaxis, during which larvae are able to detect and contrast spatial differences in the light field. Although it is not yet possible to directly link all neurons and connections in the *Platynereis* larva to phototactic behavior, the combined analysis of connectivity and behavior yielded fundamental insights into a visually guided behavior.

We concluded that spatial vision is not due to the presence of more (3–7 in our larva) photoreceptors in the eyes, since all photoreceptors from one eye synapse on the same primary interneuron. Instead, spatial vision relies on at least two eyes, pointing in different directions, and the underlying neural circuit

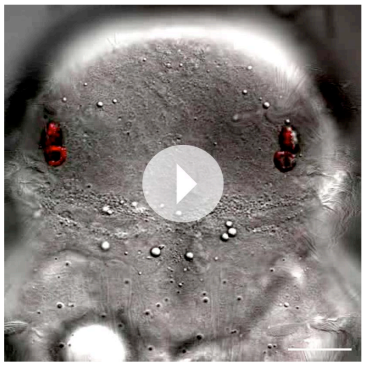

Video 9. Laser ablation of the eyes. The position of the four eyes and the two eyespots is shown by changing the imaging focus. The right eyes are ablated. The eye pigment is imaged using reflection imaging (red), and is overlaid on the DIC channel. Scale bar, 25 μm. Time increment: 1.1 s.
DOI: 10.7554/eLife.02730.043

Video 10. Uniform illumination triggers body bending following unilateral eye ablation. Both left eyes were ablated. The larva is imaged with DIC illumination with a 750 nm long-pass filter. The filter is removed to provide uniform white illumination from the microscope lamp at frame 98. The pigment of the right eye is visible. Scale bar, 50 μm. Time increment: 0.1 s.
DOI: 10.7554/eLife.02730.044

that contrasts simultaneous light inputs at the left and right eyes. Furthermore, connectomics and modularity analysis revealed that the four eyes connect to the downstream visual circuitry in a crosswise manner, showing point symmetry. The crosswise-eye-modules show mutual connections at the level of the primary interneurons. In agreement with this, ablation experiments demonstrated that a bilateral pair of eyes elicits a smaller motor response than a crosswise pair, at the same level of light-intensity contrast. The contrast enhancement takes place in the primary optic neuropil circuitry, and the IN^{ton} may relay a contrasted, one-sided signal to the secondary optic neuropil.

In the secondary optic neuropil this one-sided input could lead to the biased activation of the left or right motorneurons. Our circuit reconstructions partly explain the bimodality of the behavior (either positive or negative phototaxis). Such switching behavior requires neuronal connections between the eyes on one body side and the muscles on both body sides. We found that indeed the circuit diverges bilaterally at the level of the Schnörkel interneurons (IN^{sn}), when these cells synapse to motorneurons of both the left and right body side. The Schnörkel interneuron synapses form at axon segments either proximal or distal to the motorneuron cell bodies (***Figure 4—figure supplement 6***). The spatial organization of synapses may provide an initial bias to the system, favoring bends on one body side. Further modulatory input may influence this bias, inducing a sign switch. There are several sensory neurons, not described here, that feed into the minimal eye circuit at the middle segment of the motorneuron axons (NR, LABC, and GJ, unpublished). Further work will be needed to characterize the possible roles of these neurons in sign switching.

The sensory-motor strategy of visual phototaxis is similar to that found in the lamprey (***Ullén et al., 1997***; ***Figure 8***). In this vertebrate, unilateral illumination leads to a lateral turn away from the light during negative phototaxis. However, under some circumstances lampreys display positive phototaxis. Lesion experiments demonstrated the involvement of the pretectum and reticulospinal neurons in phototaxis, the latter forming the descending control system. Surgically severing connections between the pretectum and the ipsilateral reticulospinal neurons (***Figure 8E***) leads to a sign switch in the phototactic response when the ipsilateral side is illuminated. Transection of the ventral rhombencephalic commissure (***Figure 8E***) in turn reduces the turning angle during negative phototaxis. Thus both the *Platynereis* and the lamprey phototactic circuits are characterized by extensive midline crossing at several levels, bilateral divergence to allow context-dependent sign switching, and bilateral, probably inhibitory, interactions to enhance turning magnitude (***Figure 8D,E***).

At the cellular level, the *Platynereis* eye circuit also shows similarity in its multi-layered arrangement to the visual circuits of insects and vertebrates (***Figure 8A–C***; ***Sanes and Zipursky, 2010***). In the visual system of *Drosophila* photoreceptors project to the optic lobe that is organized into distinct ganglia

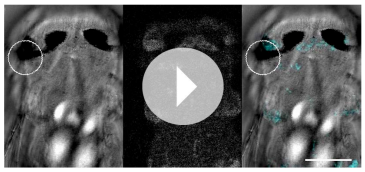

Video 11. Calcium-imaging in ventral longitudinal muscles. Calcium-imaging with GCaMP6 in the ventral longitudinal muscle during selective illumination of the right eyes. The larva is ventrally oriented, the eyes are out of focus. The circular ROI shows the illuminated area. The duration of the illuminations is visible in the DIC channel (brighter overall signal). Scale bar, 50 μm. Time increment: 0.57 s.
DOI: 10.7554/eLife.02730.045

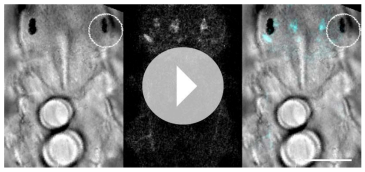

Video 12. Calcium-imaging in dorsal longitudinal muscles. Calcium-imaging with GCaMP6 in the dorsal longitudinal muscle during selective illumination of the right eyes. The larva is dorsally oriented, the eyes are visible. The circular ROI shows the illuminated area. The duration of the illuminations is visible in the DIC channel (brighter overall signal). Scale bar, 50 μm. Time increment: 0.57 s.
DOI: 10.7554/eLife.02730.046

(the lamina, medulla and lobula complex) (***Erclik et al., 2009***). Some neurons are intrinsic to one ganglion, others connect two adjacent ganglia (e.g., transmedullary neurons). Similarly, in the *Platynereis* circuit the IN^{1} and IN^{int} cells are intrinsic to the primary optic neuropil, and IN^{ton} cells link the primary and secondary neuropils. With the exception of the photoreceptors (***Arendt et al., 2002***), the evolutionary relationships of the cell types ('cell-type homology') (***Arendt, 2008***; ***Erclik et al., 2009***) in the vertebrate, insect, and annelid visual systems are unclear and more comparative work will be needed to assess the evolutionary significance of these similarities.

Additionally, our work provides a more general insight about the evolution of higher-resolution image-forming eyes. The current model of eye evolution defines four steps (***Nilsson, 2009***), from non-directional photoreception through directional scanning photoreception (spiral phototaxis) (***Jékely et al., 2008***; ***Jékely, 2009***) and low-resolution spatial vision to high-resolution spatial vision. We now extend this scheme with the concept of the two-pixel visual phototactic eye, likely predating the evolution of low-resolution spatial vision.

Simple eyes, similar to the eyes of *Platynereis* larvae, are widespread in the planktonic larval stages of several bilaterians and may often function in visual phototaxis (***Buchanan, 1986***; ***Blumer, 1994***; ***Lacalli, 2004***). More complex image-forming eyes may have repeatedly evolved from such phototactic eyes. Larval eyes sometimes directly develop into the image-forming eyes of the adults (***Cazaux, 1985***; ***Blumer, 1994***). In *Platynereis*, and several other annelids and mollusks, the larval eyes develop into the adult's eyes, which harbor hundreds or thousands of photoreceptors (***Rhode, 1992***) and mediate low-resolution image-forming vision. In *Platynereis*, we identified visual phototaxis as the first function during the development of the eyes. As in development, also during evolution the first images seen by animals may have consisted of a dark field at the bottom and a bright field at the top of the ocean.

Materials and methods

Animal culture

Platynereis larvae were obtained from an in-house breeding culture following an established protocol (***Hauenschild and Fischer, 1969***). Larvae were kept at 18°C for development. Behavioral experiments were performed at room temperature.

ssTEM

72 hr post fertilization *Platynereis* larvae, reared at 18°C, were fixed using a high-pressure freezer (HPM 010; BAL-TEC, Balzers, Liechtenstein) and transferred to liquid nitrogen. Frozen samples were cryosubstituted with 2% osmium tetroxide in acetone and 0.5% uranyl acetate in a cryosubstitution unit (EM AFS-2; Leica Microsystems GmbH, Wetzlar, Germany) over a regime of gradually rising temperatures. Samples were embedded in Epon. 40–50-nm serial sections were cut starting from the anterior end of a larva (*Platynereis* HT-9-3) on a Reichert Jung Ultracut E microtome. The sections were collected on single-slotted copper grids (NOTSCH-NUM 2 × 1 mm, Science Service, Munich, Germany)

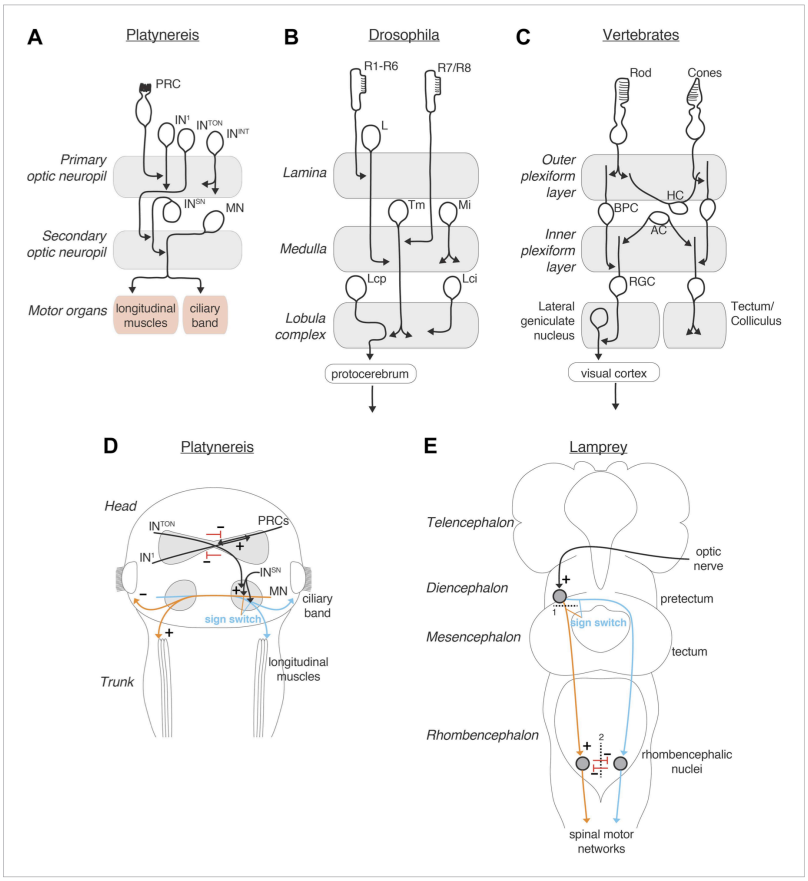

Figure 8. Comparison of the *Platynereis*, *Drosophila* and vertebrate visual circuits. Comparison of the *Platynereis* visual circuit with the *Drosophila* and vertebrate visual circuits on the neuronal level (**A**–**C**) and with the lamprey phototactic circuit on the circuit level (**D** and **E**). In (**E**) dashed line (1) represents a mesencephalic hemisection, severing connections between the pretectum and the ipsilateral reticulospinal neurons, dashed line (2) represents transection of the ventral rhombencephalic commissure. L, lamina monopolar neuron; Tm, transmedula neuron; Mi, medulla intrinsic neuron; Lcp, lobula complex projection neuron; Lci, lobula complex intrinsic neuron; BPC, bipolar cell; HC, horizontal cell, AC, amacrine cell; RGC, retinal ganglion cell. (**B** and **C**) after ***Erclik et al. (2009)***; (***Sanes and Zipursky, 2010***) (**E**) after ***Ullén et al. (1997)***.
DOI: 10.7554/eLife.02730.047

with Formvar support film, contrasted with uranyl acetate and Reynold's lead citrate, and carbon coated to stabilize the film. Image acquisition of serial sections was performed at a pixel size of 3.72 nm on a FEI TECNAI Spirit transmission electron microscope (FEI, Hillsboro, Oregon) equipped with an UltraScan 4000 4 × 4k digital camera using the image acquisition software Digital Micrograph (Gatan, Pleasanton, CA). Stitching and alignment were accomplished using TrakEM2 (***Cardona et al., 2010***). The first 1245 layers were cut at 50 nm and aligned using an elastic alignment algorithm (***Saalfeld et al., 2012***). We later found that the larva was slightly tilted, and we did not reach the

muscles and the ciliary band on the right side of the animal. We therefore sectioned a further 445 sections at 40 nm, and aligned these using the rigid alignment algorithm in TrakEM2. All structures were segmented manually as area-lists or area-trees by an expert tracer (NR). Traces were exported into 3Dviewer, Imaris and Blender. Given the simple anatomy of the neurons and the large average diameter of axons tracing was in many cases unambiguous. Neurons with several short branches or with uncertain continuation were traced again by another expert tracer (LABC).

Delineation of the eye circuit, neuron classification, nomenclature, and network visualization

The minimal eye circuit of the eyes contains only postsynaptic neurons downstream of photoreceptors. Neurons presynaptic to the minimal eye circuit at any level (with possible modulatory functions) are not included here. Five sensory cells, which are both pre- and post-synaptic to the minimal eye circuit were also excluded. 12 postsynaptic targets of the MNs in the ventral nerve cord and five between the secondary optic neuropils as well as 32 postsynaptic targets of interneurons were also excluded because of low connectivity and the occurrence of only individual synapses outside the optic neuropils.

48 neurite fragments could not be traced completely. Most of these fragments are short (<5 μm) with 1–5 synapses. They occur in regions where neurons have small short branches to receive or provide synapses. These fragments likely belong to identified neurons. Nine of the non-traceable fragments were longer (up to 44 μm).

We classified neurons according to their morphology, position, projection pattern and connectivity. Photoreceptors were identified based on the presence of a rhabdom located in the eye pigment cup. Their dominant targets are the four primary interneuron (IN^1) cells. IN^1 cells are named based on their position (anterior-left etc.). IN^1 cells are defined as a separate group based on their unique connectivity patterns, including strong input from photoreceptors and strong reciprocal contacts between the crosswise cells. The second group of interneurons is classified as IN^{int}s, with projections intrinsic to the primary optic neuropil and weak connectivity to photoreceptors and IN^1 cells. A third group is formed by the IN^{ton} cells, distinguished by their unique projection pattern from the primary to the secondary optic neuropil. Schnörkel interneurons (IN^{sn}) form a distinct class with ventral cell bodies and curved axons ('Schnörkel' is German for 'curlicue') projecting to the ipsilateral secondary optic neuropil and synapsing on the motorneurons. The dorsal interneurons (IN^{dc}) have dorsally located cell bodies and axons that project to the secondary optic neuropil. The ventral interneurons (IN^{vc}) have ventrally located cell bodies and axons that project to the secondary optic neuropil. Motorneurons were recognized based on their innervation of dorsal and ventral longitudinal muscles as well as multi-ciliated cells (prototroch or metatroch). Motorneurons form two bilateral clusters. For some motorneurons we could not find motor synapses, however, we could classify these cells as motorneurons based on their cell body position and posteriorly projecting axons. Neurons of all types are labeled based on body side (left $^{[l]}$ or right $^{[r]}$) and numbered (e.g., IN^{tonl1}).

Network analyses were done in Gephi 0.8.2. Modules were detected with an algorithm described in ***Blondel et al. (2008)*** with randomization on, using edge weights and a resolution of 1.2. Force-field-based clustering was performed using the Force Atlas 2 Plugin.

Neuron visualization

Neurons and their connections reconstructed in TrakEM2 were exported as 3D objects in a wavefront (.obj) format and imported into Blender. Cell bodies were approximated with ellipsoids and axons and dendrites with smooth curves. The approximations were performed either manually or automatically using Python scripting embedded in Blender. Muscles were kept in the original form, pigment cups and ciliated cells were approximated with simplified 3D shapes based on TrakEM2 reconstructions. The model was extended with the connectivity and synapse position information obtained from TrakEM2.

Virtual connectome atlas in blender

The virtual atlas (***Randel et al., 2014***) can be opened with Blender (http://www.blender.org/). Users new to Blender may consider watching a tutorial (http://www.blendtuts.com/2010/06/blender-25-interface.html). After opening the model file, two panels are visible in the *Tool shelf*: *Hide/Show groups* and *Highlight subnetworks* (Press 'T' if *Tool shelf* did not appear). If the panels do not appear, they can be loaded with the button *Reload Trusted* in the main menu panel (on the top). If menus still do not appear, the *Panel_show_group.py* and *Panel_synapses.py* python scripts need to be run by selecting the *Scripting* view in the main menu panel instead of *Default*. In the panel *Hide/Show groups* the cell types can be selected and hidden or displayed by pressing the *Apply* button. The panel

Highlight subnetworks enables querying pre- and post-synaptic cells by selecting a cell body of interest (right click) and pressing the *Postsynaptic* or *Presynaptic* buttons. The complete up- or downstream network of a cell can also be displayed by selecting a cell body and pressing the *Pre.subnetwork* or *Post.subnetwork* buttons. The *Show connectors* button visualizes the connectors between two cells after selecting the presynaptic cell first and then the postsynaptic cell. The *Show out connectors* button will reveal all outgoing synapses for a selected cell.

Laser ablation

Laser ablation was performed on an Olympus FV1000 confocal microscope equipped with a SIM scanner (Olympus Corporation, Tokyo, Japan). Larvae were immobilized between a slide and a coverslip in NSW containing 100 mM $MgCl_2$. Larvae were imaged with an UPLSAPO 60X NA:1.20 water immersion objective using a 635-nm laser at 2–5% and transmission imaging with DIC optics. A 351-nm pulsed laser (Teem Photonics™, Grenoble, France) at 8–15% power was used, coupled via air to the SIM scanner for controlled ablation in a region of interest. 12% corresponds to a beam power of 168 μwatts as measured with a microscope slide power sensor (S170C; Thorlabs, Newton, NJ). During eye ablations we also imaged the eye pigment by reflection imaging of the 635-nm light using a PMT. Ablated larvae were placed into NSW for recovery (1–6 hr) before behavioral experiments.

Selective eye illumination

Selective eye illumination was performed on an Olympus FV1000 confocal microscope equipped with a SIM scanner. Larvae were held by trapping them between a slide and a coverslip in natural seawater using several layers of tape as spacer. Larvae were imaged with an UPLSAPO 40X NA:0.90 air objective using a 635 nm laser at 1% and transmission imaging with DIC optics. The scanning speed was 2 μm/msec and we recorded 256 × 256 pixel images with a time increment of 0.43 s. For measuring the stimulus–response curve we used background illumination with the 488 nm laser at 10% power corresponding to 17.8 μwatts in the main scanner. For stimulations we used the 488 nm laser at 1–65% power via the SIM scanner, corresponding to a beam intensities of 0.53–20.9 μwatts. A circular region of interest of 25-pixel diameter (area of 490 pixels) covering the eyes was used for controlled illumination. The pixel dwell time of the beam was 10 μsec and the eyes were stimulated during 150 frames with the SIM scanner corresponding to a total exposure time of 735 msec during a 9.8 s trial. For the bending ***Video 8*** the stimulus laser power was at 10%. The laser power was measured with a microscope slide power sensor (S170C; Thorlabs). To record the spatial and temporal extent of the stimulus the reflected 488-nm light was imaged with a PMT. To prevent the detection of the 488-nm stimulus light by the transmitted light detector, we placed a red long-pass filter in front of the detector.

In situ hybridization and image registration

Whole-mount in situ hybridization and image registration were performed as previously described (***Asadulina et al., 2012***). For probe generation we used expressed sequence tag clones or PCR-amplified fragments of already published *Platynereis* genes. The GeneBank accessions are: *TyrH*—JZ446954, *TrpH*–JZ446141, *VGlut*—JZ395359, *hdc*—JZ396646, *VAChT*—JZ402823, *ChAT*—JZ402100, *gad*—GU169427, dbh—KJ855061.

For registering gene expression patterns of 3-day-old larvae we generated a reference template (***Randel et al., 2014***) where we removed the bias present in the earlier reference, due to the use of a single larva as a starting template (***Asadulina et al., 2012***). In brief, we identified a median-size larva and registered it to every single image stack used for template generation (40 stacks), computed the average transformation and applied it to the median-size larva. The corrected larva was used as the starting point for the iteratively template generation (***Asadulina et al., 2012***). We registered minimum four individual larval whole-body scans for each gene to create an average expression pattern.

Phototaxis assay

Larval phototaxis was assayed in a horizontal 6 × 15 mm rectangular glass cuvette with 3 mm high walls. The cuvette was illuminated uniformly through a light diffuser with white light from a 150-watt halogen cold light source (Schott KL 2500 LCD, Schott AG, Mainz, Germany). Larval behavior was recorded at 21 frames per second on a Zeiss Stemi 2000-CS stereomicroscope equipped with an AxioCam MRm camera (Carl Zeiss AG, Jena, Germany). Phototaxis efficiency was measured using a custom ImageJ macro that calculated larval density at the left and right side of the cuvette before and after the light stimulus (***Randel et al., 2014***).

Calcium imaging

Fertilized eggs were injected with capped and polyA-tailed GCaMP6 (*Chen et al., 2013*) RNA generated from a vector (pUC57-T7-RPP2-GCaMP6) containing the GCaMP6 ORF fused to a 169 base pair 5′ UTR from the *Platynereis* 60S acidic ribosomal protein P2. 3-day-old larvae were held as described above. Imaging was performed on an Olympus FV1000 confocal microscope equipped with a SIM scanner. Larvae were imaged with an UPLSAPO 60X NA:1.20 water immersion objective using a 635-nm laser at 10% and transmission imaging with DIC optics. The GCaMP6 signal was imaged with a 488-nm laser at 2% intensity. The eyes were stimulated with the 488-nm laser in a region of interest using the SIM scanner. GCaMP6 signals were recorded simultaneously.

Acknowledgements

We thank Dan Bumbarger and members of the Jékely group for comments on the manuscript, Ferdinand Kluge for help with tracing, Aurora Panzera for help with microscopy and microinjection, and Martin Gühmann for help with phototaxis scoring. The research leading to these results received funding from the European Research Council under the European Union's Seventh Framework Programme (FP7/2007-2013)/European Research Council Grant Agreement 260821.

Author contributions

GJ designed the research. NR prepared and sectioned the sample. RS imaged the sample. NR traced and assembled the connectome with help from AA and GJ. LABC and CV helped with the tracing and proofreading. NR and GJ performed laser ablations and behavioral experiments. EAW and MC performed gene expression analyses. AA visualized neuronal morphologies. GJ wrote the paper, with contributions from NR and AA.

Additional information

Funding

Funder	Author
European Commission (EC)	Nadine Randel, Albina Asadulina, Elizabeth A Williams, Markus Conzelmann, Réza Shahidi
Max Planck Society	Luis A Bezares-Calderón, Csaba Verasztó, Gáspár Jékely

The funders had no role in study design, data collection and interpretation, or the decision to submit the work for publication.

Author contributions

NR, GJ, Conception and design, Acquisition of data, Analysis and interpretation of data, Drafting or revising the article; AA, Conception and design, Analysis and interpretation of data, Drafting or revising the article; LAB-C, CV, Analysis and interpretation of data, Drafting or revising the article; EAW, MC, RS, Acquisition of data, Analysis and interpretation of data, Drafting or revising the article

Ethics

Animal experimentation: This study only used invertebrate animals.

Additional files

Major dataset

The following dataset was generated:

Author(s)	Year	Dataset title	Dataset ID and/or URL	Database, license, and accessibility information
Randel N, Asadulina A, Bezares-Calderón LA, Verasztó C, Williams EA, Conzelmann M, Shahidi R, Jékely G	2014	Data from: Neuronal connectome of a sensory-motor circuit for visual navigation	doi: 10.5061/dryad.6f267	Available at Dryad Digital Repository under a CC0 Public Domain Dedication.

References

Arendt D. 2008. The evolution of cell types in animals: emerging principles from molecular studies. *Nature Reviews Genetics* **9**:868. doi: 10.1038/nrg2416.

Arendt D, Tessmar K, de Campos-Baptista M-IM, Dorresteijn A, Wittbrodt J. 2002. Development of pigment-cup eyes in the polychaete Platynereis dumerilii and evolutionary conservation of larval eyes in Bilateria. *Development* **129**:1143–1154.

Asadulina A, Panzera A, Verasztó C, Liebig C, Jékely G. 2012. Whole-body gene expression pattern registration in Platynereis larvae. *EvoDevo* **3**:27. doi: 10.1186/2041-9139-3-27.

Backfisch B, Veedin Rajan VB, Fischer RM, Lohs C, Arboleda E, Tessmar-Raible K, Raible F. 2013. Stable transgenesis in the marine annelid Platynereis dumerilii sheds new light on photoreceptor evolution. *Proceedings of the National Academy of Sciences of the United States of America* **110**:193–198. doi: 10.1073/pnas.1209657109.

Blondel VD, Guillaume J-L, Lambiotte R, Lefebvre E. 2008. Fast unfolding of communities in large networks. *Journal of Statistical Mechanics* **2008**:P10008. doi: 10.1088/1742-5468/2008/10/P10008.

Blumer M. 1994. The ultrastructure of the eyes in the veliger-larvae of Aporrhais sp. and Bittium reticulatum (Mollusca, Caenogastropoda). *Zoomorphology* **114**:149–159. doi: 10.1007/BF00403262.

Bock DD, Lee W-CA, Kerlin AM, Andermann ML, Hood G, Wetzel AW, Yurgenson S, Soucy ER, Kim HS, Reid RC. 2011. Network anatomy and in vivo physiology of visual cortical neurons. *Nature* **471**:177–182. doi: 10.1038/nature09802.

Briggman KL, Helmstaedter M, Denk W. 2011. Wiring specificity in the direction-selectivity circuit of the retina. *Nature* **471**:183–188. doi: 10.1038/nature09818.

Buchanan J. 1986. Ultrastructure of the larval eyes of Hermissenda-Crassicornis (Mollusca, Nudibranchia). *Journal of Ultrastructure and Molecular Structure Research* **94**:52–62. doi: 10.1016/0889-1605(86)90051-0.

Bumbarger DJ, Riebesell M, Rödelsperger C, Sommer RJ. 2013. System-wide Rewiring Underlies behavioral differences in Predatory and Bacterial-Feeding Nematodes. *Cell* **152**:109–119. doi: 10.1016/j.cell.2012.12.013.

Burgess HA, Schoch H, Granato M. 2010. Distinct retinal pathways drive spatial orientation behaviors in zebrafish navigation. *Current Biology* **20**:381–386. doi: 10.1016/j.cub.2010.01.022.

Cardona A, Saalfeld S, Preibisch S, Schmid B, Cheng A, Pulokas J, Tomancak P, Hartenstein V. 2010. An integrated micro- and macroarchitectural analysis of the Drosophila brain by computer-assisted serial section electron microscopy. *PLOS Biology* **8**:e1000502. doi: 10.1371/journal.pbio.1000502.

Cazaux C. 1985. Développement larvaire de l'annelide polychete Phyllodocidae Eteone picta Quatrefages 1865 dans le Bassin d'Arcachon. *Journal Of Experimental Marine Biology And Ecology* 191–209.

Chen T-W, Wardill TJ, Sun Y, Pulver SR, Renninger SL, Baohan A, Schreiter ER, Kerr RA, Orger MB, Jayaraman V, Looger LL, Svoboda K, Kim DS. 2013. Ultrasensitive fluorescent proteins for imaging neuronal activity. *Nature* **499**:295–300. doi: 10.1038/nature12354.

Denes AS, Jékely G, Steinmetz PRH, Raible F, Snyman H, Prud'homme B, Ferrier DE, Balavoine G, Arendt D. 2007. Molecular architecture of annelid nerve cord supports common origin of nervous system centralization in bilateria. *Cell* **129**:277–288. doi: 10.1016/j.cell.2007.02.040.

Erclik T, Hartenstein V, McInnes RR, Lipshitz HD. 2009. Eye evolution at high resolution: the neuron as a unit of homology. *Developmental Biology* **332**:70–79. doi: 10.1016/j.ydbio.2009.05.565.

Garm A, O'connor M, Parkefelt L, Nilsson D-E. 2007. Visually guided obstacle avoidance in the box jellyfish Tripedalia cystophora and Chiropsella bronzie **210**:3616–3623. doi: 10.1242/jeb.004044.

Hauenschild C, Fischer A. 1969. *Platynereis dumerilii. Mikroskopische Anatomie, Fortpflanzung, Entwicklung*. Stuttgart: Gustav Fischer. p. 1.

Helmstaedter M, Briggman KL, Turaga SC, Jain V, Seung HS, Denk W. 2013. Connectomic reconstruction of the inner plexiform layer in the mouse retina. *Nature* **500**:168–174. doi: 10.1038/nature12346.

Huang K-H, Ahrens MB, Dunn TW, Engert F. 2013. Spinal projection neurons control turning behaviors in zebrafish. *Current Biology* **23**:1566–1573. doi: 10.1016/j.cub.2013.06.044.

Jarrell TA, Wang Y, Bloniarz AE, Brittin CA, Xu M, Thomson JN, Albertson DG, Hall DH, Emmons SW. 2012. The connectome of a decision-making neural network. *Science* **337**:437–444. doi: 10.1126/science.1221762.

Jékely G. 2009. Evolution of phototaxis. *Philosophical Transactions of the Royal Society B: Biological Sciences* **364**:2795–2808. doi: 10.1098/rstb.2009.0072.

Jékely G, Colombelli J, Hausen H, Guy K, Stelzer EHK, Nédélec F, Arendt D. 2008. Mechanism of phototaxis in marine zooplankton. *Nature* **456**:395–399. doi: 10.1038/nature07590.

Kandarian B, Sethi J, Wu A, Baker M, Yazdani N, Kym E, Sanchez A, Edsall L, Gaasterland T, Macagno E. 2012. The medicinal leech genome encodes 21 innexin genes: different combinations are expressed by identified central neurons. *Development Genes and Evolution* **222**:29–44. doi: 10.1007/s00427-011-0387-z.

Kane EA, Gershow M, Afonso B, Larderet I, Klein M, Carter AR, de Bivort BL, Sprecher SG, Samuel AD. 2013. Sensorimotor structure of Drosophila larva phototaxis. *Proceedings of the National Academy of Sciences of the United States of America* **110**:E3868–E3877. doi: 10.1073/pnas.1215295110.

Lacalli TC. 2004. Sensory systems in amphioxus: a window on the ancestral chordate condition. *Brain, Behavior and Evolution* **64**:148–162. doi: 10.1159/000079744.

Land MF, Nilsson D-E. 2002. *Animal eyes*. New York: Oxford University Press. 1st edition.

Marsden JR. 1990. Light responses of the planktotrophic larva of the serpulid polychaete Spirobranchus polycerus. *Marine Ecology Progress Series* **58**:225–233.

Muller KJ, Carbonetto S. 1979. Morphological and Physiological Properties of a Regenerating Synapse in the C.N.S. of the Leech. *Journal of Comparative Neurology* **185**:485–516. doi: 10.1002/cne.901850305.

Nilsson D-E. 2009. The evolution of eyes and visually guided behaviour. *Philosophical Transactions of the Royal Society B: Biological Sciences* **364**:2833–2847. doi: 10.1098/rstb.2009.0083.
Orger MB, Kampff AR, Severi KE, Bollmann JH, Engert F. 2008. Control of visually guided behavior by distinct populations of spinal projection neurons. *Nature Neuroscience* **11**:327–333. doi: 10.1038/nn2048.
Randel N, Asadulina A, Bezares-Calderón LA, Verasztó C, Williams EA, Conzelmann M, Shahidi R, Jékely G. 2014. Data from: Neuronal connectome of a sensory-motor circuit for visual navigation. Dryad Digital Repository. doi: 10.5061/dryad.6f267.
Randel N, Bezares-Calderón LA, Gühmann M, Shahidi R, Jékely G. 2013. Expression dynamics and protein localization of rhabdomeric opsins in platynereis larvae. *Integrative and Comparative Biology* **53**:7–16. doi: 10.1093/icb/ict046.
Rhode B. 1992. Development and differentiation on the eye in Platynereis dumerilii (Annelida, Polychaeta). *Journal of Morphology* **212**:71–85. doi: 10.1002/jmor.1052120108.
Rivera-Alba M, Vitaladevuni SN, Mishchenko Y, Lu Z, Takemura S-Y, Scheffer L, Meinertzhagen IA, Chklovskii DB, de Polavieja GG. 2011. Wiring economy and volume exclusion determine neuronal placement in the Drosophila brain. *Current Biology* **21**:2000–2005. doi: 10.1016/j.cub.2011.10.022.
Saalfeld S, Fetter R, Cardona A, Tomancak P. 2012. Elastic volume reconstruction from series of ultra-thin microscopy sections. *Nature Methods* **9**:717–720. doi: 10.1038/nmeth.2072.
Sanes JR, Zipursky SL. 2010. Design principles of insect and vertebrate visual systems. *Neuron* **66**:15–36. doi: 10.1016/j.neuron.2010.01.018.
Shen D-W, Lu Q-W, Wang L, Zhang R-J. 2002. Ultrastructure of electrical synapses between nociceptive and anterior pagoda neurons in the CNS of the leech (Whitmania pigra). *Invertebrate Neuroscience*. **4**:193–198.
Sprecher SG, Cardona A, Hartenstein V. 2011. The Drosophila larval visual system: high-resolution analysis of a simple visual neuropil. *Developmental Biology* **358**:33–43. doi: 10.1016/j.ydbio.2011.07.006.
Stuart AE. 1999. From fruit flies to barnacles, histamine is the neurotransmitter of arthropod photoreceptors. *Neuron* **22**:431–433. doi: 10.1016/S0896-6273(00)80699-6.
Takemura S-Y, Bharioke A, Lu Z, Nern A, Vitaladevuni S, Rivlin PK, Katz WT, Olbris DJ, Plaza SM, Winston P, Zhao T, Horne JA, Fetter RD, Takemura S, Blazek K, Chang LA, Ogundeyi O, Saunders MA, Shapiro V, Sigmund C, Rubin GM, Scheffer LK, Meinertzhagen IA, Chklovskii DB. 2013. A visual motion detection circuit suggested by Drosophila connectomics. *Nature* **500**:175–181. doi: 10.1038/nature12450.
Takemura S-Y, Karuppudurai T, Ting C-Y, Lu Z, Lee C-H, Meinertzhagen IA. 2011. Cholinergic circuits integrate neighboring visual signals in a Drosophila motion detection pathway. *Current Biology* **21**:2077–2084. doi: 10.1016/j.cub.2011.10.053.
Thorson G. 1964. Light as an ecological factor in the dispersal and settlement of larvae of marine bottom invertebrates. *Ophelia* **1**:167–208. doi: 10.1080/00785326.1964.10416277.
Tomer R, Denes AS, Tessmar-Raible K, Arendt D. 2010. Profiling by image registration reveals common origin of annelid mushroom bodies and vertebrate pallium. *Cell* **142**:800–809. doi: 10.1016/j.cell.2010.07.043.
Ullén F, Deliagina TG, Orlovsky GN, Grillner S. 1997. Visual pathways for postural control and negative phototaxis in lamprey. *Journal of Neurophysiology* **78**:960–976.
Wells J, Besso JA, Boldosser WG, Parsons RL. 1972. The fine structure of the nerve cord of Myxicola infundibulum (Annelida, Polychaeta). *Zeitschrift für Zellforschung und mikroskopische Anatomie* **131**:141–148. doi: 10.1007/BF00306923.
Young CM, Chia F-S. 1982. Ontogeny of phototaxis during larval development of the sedentary polychaete, Serpula vermicularis (L.). *The Biological Bulletin* **162**:457–468. doi: 10.2307/1540996.

Figure 1–figure supplement 1.

Morphology of photoreceptor cells reconstructed from serial TEM sections.

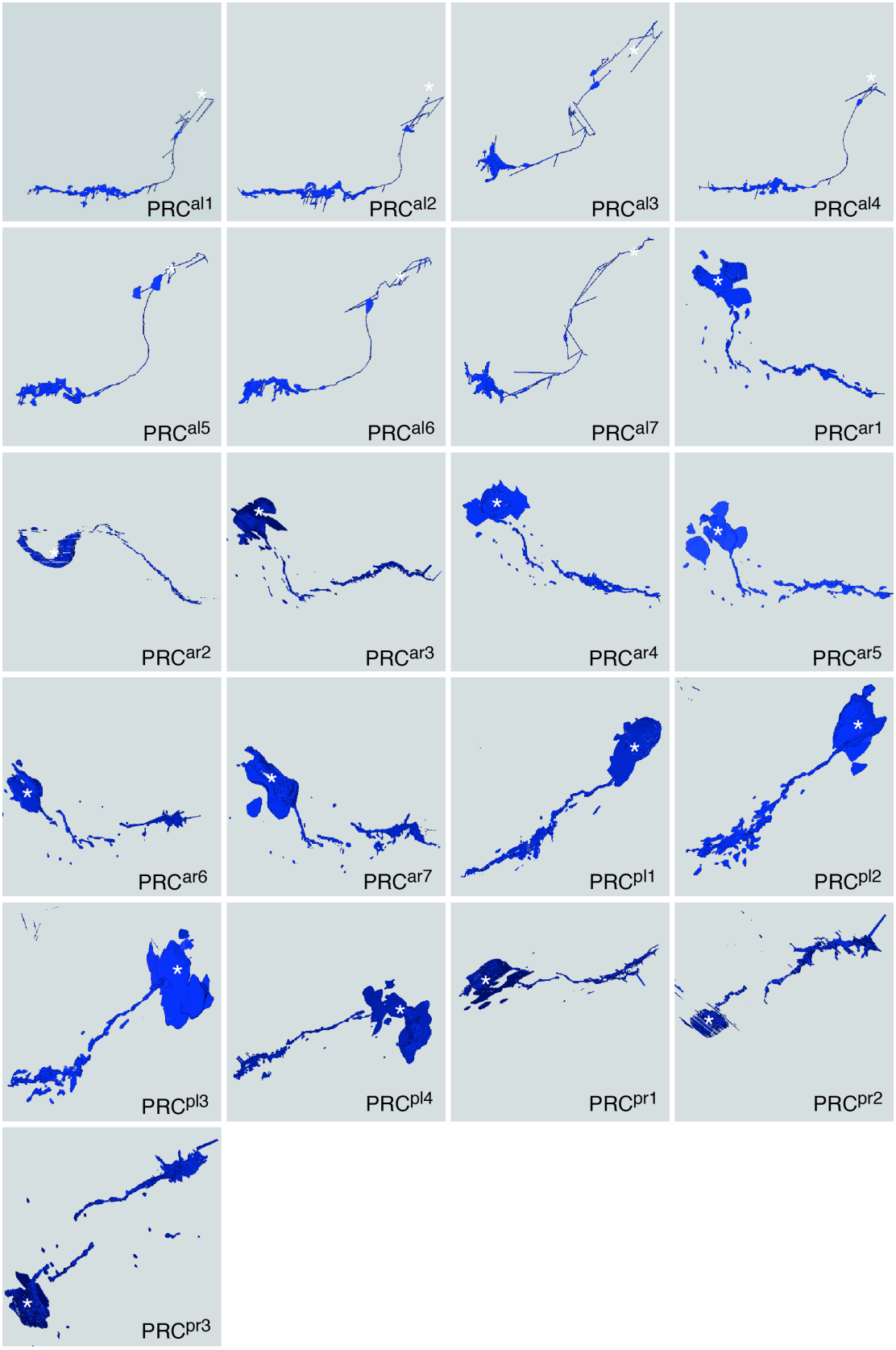

Figure 1–figure supplement 2.

Morphology of IN^{1}, IN^{ton}, IN^{sn}, and IN^{dc} cells reconstructed from serial TEM sections.

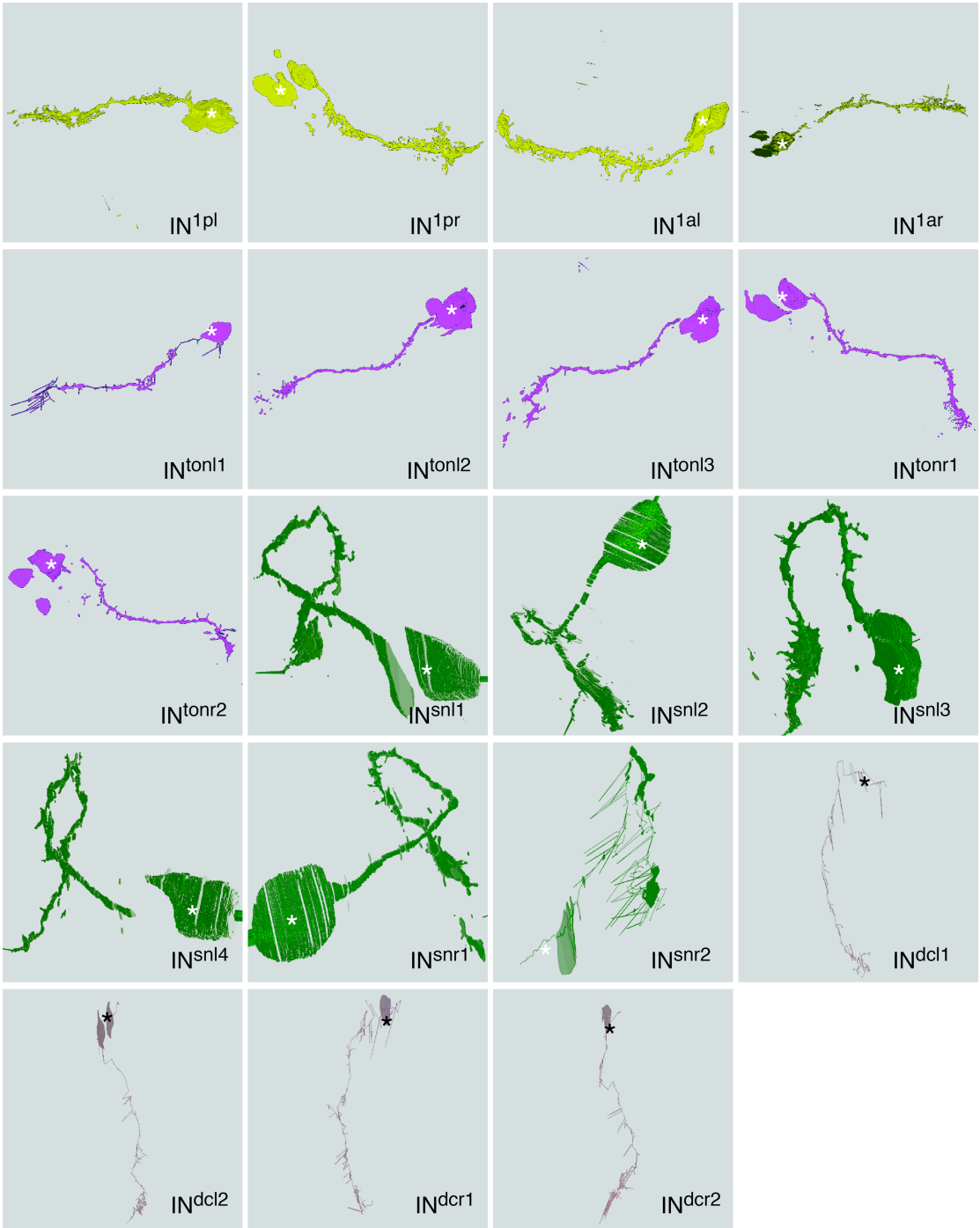

Figure 1–figure supplement 3.

Morphology of IN^{int} and IN^{vc} cells reconstructed from serial TEM sections.

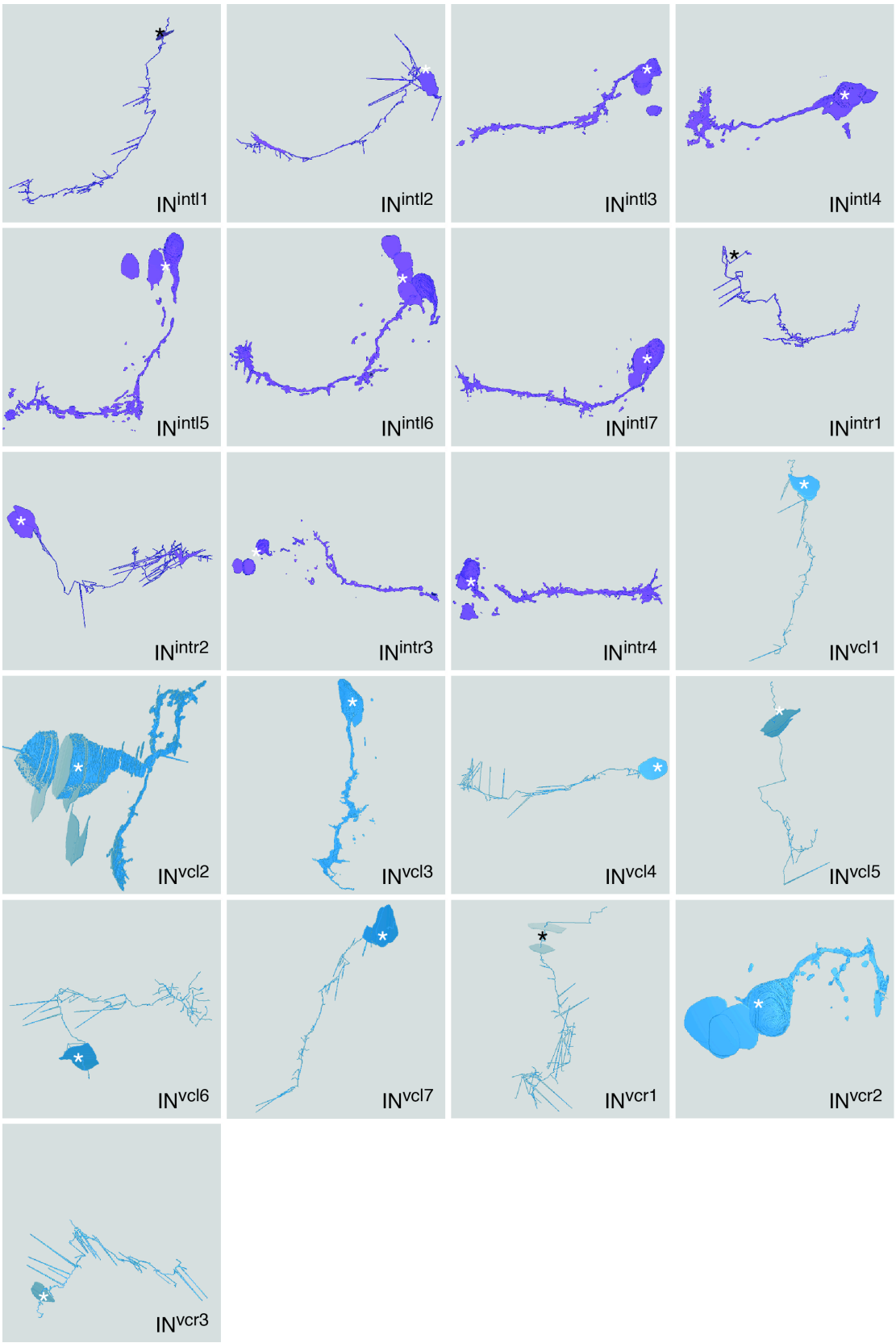

Figure 1–figure supplement 4.

Morphology of motorneurons reconstructed from serial TEM sections.

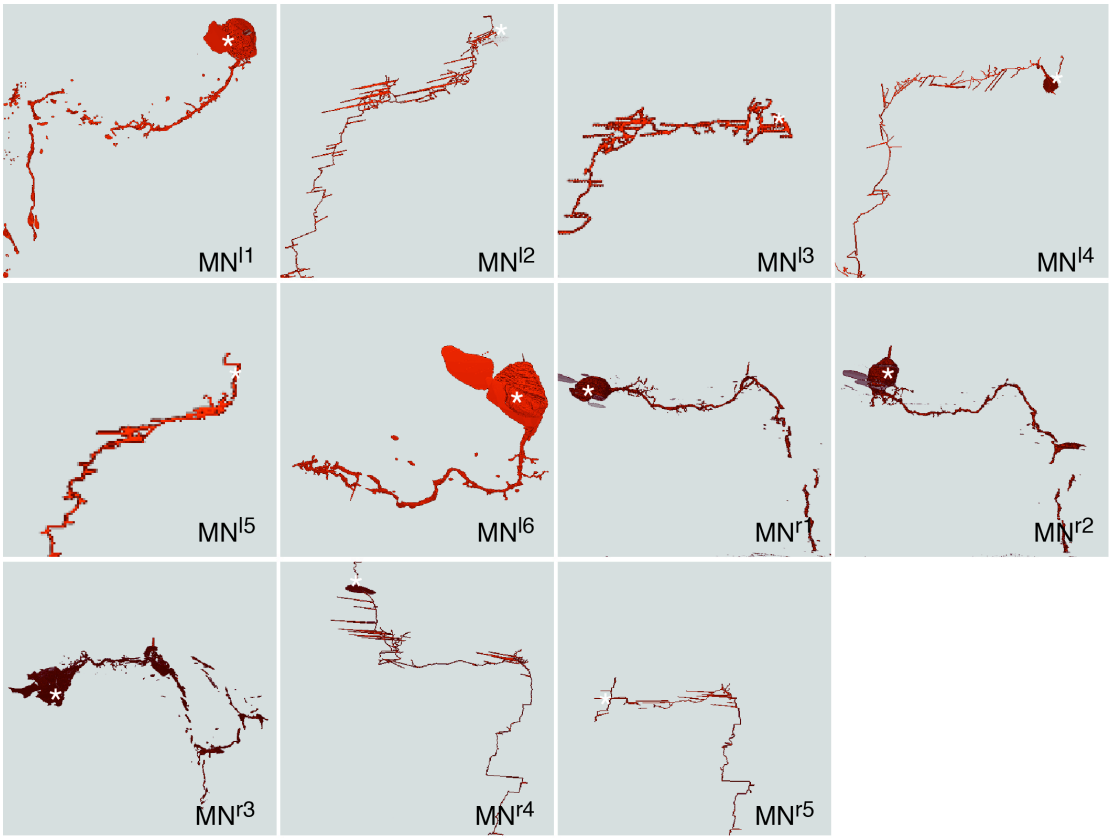

Figure 1–figure supplement 5.

Axon diameter and synapse size in the *Platynereis* larval connectome.

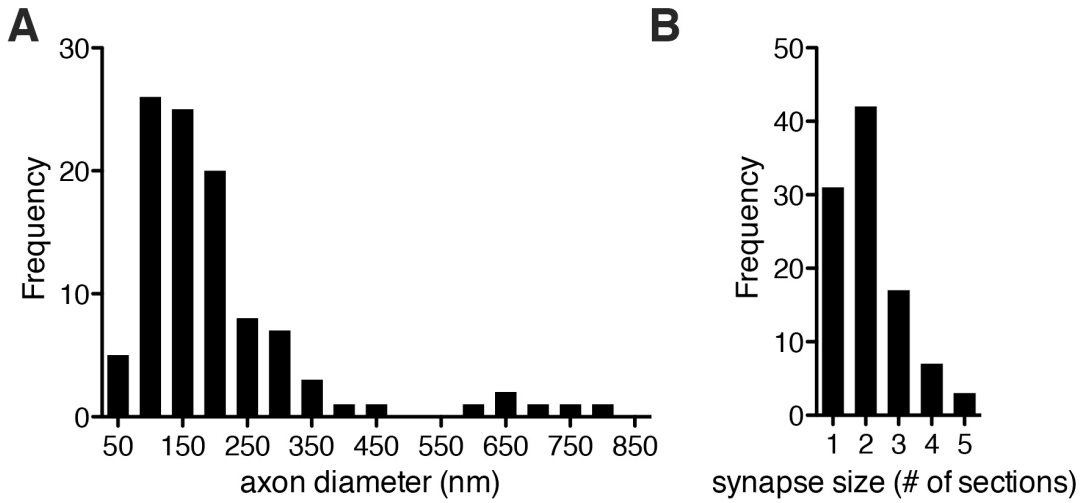

Figure 1–figure supplement 6.

Synapses of photoreceptors and IN[1] cells.

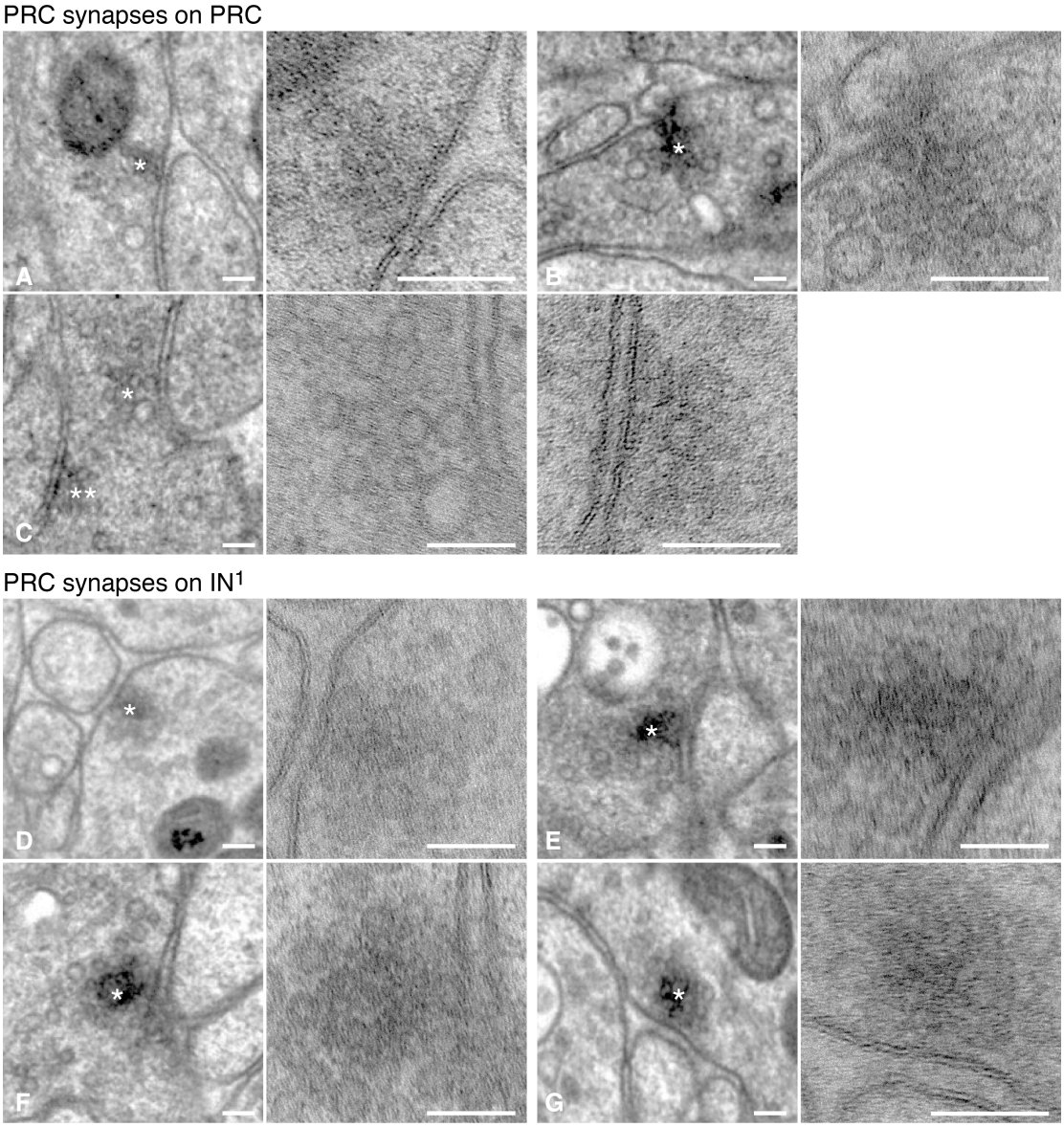

Figure 1–figure supplement 7.

Synapses of IN^1 cells.

IN^1 synapses on IN^1

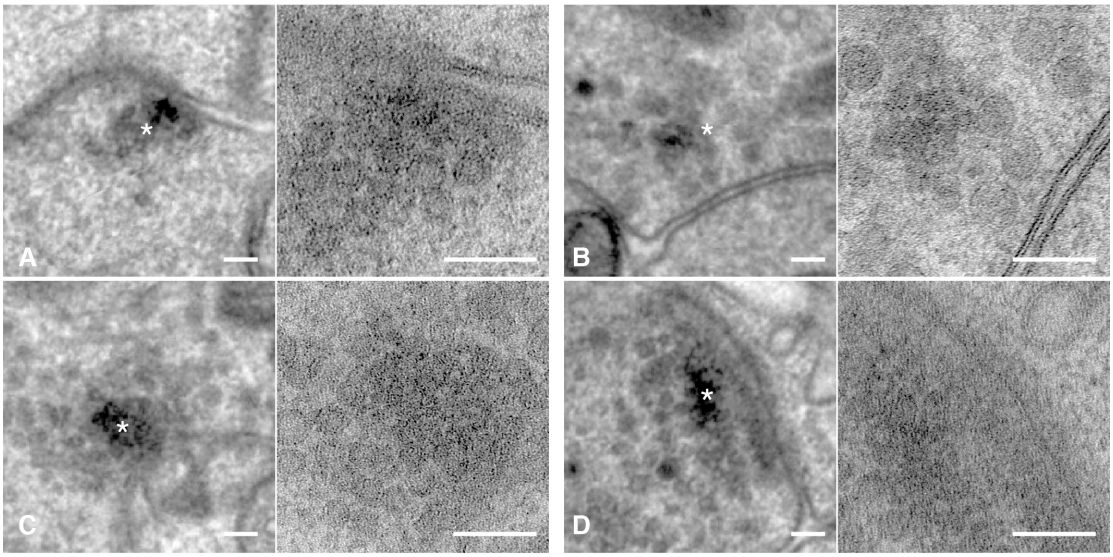

IN^1synapses on IN^{ton}

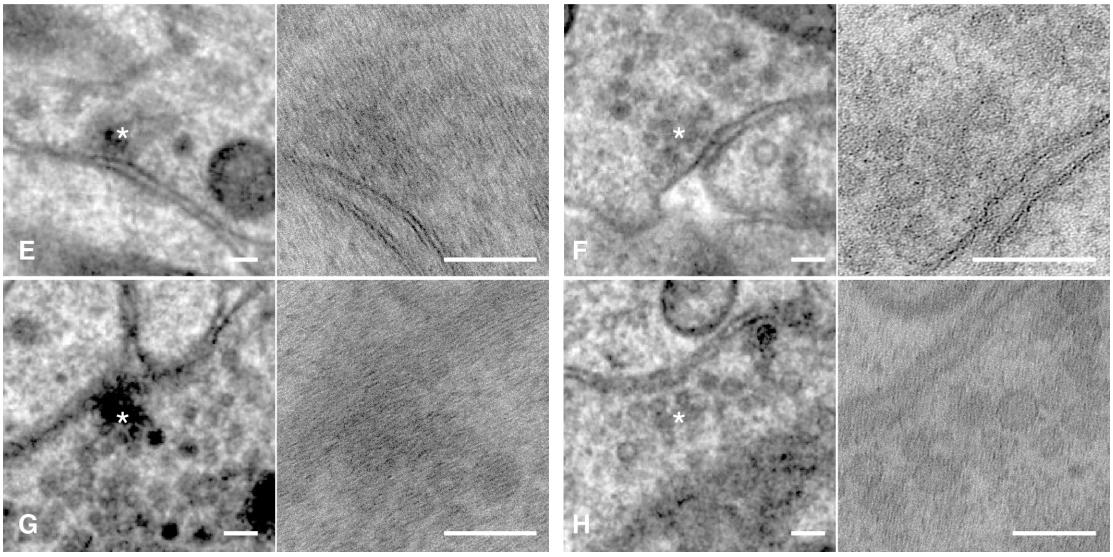

Figure 1–figure supplement 8.

Synapses of IN^{ton} cells and IN^{sn} cells.

IN^{ton} synapses on IN^{sn}

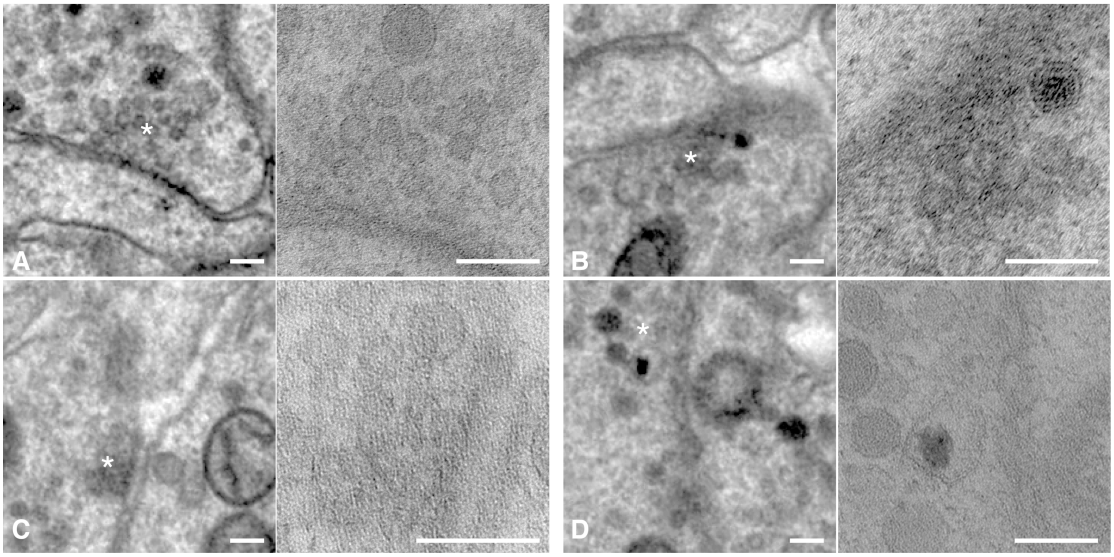

IN^{sn} synapses on MN

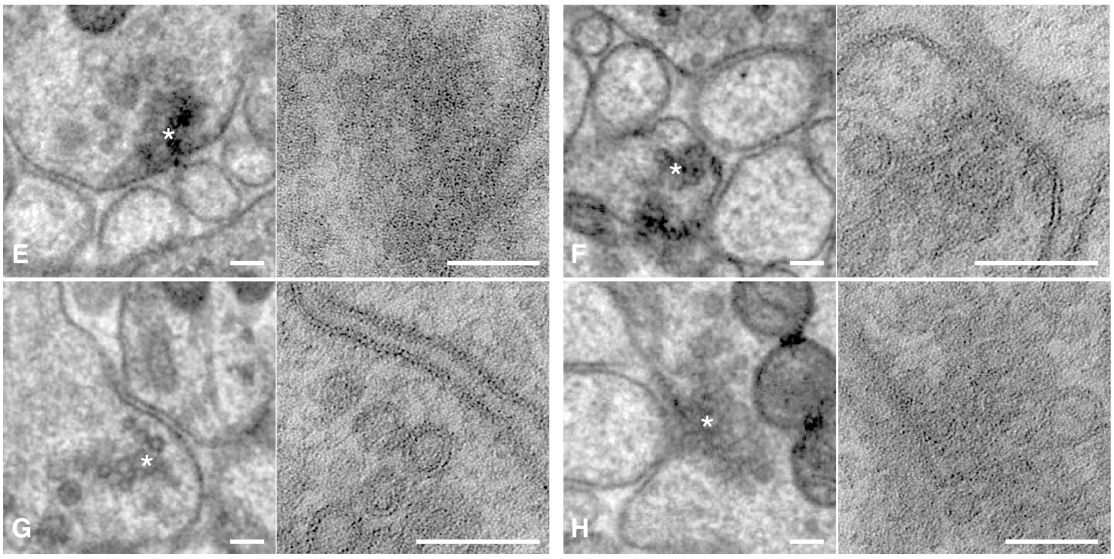

Figure 1–figure supplement 9.

Synapses of motorneurons.

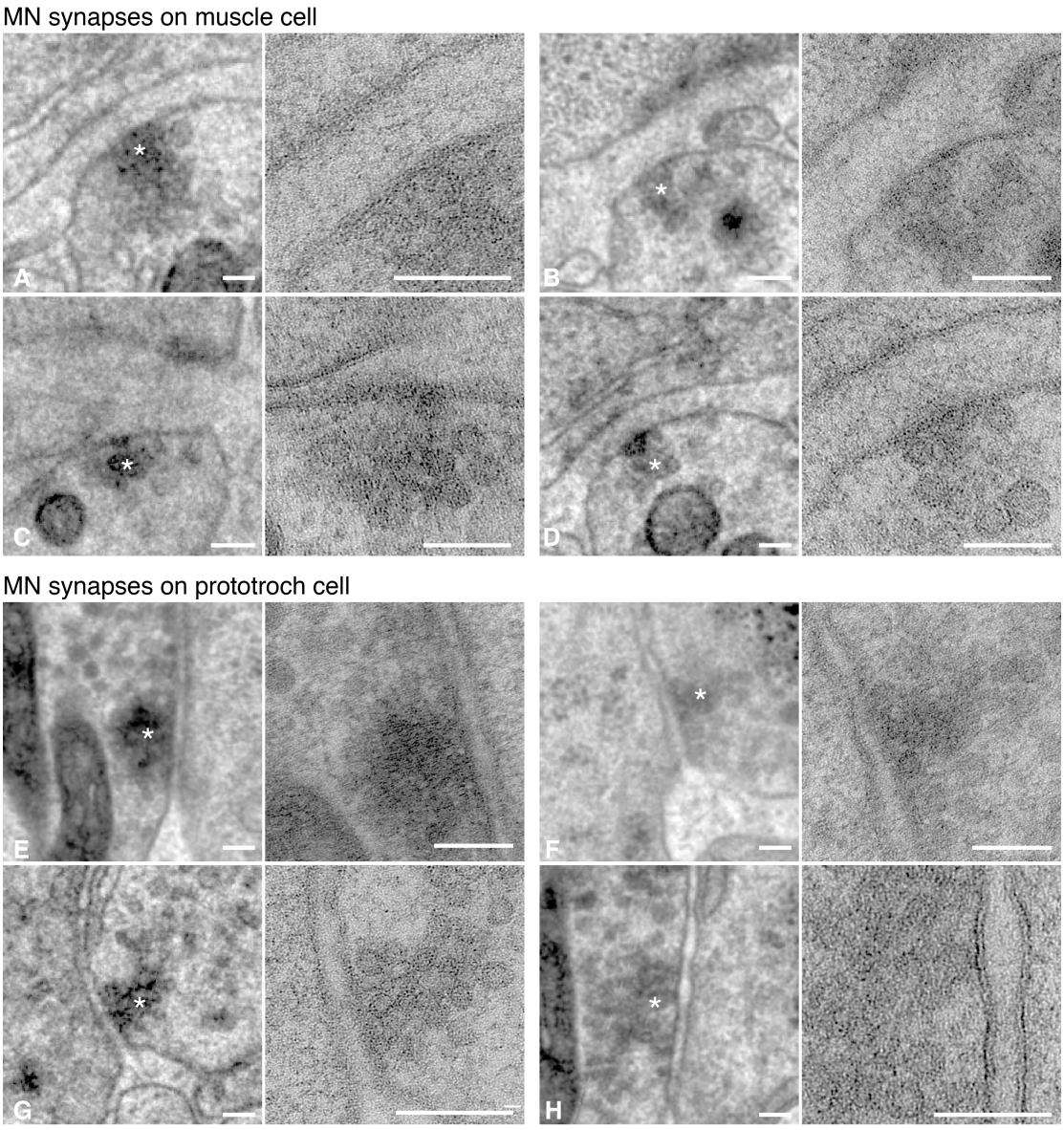

Figure 2–figure supplement 1.

Muscles and ciliary bands in 3-day old larvae.

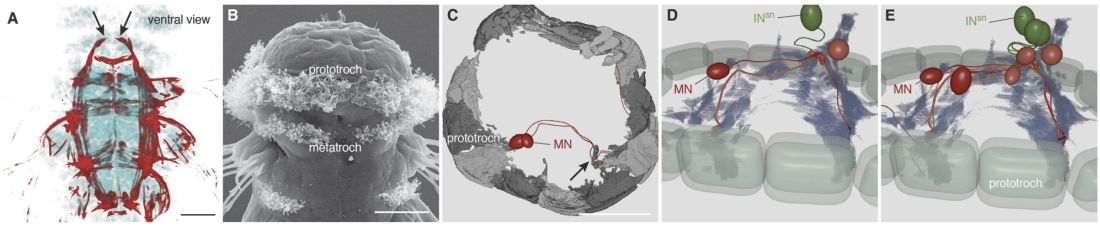

Figure 3–figure supplement 1.

Synaptic vesicle diameter for different synapse types.

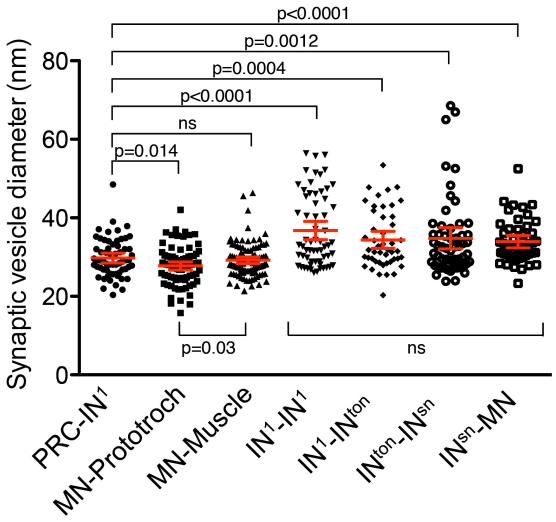

Figure 3–figure supplement 2.

Expression of neurotransmitter markers in the head of *Platynereis* larva.

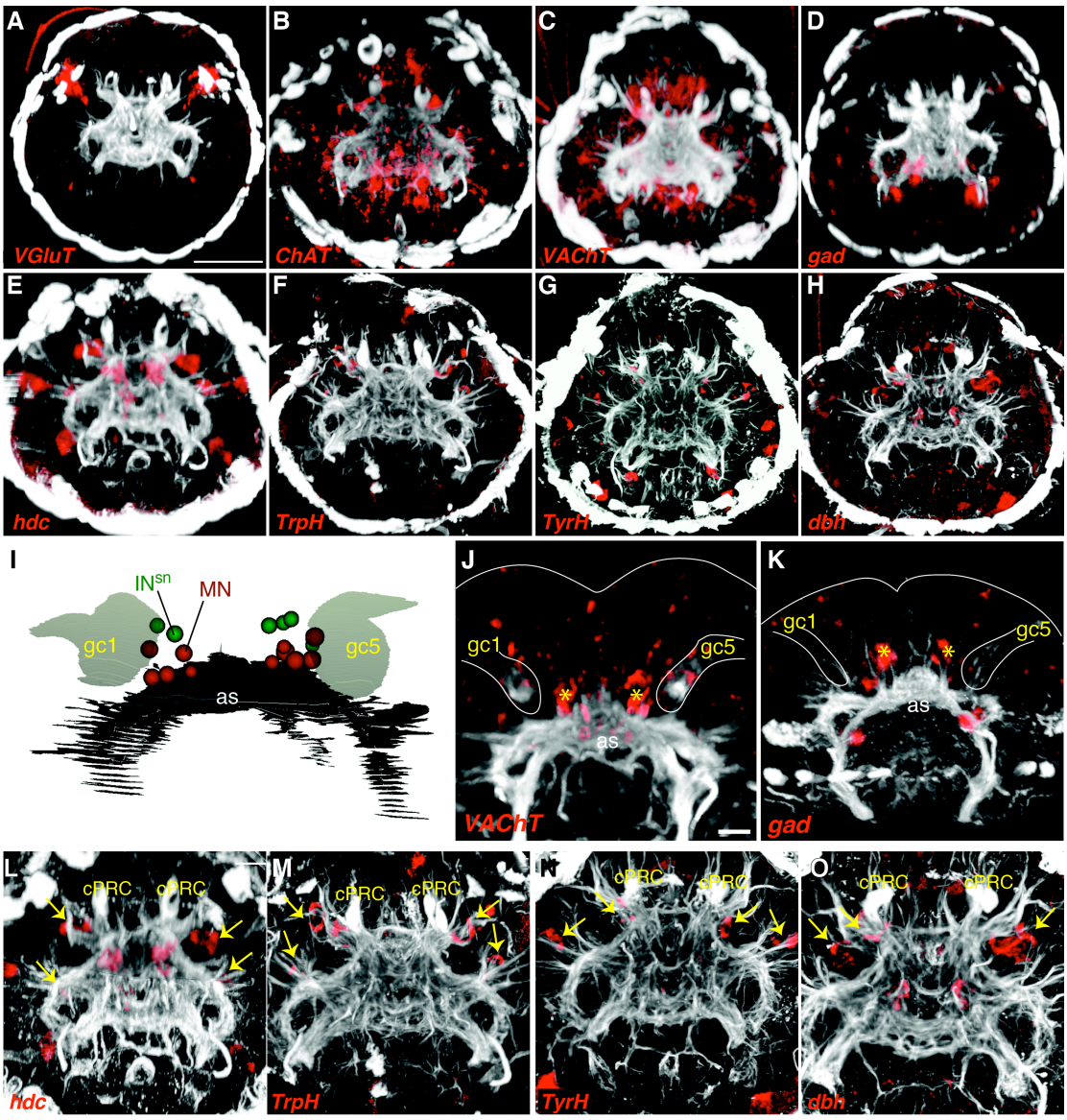

Figure 3–figure supplement 3.

Neurotransmitter marker gene expression profiling.

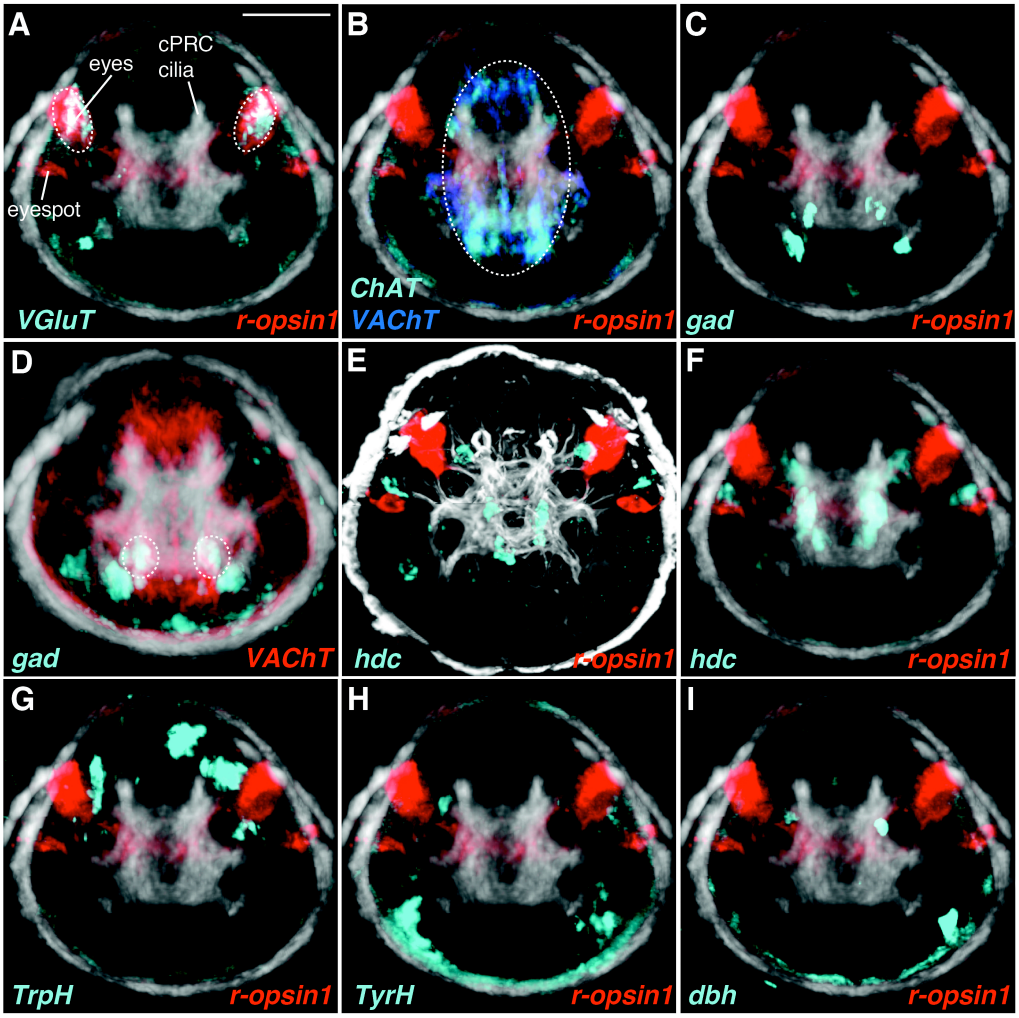

Figure 4–figure supplement 1.

Synaptic connectivity matrix of the *Platynereis* larval visual circuit.

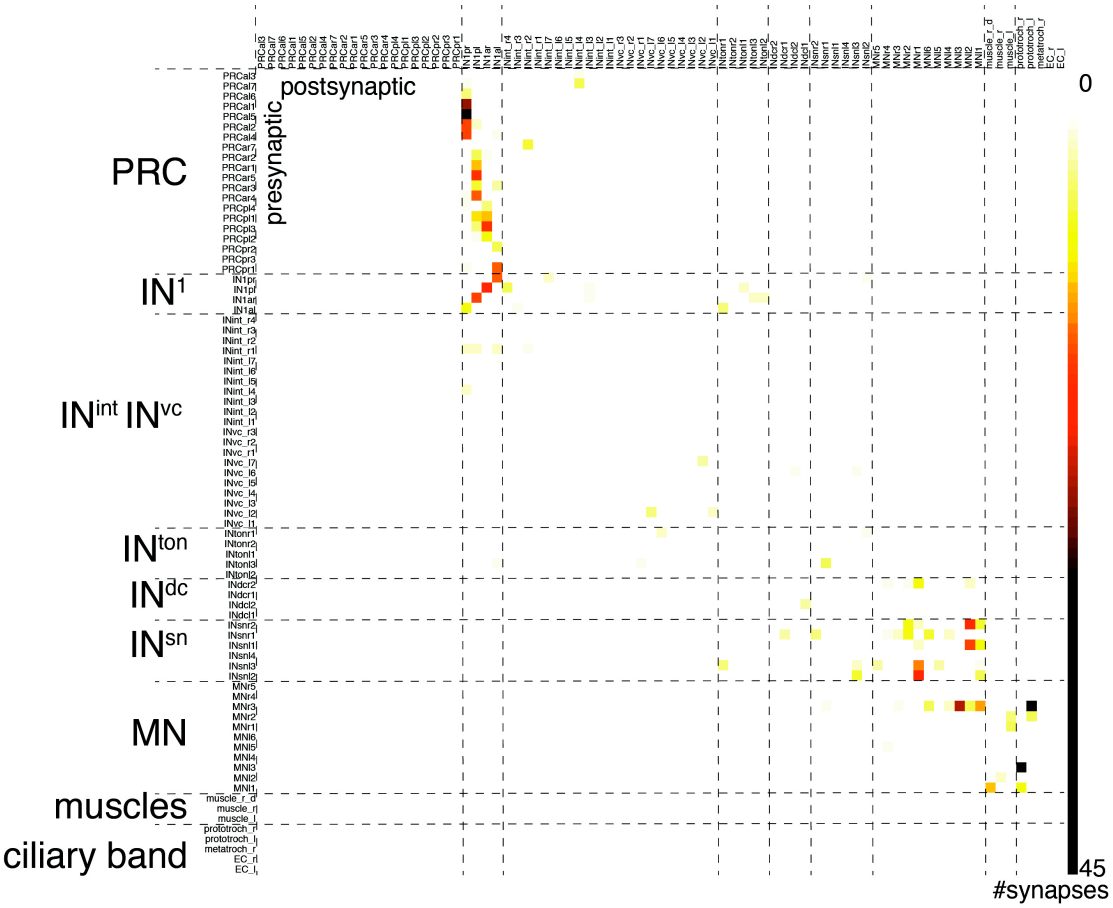

Figure 4–figure supplement 2.

Connectivity graphs of the *Platynereis* larval visual circuit.

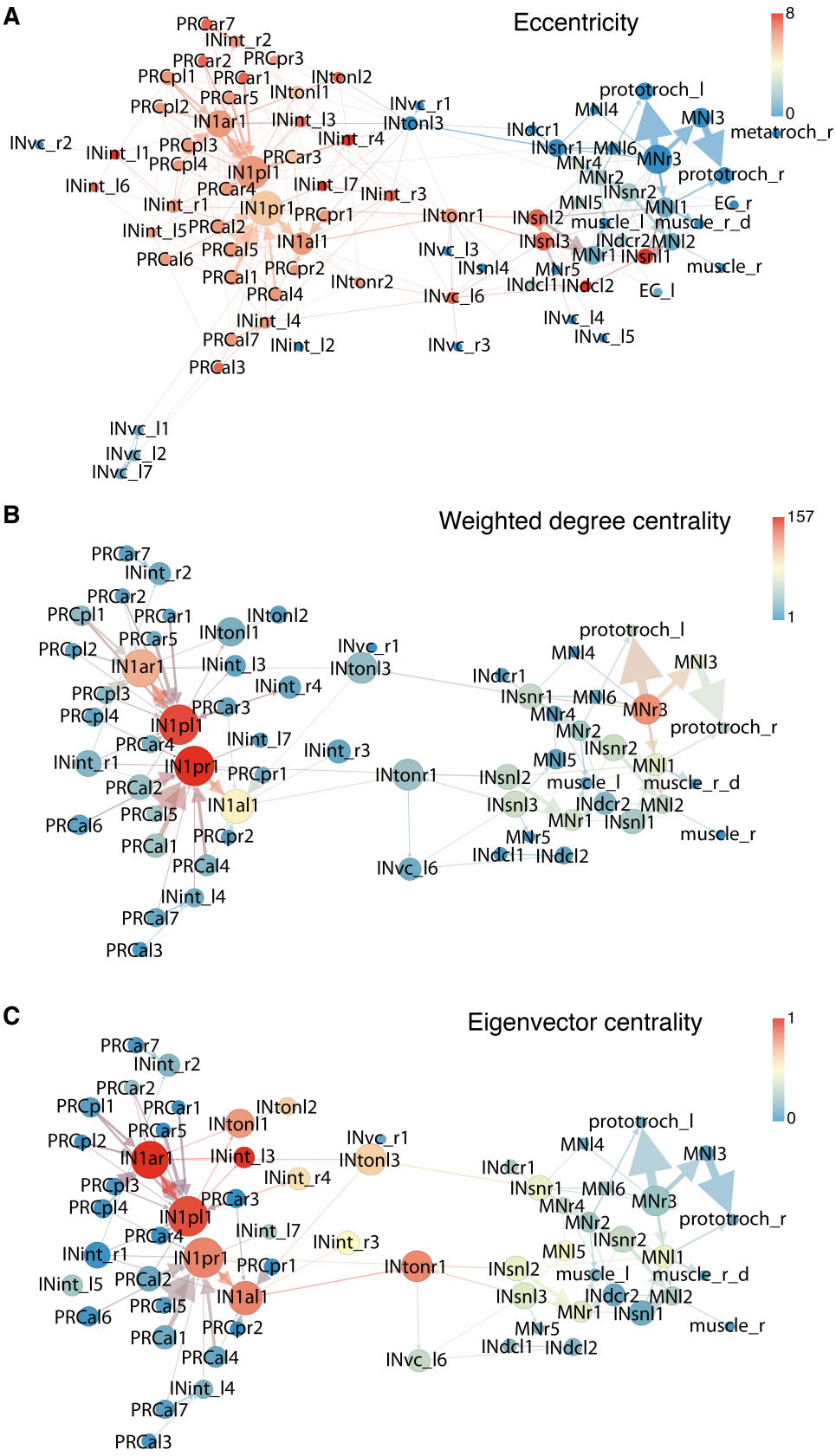

Figure 4–figure supplement 3.

Modules in the eye connectivity graph.

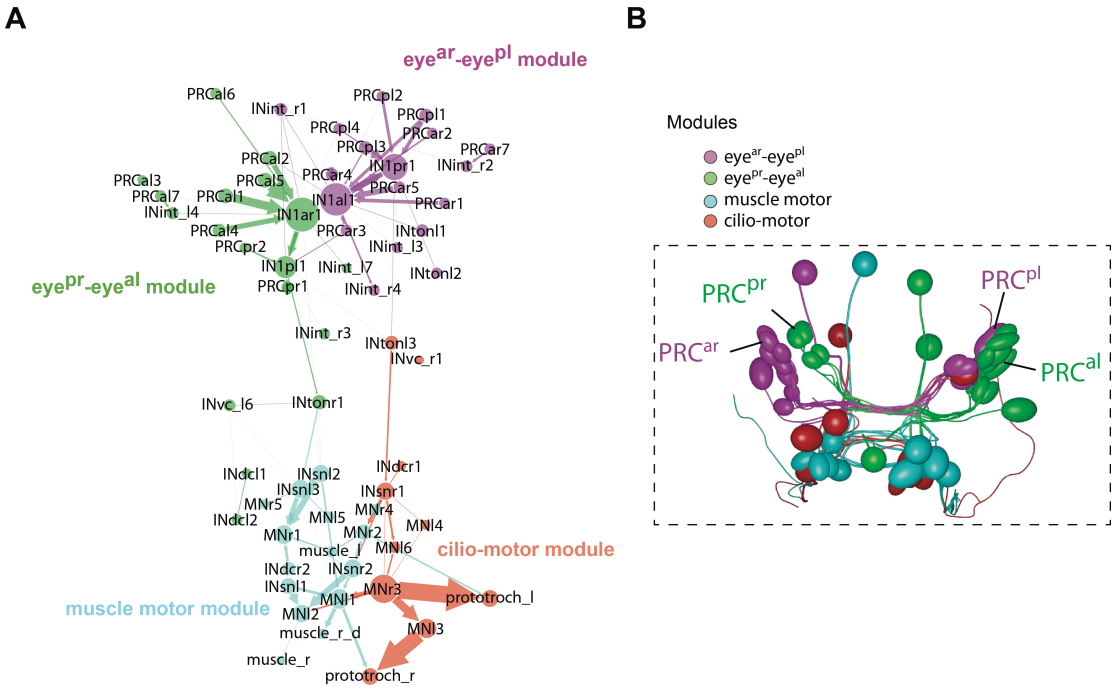

Figure 4–figure supplement 4.

Connectivity matrix of the left and right body sides.

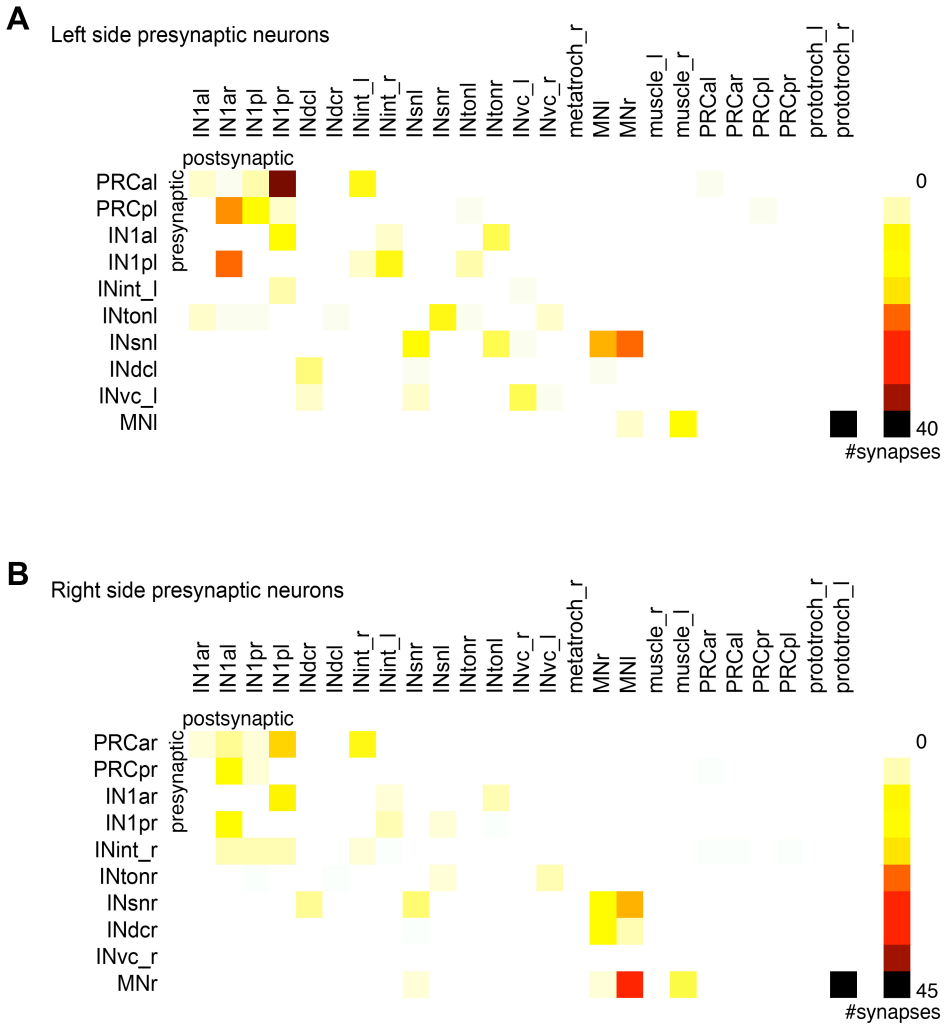

Figure 4–figure supplement 5.

Stereotypy of synapse distribution on IN^1 cells.

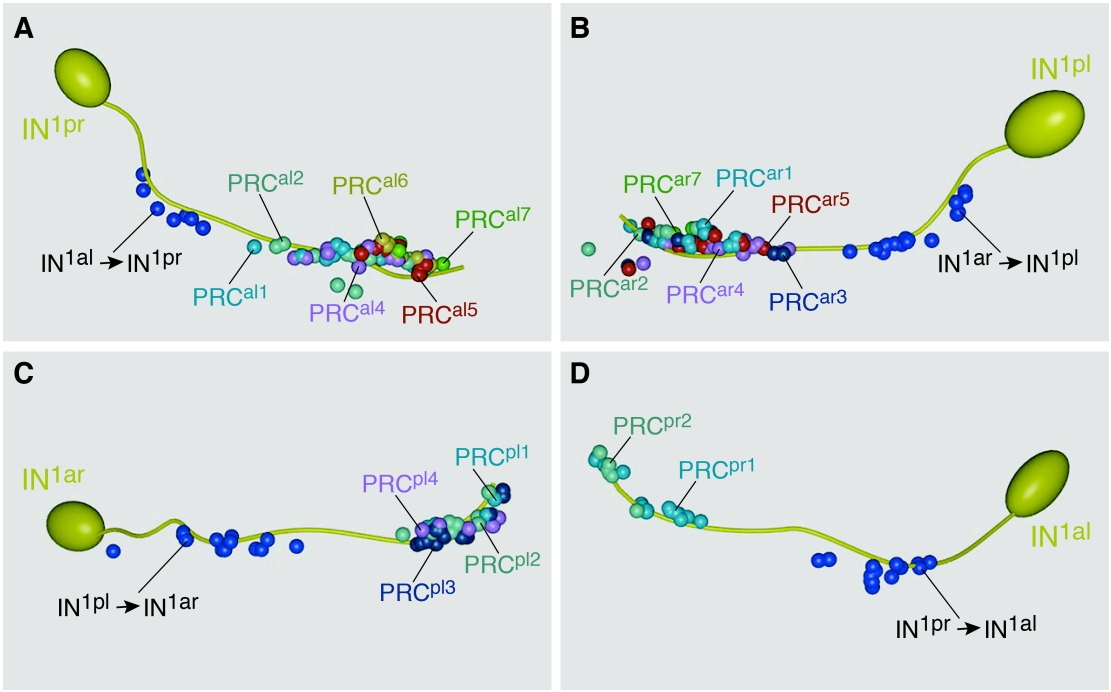

Figure 4–figure supplement 6.

Stereotypy of synapse distribution on IN^{ton} IN^{sn} and MN cells.

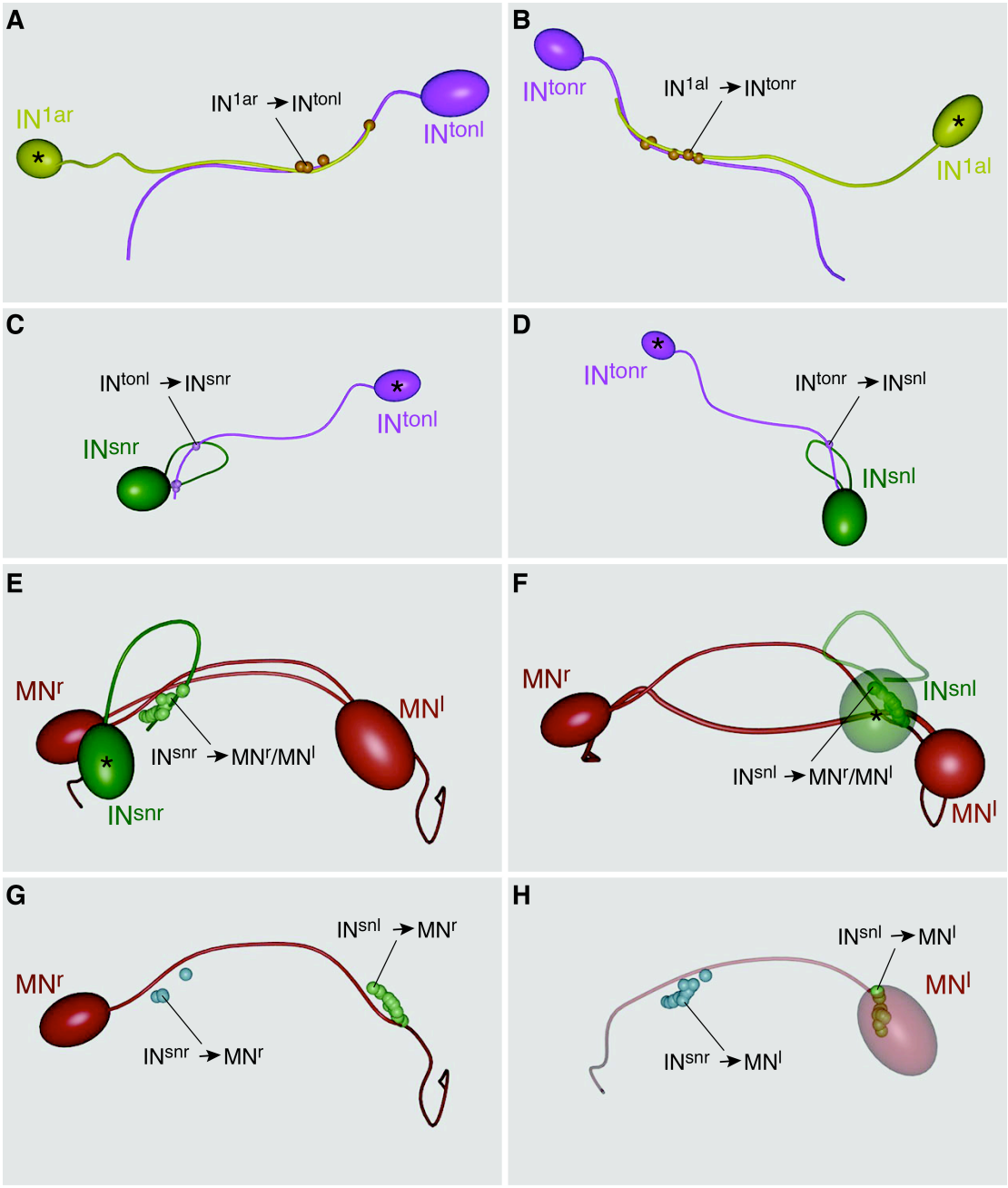

Figure 6–figure supplement 1.

Inhibition of phototaxis by a cholinergic antagonist.

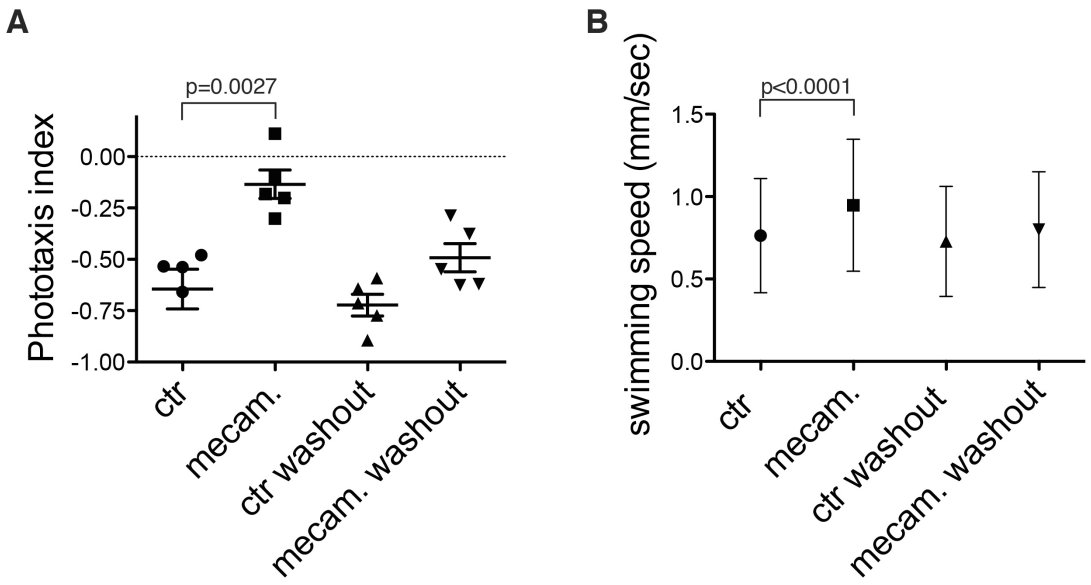

Figure 6–figure supplement 2.

Efficiency of phototaxis depends on contrast, not absolute light levels.

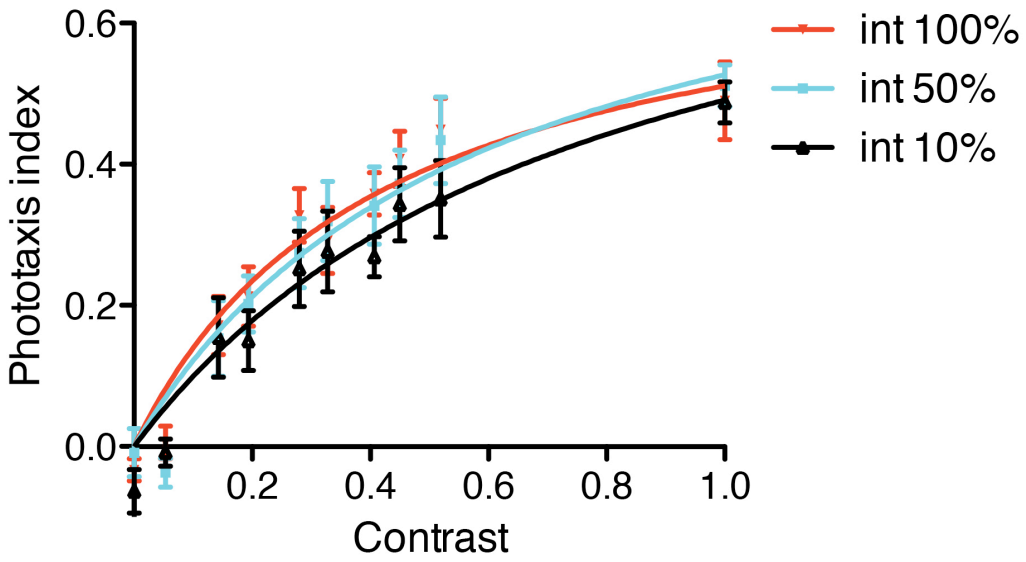

Figure titles and legends

Figure 1–figure supplement 1.

Morphology of photoreceptor cells reconstructed from serial TEM sections.

Tracing of the cell skeletons was complemented with partial volume reconstructions. The position of the cell body is marked with an asterisk.

Figure 1–figure supplement 2.

Morphology of IN^{1}, IN^{ton}, IN^{sn}, and IN^{dc} cells reconstructed from serial TEM sections.

Tracing of the cell skeletons was complemented with partial volume reconstructions. The position of the cell body is marked with an asterisk.

Figure 1–figure supplement 3.

Morphology of IN^{int} and IN^{vc} cells reconstructed from serial TEM sections.

Tracing of the cell skeletons was complemented with partial volume reconstructions. The position of the cell body is marked with an asterisk.

Figure 1–figure supplement 4.

Morphology of motorneurons reconstructed from serial TEM sections.

Tracing of the cell skeletons was complemented with partial volume reconstructions. The position of the cell body is marked with an asterisk.

Figure 1–figure supplement 5.

Axon diameter and synapse size in the *Platynereis* larval connectome.

(**A**) Histogram showing axon diameter (n=102). (**B**) Histogram showing synapse size defined as the number of consecutive sections in which a synapse was visible (n=100).

Figure 1–figure supplement 6.

Synapses of photoreceptors and IN^{1} cells.

Examples of PRC to PRC (**A**-**C**) and PRC to IN^{1} synapses (**D**-**G**). The left and right panels show the same synapse at different resolution (left: 3.7 nm/pixel, right: 0.2 nm/pixel). Asterisks mark the synapse, which is shown at higher resolution in the right panel. Scale bar, 100 nm.

Figure 1–figure supplement 7.

Synapses of IN^{1} cells.

Examples of IN^{1} to IN^{1} (**A**-**D**) and IN^{1} to IN^{ton} synapses (**E**-**H**). The left and right panels show the same synapse at different resolution (left: 3.7 nm/pixel, right: 0.2 nm/pixel). Asterisks mark the synapse, which is shown at higher resolution in the right panel. Scale bar, 100 nm.

Figure 1–figure supplement 8.

Synapses of IN^{ton} cells and IN^{sn} cells.

Examples of IN^{ton} to IN^{sn} (**A**-**D**) and IN^{sn} to MN synapses (**E**-**H**). The left and right panels show the same synapse at different resolution (left: 3.7 nm/pixel, right: 0.2 nm/pixel). Asterisks mark the synapse, which is shown at higher resolution in the right panel. Scale bar, 100 nm.

Figure 1–figure supplement 9.

Synapses of motorneurons.

Examples of MN to muscle cell (**A**-**D**) and MN to prototroch cell synapses (**E**-**H**). The left and right panels show the same synapse at different resolution

(left: 3.7 nm/pixel, right: 0.2 nm/pixel). Asterisks mark the synapse, which is shown at higher resolution in the right panel. Scale bar, 100 nm.

Figure 2–figure supplement 1.

Muscles and ciliary bands in 3-day old larvae.

(**A**) Phalloidin staining of the musculature (red) in a 3-day-old larva, ventral view. Arrows point at the most anterior tip of the dorsal longitudinal muscles. Nuclei are labeled with DAPI (cyan). (**B**) SEM micrograph of a 3-day old larva (ventral view) showing the prototroch and metatroch ciliary bands. (**C**) ssTEM reconstruction of the prototroch cells. Two MN cells are also shown. One of the prototroch cells extends a long projection towards the MN axons and receives synaptic input there (arrow). (**D**,**E**) Bilateral divergence of the circuit at the level of the MNs. SN cells connect to both ipsilateral and contralateral MNs at their proximal or distal axon segments respectively. The position of synapses from SN to MN cells are shown. In (**D**) only two MNs are shown for clarity. Scale bars 30 µm.

Figure 3–figure supplement 1.

Synaptic vesicle diameter for different synapse types.

Scatter plot of the diameter of synaptic vesicles of different synapse types. The labels indicate the pre- and postsynaptic neurons. Vesicle diameter was measured from high-resolution (0.2 nm/pixel) images. Mean with 95% confidence interval are shown. n >47 vesicles for each synapse type. p-values of an unpaired t test with Welch's correction are indicated relative to synaptic vesicles of the photoreceptors.

Figure 3–figure supplement 2.

Expression of neurotransmitter markers in the head of *Platynereis* larva.

(A-**H)** Whole mount RNA *in situ* hybridization in 3-day-old larvae for neurotransmitter marker genes (red), counterstained with acetylated tubulin antibody (white). (**A**) Glutamatergic marker *vesicular glutamate transporter*

(*VGluT*), (**B**,**C**) cholinergic markers *choline acetyltransferase* (*ChAT*) and *vesicular acetylcholine transporter* (*VAChT*), (**D**) GABAergic marker *glutamate decarboxylase* (*gad*), (**E**) histaminergic marker *histidine decarboxylase* (*hdc*), (**F**) serotonergic marker *tryptophan hydroxylase* (*TrpH*), (**G**) dopaminergic marker *tyrosine hydroxylase* (*TyrH*), and (**H**) adrenergic marker *dopamine beta hydroxylase* (*dbh*). (**I**) Ventral view schematic based on EM data of cell body positions of motorneurons (MN) and Schnörkel interneurons (IN^{sn}) relative to the larval axonal scaffold (as) and two gland cells (gc1, gc5). (**J**,**K**) Close-up of whole mount RNA *in situ* hybridization of (**J**) cholinergic marker *VAChT* and (**K**) GABAergic marker *gad*. Gland cells (gc) are indicated by a white outline. Yellow asterisks mark the ventral domain of gene expression. (**L**-**O**) Close-up of panels (E-H) showing whole mount RNA *in situ* hybridizations of (**L**) *hdc* (**M**) *TrpH* (**N**) *TyrH* (**O**) *dbh*. Yellow arrows indicate areas of gene expression in the region of the interneurons. The sensory cilia of the ciliary photoreceptor cells (cPRC) are indicated. (**A**-**H**, **L**-**O**) are anterior views, (**I**-**K**) are ventral views. Scale bar: (**A**-**H**) 50 µM, (**J**-**O**) 10 µM.

Figure 3–figure supplement 3.

Neurotransmitter marker gene expression profiling.

The spatial relationships and colocalization of neurotransmitter marker genes were characterized by image registration and double RNA *in-situ* hybridization in 3-day-old *Platynereis* larvae. (**A**-**D**, **F**-**I**) Average expression patterns of neurotransmitter marker genes and *r-opsin1* projected onto a common whole-body nuclear reference template. An average acetylated tubulin signal (white) was also projected onto the reference. Colocalization of registered genes in the average gene expression 3D image stacks is indicated by white and highlighted by dashed circles. **(E)** Double whole mount RNA *in-situ* hybridization for *hdc* (cyan) and *r-opsin-1* (red) counterstained with acetylated tubulin antibody (white). All images are anterior views. Scale bar 50 µM. Average 3D image stacks are available in (21).

Figure 4–figure supplement 1.

Synaptic connectivity matrix of the *Platynereis* larval visual circuit.

The synaptic connectivity matrix represents synaptic connections between 71 neurons and 8 effectors.

Figure 4–figure supplement 2.

Connectivity graphs of the *Platynereis* larval visual circuit.

Nodes correspond to single neurons, edges represent connections, weighted by synapse number. The layout is based on force field clustering. Nodes in the full (**A**) or the trimmed (**B**, **C**) graphs were colored by eccentricity (**A**), weighted degree centrality (**B**) or eigenvector centrality (**C**). In (**A**) all cells and connections of the minimal eye circuit are shown, in (**B**, **C**) cells connected with <3 synapses and edges <3 synapses were removed.

Figure 4–figure supplement 3.

Modules in the eye connectivity graph.

(**A**) Trimmed connectomic graph of the visual eye circuit including 56 neurons and 5 effectors (muscles and ciliary band cells). Colors indicate the four modules of the network. Edges are colored as their source node. (**B**) Anatomical position of the cells of the four modules. The cells are colored as in (**A**), according to their module association.

Figure 4–figure supplement 4.

Connectivity matrix of the left and right body sides.

Synaptic connectivity matrix of cells with a cell body on the left (**A**) and right (**B**) body side.

Figure 4–figure supplement 5.
Stereotypy of synapse distribution on IN^1 cells.

Spatial distribution of synapses onto axons of the posterior right (**A**), posterior left (**B**), anterior right (**C**), and anterior left (**D**) IN^1 axons. Synapses of individual PRCs to IN^1 axons are shown in different colors. The cell-body proximal synapses from the axons of the respective crosswise IN^1 cell are also shown.

Figure 4–figure supplement 6.

Stereotypy of synapse distribution on IN^{ton} IN^{sn} and MN cells.

Spatial distribution of synapses between (**A**, **B**) IN^1 and IN^{ton}, (**C**, **D**) IN^{ton} and IN^{sn} and (**E**-**H**) IN^{sn} and MN cells. Asterisks mark the presynaptic neuron.

Figure 6–figure supplement 1.

Inhibition of phototaxis by a cholinergic antagonist

Phototaxis index (**A**) and swimming speed (**B**) of control 3-day-old larvae and larvae treated with the acetylcholine receptor antagonist mecamylamine (50 μm). Data are shown as scatter plots with mean ± s.e.m. The phototaxis index is a population measure, the data are from five replicate experiments, each with >14 larvae. Swimming speed was averaged for single larvae (n>14 larvae). P-values of unpaired t-tests relative to control larvae are shown. Source data are available from (21)

Figure 6–figure supplement 2.

Efficiency of phototaxis depends on contrast, not absolute light levels.

Larval phototaxis was measured in a cuvette illuminated from both sides. The stimulus light was dimmed on one side by adding progressively more 10% or 25% neutral density filters. The experiment was performed with 100%, 50% and 10% starting white light intensity. Data are shown as mean ± s.e.m. The data points were fitted with a saturation binding-curve. Contrast is defined as $(I_{max}-I_{min})/(I_{max}+I_{min})$ where I_{max} and I_{min} are maximum and minimum intensity.

Expression dynamics and protein localization of rhabdomeric opsins in *Platynereis* larvae

Integrative and Comparative Biology Advance Access published May 10, 2013

Integrative and Comparative Biology

Integrative and Comparative Biology, pp. 1–10
doi:10.1093/icb/ict046

Society for Integrative and Comparative Biology

SYMPOSIUM

Expression dynamics and protein localization of rhabdomeric opsins in *Platynereis* larvae

Nadine Randel, Luis A. Bezares-Calderón, Martin Gühmann, Réza Shahidi and Gáspár Jékely[1]

Max Planck Institute for Developmental Biology, Spemannstrasse 35, 72076 Tuebingen, Germany

From the symposium "Integrating Genomics with Comparative Vision Research of the Invertebrates" presented at the annual meeting of the Society for Integrative and Comparative Biology, January 3–7, 2013 at San Francisco, California.

[1]E-mail: gaspar.jekely@tuebingen.mpg.de

Synopsis The larval stages of polychaete annelids are often responsive to light and can possess one to six eyes. The early trochophore larvae of the errant annelid *Platynereis dumerilii* have a single pair of ventral eyespots, whereas older nectochaete larvae have an additional two pairs of dorsal eyes that will develop into the adult eyes. Early *Platynereis* trochophores show robust positive phototaxis starting on the first day of development. Even though the mechanism of phototaxis in *Platynereis* early trochophore larvae is well understood, no photopigment (opsin) expression has yet been described in this stage. In late trochophore larvae, a rhabdomeric-type opsin, *r-opsin1*, expressed in both the eyespots and the adult eyes has already been reported. Here, we identify another *Platynereis* rhabdomeric opsin, *r-opsin3*, that is expressed in a single photoreceptor in the eyespots in early trochophores, suggesting that it mediates early larval phototaxis. We also show that *r-opsin1* and *r-opsin3* are expressed in adjacent photoreceptor cells in the eyespots in later stages, indicating that a second eyespot-photoreceptor differentiates in late trochophore larvae. Using serial transmission electron microscopy (TEM), we identified and reconstructed both photoreceptors and a pigment cell in the late larval eyespot. We also characterized opsin expression in the adult eyes and found that the two opsins co-express there in several photoreceptor cells. Using antibodies recognizing r-opsin1 and r-opsin3 proteins, we demonstrate that both opsins localize to the rhabdomere in all six eyes. In addition, we found that *r-opsin1* mRNA is localized to, and translated in, the projections of the adult eyes. The specific changes we describe in opsin transcription and translation and in the cellular complement suggest that the six larval eyes undergo spectral and functional maturation during the early planktonic phase of the *Platynereis* life cycle.

Introduction

Positive phototaxis of early larval stages is a widespread phenomenon among marine invertebrates, characteristic of approximately 80% of the benthic invertebrates with a pelagic larva (Thorson 1964). Simple larval eyes, sometimes consisting of only a single photoreceptor cell with shading pigment (Nordström et al. 2003), or a photoreceptor cell and a pigment cell (Jékely et al. 2008), are known to mediate larval phototaxis. Simple larval eyes are widespread among marine invertebrates and have been characterized morphologically in the larval stages of sponges (Leys and Degnan 2001), cnidarians (Nordström et al. 2003), annelids (Bartolomaeus 1992a), mollusks (Bartolomaeus 1992b), nemerteans (Döhren and Bartolomaeus 2007), flatworms (Eakin and Brandenburger 1981), brachiopods (Passamaneck et al. 2011), hemichordates (Brandenburger et al. 1973), cephalochordates (Lacalli 1996), and crustaceans (Lacalli 2009). In contrast to the wealth of morphological studies, few studies have focused on the molecular and functional characterization of larval eyes (Jékely et al. 2008; Passamaneck et al. 2011; Vopalensky et al. 2012). A better understanding of the molecular and functional characteristics of the eyes of larval marine invertebrates would allow a more reliable reconstruction of early stages of evolution of eyes in bilaterians, because the eyes of some larvae may have retained an ancestral organization (Arendt and Wittbrodt 2001; Jékely et al. 2008). In particular, opsins, the seven-transmembrane

G-protein-coupled receptors responsible for light detection, have received most attention in comparative studies of photoreceptors. Opsins are phylogenetically stable markers of photoreceptor types and their molecular divergences may have paralleled the functional divergence of photoreceptors (Arendt 2003). Divergences of opsins also contribute to the evolution of spectral diversity among photoreceptors (Porter et al. 2009).

The larval eyespots of the marine annelid *Platynereis dumerilii* are among the most well-characterized simple larval eyes (Jékely et al. 2008). *Platynereis* eyespots develop laterally in the episphere of the early trochophore larva (for staging see Fischer et al. 2010) and are present throughout larval stages, and might persist in the adult as frontolateral eyelets (Backfisch et al. 2013). The eyespots consist of a rhabdomeric photoreceptor cell and an associated shading pigment cell (Rhode 1992), and mediate positive phototaxis of the helical-swimming larva from 24 hours post fertilization (hpf) onward (developing at 18 °C). The axon of the eyespot photoreceptor directly synapses on the ipsilateral multiciliated cells of the ciliary band (prototroch) and upon stimulation, cholinergic signals from the photoreceptor reduce the frequency of ciliary beats and change the ciliary stroke pattern in the adjacent prototroch cells (Jékely et al. 2008). These changes are triggered at every 180° rotation by the alternating illumination of the two eyespots and steer the helical trajectories toward the light source. Despite these advances, no opsin has yet been described in the eyespots of the early *Platynereis* trochophore.

In late trochophore larvae (40–48 hpf), two additional pairs of eyes start to develop in the dorsal episphere (Rhode 1992; Arendt et al. 2002). The newly developing eyes represent the precursors of the adults' pigment-cup eyes (henceforth referred to as 'adult eyes', also when discussing larval stages). These are everse, cerebral eyes consisting of several pigment and photoreceptor cells, the number of which increases with age. The adult eyes also have a lens, formed by the apical protrusions of the pigment cells. The photoreceptor rhabdomeres are located inside the pigment cup (Rhode 1992). The adult eyes express a rhabdomeric opsin (r-opsin), *r-opsin1* (Arendt et al. 2002). This opsin is also expressed in the eyespots after 2 days post fertilization (dpf), long after the onset of phototactic behavior (Arendt et al. 2002). Three other *Platynereis* opsins *r-opsin2* (D. Arendt, EMBL, personal communication), *r-opsin3*, and *r-opsin-4* have been identified, but their expression patterns have not yet been characterized.

Here, we characterize the expression of *Platynereis r-opsin3* and characterize its co-expression with *r-opsin1* both at the transcript level and at the protein level. Using serial TEM, we also reconstruct the morphology of the cellular complements of the eyespots in the nectochaete larva. Our results indicate a spectral and functional maturation of the eyes of the *Platynereis* nectochaete larva.

Materials and methods

Molecular phylogeny

We selected a subset of arthropod and lophotrochozan r-opsin sequences from the NCBI non-redundant and EST databases, and from the *Capitella teleta* and *Lottia gigantea* genome projects at JGI (http://genome.jgi.doe.gov/). r-Opsin protein sequences were aligned with MUSCLE (Edgar 2004). The profile thus obtained was merged to an alignment of ciliary opsins using PRANK (Loytynoja and Goldman 2008). The resulting alignment was cropped at both ends to remove poorly aligned regions.

We inferred opsin phylogeny using two methods. First, we performed a maximum-likelihood analysis using PhyML3.0 (Guindon et al. 2010) and the aLRT statistics to evaluate the likelihood of each node. We used an LG + G + I model and the best of NNI + SPR search strategies for the inference. Next, we ran a Bayesian analysis with MrBayes 3.2 (Ronquist et al. 2012) using the following parameters: two million generations with sampling each 100 generations, four chains per each of two independent runs, a chain temperature of 0.25, and an initial burn-in fraction of 0.5. We estimated the substitution model, the gamma parameter, and invariant sites. We stopped the analysis after the average standard deviation of split frequencies was equal to or less than 0.01. The resulting analysis reached this point after 220 000 generations. After analyzing convergence criteria with Tracer and with the compare function of AWTY (Nylander et al. 2008), we summarized the parameters and trees with a burn-in fraction of 0.5 (11 100 samples).

Generation of antibodies

Rabbits were immunized with synthetic peptides (CSEVLVPGSMSLDGLLTTAH for r-opsin1 and CSKPQAAPKGKGGKDN for r-opsin3) coupled to an adjuvant (lipoadjuvant Pam3) via an N-terminal Cys. Sera were affinity-purified on the respective peptide epitopes coupled to a SulfoLink resin (Thermo Scientific, Rockford, IL), as described by Conzelmann and Jékely (2012). Upon elution, we fractionated the bound antibodies using a 100 mM

glycine buffer of decreasing pH (4.7 to 2.0). For the r-opsin3 antibody, the yield of high-affinity antibody was very low; therefore, we are unable to provide it.

Staining of tissues

Single and double *in situ* hybridization and immunostaining were performed as previously described (Tessmar-Raible et al. 2005; Conzelmann and Jékely 2012).

Transmission electron microscopy

Seventy-two-hpf *Platynereis* larvae were fixed using a high-pressure freezer (BAL-TEC HPM 010, Balzers, Liechtenstein) and transferred to liquid nitrogen. Frozen samples were cryosubstituted with 2% osmium tetroxide in acetone and 0.5% uranyl acetate in a cryosubstitution unit (Leica EM AFS-2) over a regime of gradually rising temperatures. Samples were embedded in Epon. Fifty nanometer (nm) serial sections were cut on a Reichert Jung Ultracut E microtome. The sections were collected on single-slotted copper grids (NOTSCH-NUM 2 × 1 mm, Science Service, München) with Formvar support film, contrasted with uranyl acetate and Reynold's lead citrate, and carbon coated to stabilized the film. Image acquisition of serial sections was performed at a pixel size of 3.72 nm on a FEI TECNAI Spirit transmission electron microscope equipped with an UltraScan 4000 4X4k digital camera using the image acquisition software Digital Micrograph (Gatan Software Team Inc., Pleasanton). Stitching and alignment were accomplished using TrakEM2 (Cardona et al. 2010). All structures were segmented manually as area-lists, and exported into 3Dviewer and Blender.

Results

Identification of a novel r-opsin in *P. dumerilii*

In an unpublished mixed-stages *Platynereis* EST library (available at http://jekely-lab.tuebingen.mpg.de/), we identified a partial and a full-length clone encoding two different rhabdomeric-type opsins. Using Rapid Amplification of cDNA Ends (RACE), we obtained the missing coding region and the 5′-UTR for the partial clone, allowing us to isolate a full-length sequence from *Platynereis* cDNA. Both cDNAs encode an opsin protein with seven predicted transmembrane helices and a conserved lysine in the seventh transmembrane helix, a defining feature of opsins (Terakita 2005). Following the seventh transmembrane helix, the opsins have a highly conserved histidine–proline–arginine (HPR) tripeptide motif that is shared with other r-opsins (HPK or HPR) (Arendt 2004), identifying them as r-opsins. We named these *Platynereis* opsin genes *r-opsin3* (KC810971) and *r-opsin4* (KC810972). We will refer to the first identified r-opsin as *r-opsin1* (Arendt et al. 2002).

To better understand the relationship of r-opsin3 and r-opsin4 to other r-opsins, we performed molecular phylogenetic analyses. In a tree of select opsins, r-opsin3 clustered together with high support with an opsin from the sedentary annelid *C. teleta*. The r-opsin1 sequence was an outgroup to the r-opsin3 sequences (Fig. 1). This tree topology indicates that the duplication event giving rise to the *r-opsin1* and *r-opsin3* paralogs predates the divergence of the two major annelid lineages, Errantia and Sedentaria (Struck et al. 2011). These opsins formed a well-supported clade (Clade II) with some mollusk r-opsins. We could identify another stable r-opsin clade (Clade I) with both mollusk and annelid sequences. This clade includes the *Platynereis r-opsin4* and a *C. teleta* r-opsin.

Spatial and temporal pattern of expression of *r-opsin3* and *r-opsin1* in *Platynereis* larval stages

To analyze the expression of *r-opsin3* during the development of *Platynereis*, we performed whole-mount *in situ* hybridization on various larval stages and adults (Fig. 2A–E). In contrast to *r-opsin1*, which is not expressed until the onset of differentiation of the photoreceptor in the adult eye at 43 hpf (Arendt et al. 2002), we detected prominent expression of *r-opsin3* already in 24-hpf larvae (Fig. 2F). The *r-opsin3* is expressed in single cells in the position of the eyespots. The *in situ* signal in each cell is associated with an apical dendrite labeled by acetylated-tubulin.

To characterize the expression of *r-opsin3* in the eyespots at cellular resolution, we performed double *in situ* hybridization with *r-opsin3*-specific and *FVRIamide-precursor*-specific probes. *FVRIamide precursor* is a proneuropeptide gene expressed in the eyespot photoreceptor in early *Platynereis* larvae (Jékely et al. 2008). An antibody against the active FVRIamide neuropeptide labels the axonal projection of the photoreceptor cell to the ciliary band (Jékely et al. 2008). Confocal microscopic imaging of double *in situ* hybridization samples revealed cellular co-expression of the two genes in 24-hpf larvae (Fig. 2P). We also detected the expression of *r-opsin3* in the eyespots in 48-hpf and 72-hpf larvae, but not in 5-dpf and 15-dpf larvae (Fig. 2G–J). The *r-opsin3* is also expressed in the adult eyes from 48 hpf onward including adult stages (Fig. 2G–J,

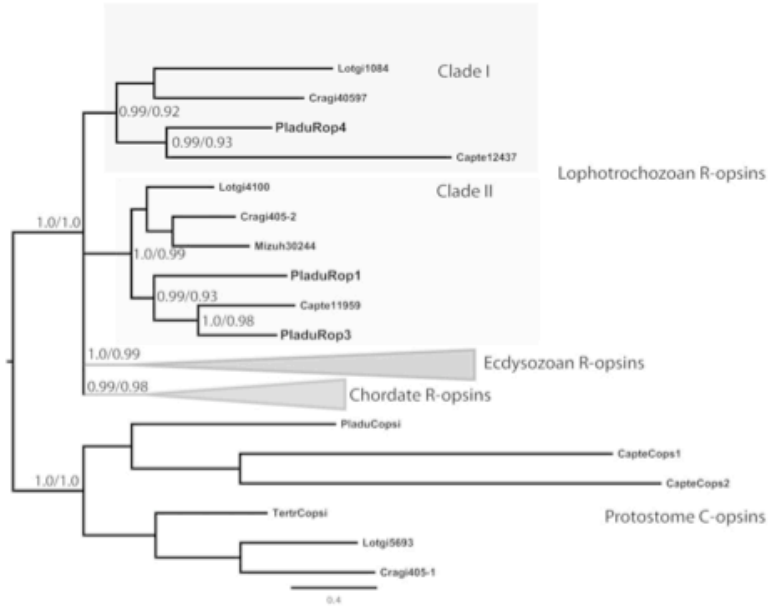

Fig. 1 Phylogenetic tree of protostome r-opsins. Bayesian phylogenetic tree inferred from a protein alignment of protostome r-opsins and c-opsins. The tree shows that r-opsin1 and r-opsin3 diverged early during the evolution of annelids. Posterior probabilities of a Bayesian phylogeny (Bayesian posterior probability/aLRT value) and bootstrap values of a maximum-likelihood tree are indicated at the main nodes.

Supplementary Fig. S1). We could also detect expression of *r-opsin3* in the adult notopodia, in a position similar to that recently described for *r-opsin1* (Supplementary Fig. S1) (Backfisch et al. 2013).

In contrast to *r-opsin3*, *r-opsin1* is not expressed in the eyespots until the late trochophore stage (Arendt et al. 2002) (Fig. 2K). We also found strong *r-opsin1* expression in the eyespots at 15 dpf indicating that *r-opsin1* expression is maintained longer than that of *r-opsin3* (Fig. 2L–O). Expression of *r-opsin1* is strong in the adult eyes from 48 hpf onward and could also be detected in juveniles and adults (Figs. 2K–O and 3).

The late onset of *r-opsin1* expression in the eyespots suggested that the two opsins could co-express in the eyespot photoreceptor. To test this, we performed double *in situ* hybridization and confocal microscopy imaging experiments with *r-opsin1* and *r-opsin3*. We found that the two opsins are expressed in two adjacent cells in the eyespots in 56-hpf late trochophore larvae with *r-opsin1* labeling the more medial cell (Fig. 2Q and R). In 72-hpf nectochaete larvae, weak *r-opsin3* expression could also be detected in the more medial cell, co-expressing with *r-opsin1* (Fig. 2S). These findings were surprising, since previous ultrastructural work revealed the presence of only one photoreceptor in the eyespot. In contrast to the eyespots, in the adult eyes, we detected co-expression of the two opsins in the same photoreceptor cells (Fig. 2T). Co-expression of the two opsins in single photoreceptor cells was verified by detecting the cell borders with acetylated tubulin staining. The two signals from the double *in situ* hybridization show little overlap within the same cell due to the strong shadowing effect of the NBT/BCIP precipitate (Jékely and Arendt 2007). We could not detect the expression of r-opsin4 in various larval stages using *in situ* hybridization.

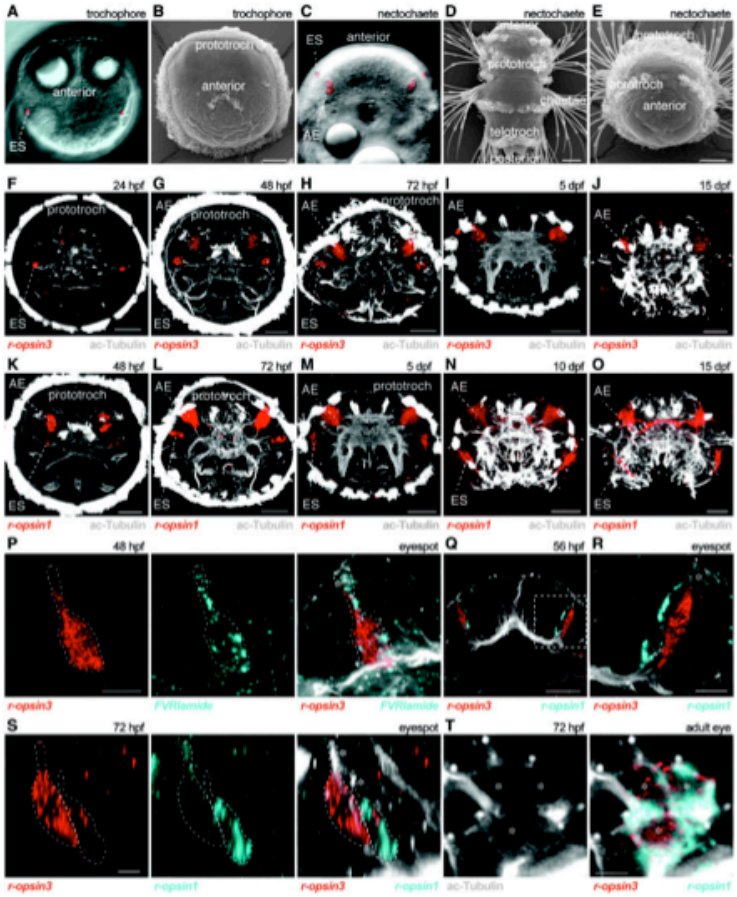

Fig. 2 Expression of *r-opsin3* and *r-opsin1* in *Platynereis* trochophore and nectochaete larvae. (**A**) Differential interference contrast (DIC) image of a 48-hpf larva with eyespots (red). (**B**) SEM image of a trochophore (48 hpf) larva. (**C**) DIC image of a 72-hpf larva with eyespots and adult eyes (red). (**D**, **E**) SEM images of nectochaete larvae (72 hpf) oriented dorsally (D) or anteriorly (E). (**F–J**) *In situ* hybridization in the indicated larval stages for *r-opsin3* (red) counterstained for acetylated tubulin (white). (**K–O**) *In situ* hybridization in the indicated larval stages for *r-opsin1* (red) counterstained for acetylated tubulin (white). (**P**) Double *in situ* hybridization for *r-opsin3* (red) and *FVRIamide precursor* (cyan) counterstained for acetylated tubulin (white) in a 48-hpf larva reveals co-expression in the photoreceptor cell of the eyespot. (**Q–T**) Double *in situ* hybridization for *r-opsin3* (red) and *r-opsin1* (cyan) counterstained for acetylated tubulin (white) in 56-hpf (Q, R) and 72-hpf (S, T) larvae reveals the expression of the two opsins in two adjacent photoreceptor cells of the eyespot (Q–S), and co-expression in the adult eye (T). In (A, C), the eyespot's pigment was highlighted using the reflection of the laser light in the confocal microscope. In (P–S), asterisks label the dendrites of the photoreceptor cells, in (T) the cell bodies of the photoreceptors. In (P, S), dashed lines mark the boundaries of the photoreceptor cells as revealed by the *in situ* and the acetylated-tubulin signals. The boxed area in (Q) is shown enlarged in (R). AE, adult eye; ES, eyespot. Scale bars: (B, D, E–O, Q): 30 µm, (P, R, S, T) 5 µm.

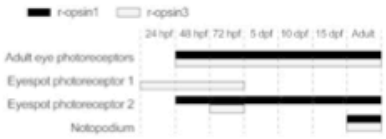

Fig. 3 Summary diagram of the expression patterns of *Platynereis* r-*opsin1* and r-*opsin3* in the photoreceptor cells of the adult eyes, eyespots, and parapodia in various larval and adult stages, based on the data in this article and Backfisch et al. (2013).

Serial TEM reconstruction of the morphology of the eyespot in a nectochaete larva

The results of the double *in situ* hybridization indicated that the eyespots differentiate a second photoreceptor in the late trochophore stage. An alternative possibility is that the pigment cell starts to express *r-opsin1*. To distinguish between these two possibilities, we performed serial-sectioning TEM (serial TEM) on 72-hpf nectochaete larvae and examined the ultrastructure of their eyespots. In contrast to the early trochophore larval stage, in which only one photoreceptor had been described in the eyespots (Rhode 1992; Jékely et al. 2008), we identified two photoreceptors and a pigment cell (Fig. 4A–E and H). The distal end of both photoreceptors had parallel microvilli protruding into the cup-shaped depression of the pigment cell (Fig. 4A and B). The photoreceptor with the more laterally located cell body had one cilium; the photoreceptor with the more medial cell body had two cilia with 9 + 0 microtubule doublets and associated basal bodies (Fig. 4C).

It has been shown that the single eyespot photoreceptor cell, expressing *FVRIamide-precursor*, synapses on the prototroch ciliary band in young trochophore larvae (Jékely et al. 2008). To test which of the two photoreceptors identified in the TEM sections corresponds to this cell (i.e., the cell that also expresses *r-opsin3*, based on the results of our double *in situ* hybridization) (Fig. 2P), we traced the axonal projection of both photoreceptors in several serial sections. The lateral cell projected an axon to, and synapses on, the cells of the ciliary band (Fig. 4F–H), identifying it as the *r-opsin3*-expressing photoreceptor. This axon then turns and projects toward the anterior axonal scaffold along the ventral branch of the circumaesophageal connectives (Fig. 4H and J). The axon of the medial, *r-opsin1*-expressing photoreceptor projects along the dorsal branch of the circumaesophageal connectives toward the anterior axonal scaffold (Fig. 4H and J). These results reveal an elaboration of the eyespot circuitry and point at possible functional changes.

Localization of the opsin proteins to the photoreceptor rhabdomere

Both the adult eye and the eyespot photoreceptors are of the rhabdomeric type and have apical membrane extensions characteristic of these photoreceptors (Rhode 1992). The r-opsins are most commonly localized to apical microvillar extensions in rhabdomeric photoreceptors, with some exceptions such as the vertebrate melanopsins (Hattar et al. 2002) and a sea urchin r-opsin (Ullrich-Lüter et al. 2011), which localize to the photoreceptor cell body, dendrites, and axons or to intracellular vesicles, respectively. Given these exceptions, it was important to test whether both r-opsin1 and r-opsin3 proteins localize to the apical microvilli in the eyes of *Platynereis* larvae. We developed affinity-purified specific antibodies against both r-opsins. Immunolabelings with both antibodies revealed strong and specific signals in the photoreceptor rhabdoms both in the adult eyes and in the eyespots, indicating that the antibodies are specific to the opsins (Fig. 4K–P).

In the eyespots, we could detect r-opsin3 in two structures associated with acetylated-tubulin signal, corresponding to the rhabdomeres of the two photoreceptors, consistent with the results from *in situ* hybridization (Fig. 4K and L). The r-opsin1 could only be detected in one apical structure associated with acetylated-tubulin signal, and also in the body of the photoreceptor cell (Fig. 4N and O).

In the adult eyes, we could detect both opsins in the photoreceptor's rhabdomeres and cell bodies (Fig. 4K, M, N, and P). Given that the pigment content of the adult eyes was preserved during fixation, we could correlate the antibody signal with the position of the pigment cup (Fig. 4M and P). In agreement with the morphology of the adult eyes (Rhode 1992) (Fig. 4I), the antibodies showed labeling inside the pigment cup, confirming that both opsins are also localized in the photoreceptor's rhabdomeres (Fig. 4M and P).

Using the r-opsin1 antibody, we also detected protein signal in the median brain of larvae. The signal localized to the area where the photoreceptors of the adult eyes project (Fig. 4R and S) (Backfisch et al. 2013). The photoreceptor projections were revealed by *in situ* hybridizations using the *r-opsin1* probe, also indicating that the *r-opsin1* mRNA is localized to the photoreceptor's axons (Fig. 4Q), as previously observed (Jékely and Arendt 2007). These results suggest that the *r-opsin1* mRNA is locally translated

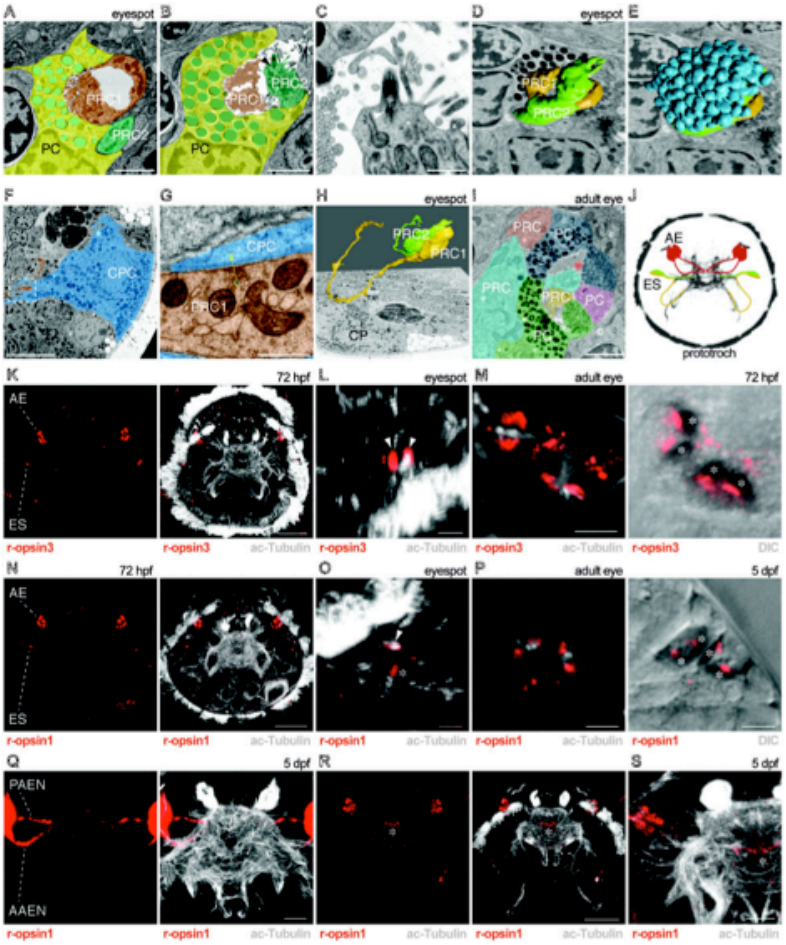

Fig. 4 Ultrastructure of eyes and immunohistochemical localization of opsins in *Platynereis* rhabdomeric photoreceptors. (**A–H**) Ultrastructure of an eyespot and the projection of the photoreceptor cells in a 72-hpf larva. (A, B) TEM images of an eyespot with the two rhabdomeric photoreceptor cells (orange, green), the pigment cell (yellow) and pigment granules (cyan) in two different layers. (C) TEM image of the apical end of a photoreceptor cell with a cilium. (D, E) TEM images of the eyespot with the reconstructed 3D structure of the two rhabdomers (D) and the pigment granules (E). (F, G) TEM images of the prototroch region. (F) Axon of a photoreceptor cell (orange) in close contact with a prototroch cell (cyan). (G) Close-up image of a synapse between the photoreceptor cell (orange) and the prototroch cell (cyan). (H) TEM image of the prototroch region with the reconstructed photoreceptor cells and their axons. (I) TEM image of an adult eye. Each cell is labeled with a different color. (J) Schematic drawing of the eyes and their projections to the apical nerve plexus. (K–M) Immunostaining for r-opsin3 (red) in 72-hpf larvae counterstained for acetylated tubulin

(continued)

in the axon terminals of the photoreceptors of the adult eyes.

Discussion

The identification of a second r-opsin in *Platynereis* broadens our molecular perspective on the light responses by the larvae of this model annelid. The onset of expression of *r-opsin3* in the eyespots correlates with the appearance of positive phototaxis in the larvae. This, together with the localization of the r-opsin3 protein to the photoreceptor's rhabdomere suggests that r-opsin3 is a functional phototaxis photoreceptor in early trochophore larvae. Given the relatively broad action spectrum (365–545 nm) of phototaxis in early larvae (Jékely et al. 2008), r-opsin3 may not be the only opsin mediating this behavior. The presence of two distinct photoreceptors expressing distinct opsins in the eyespots in later larval stages suggests that in older larvae, the eyespots may develop another function in addition to the regulation of phototaxis. The phototactic function of the eyespot may be maintained until *r-opsin3* is expressed in the ventral eyes. The sustained expression of *r-opsin1* in the eyespot throughout larval and juvenile stages indicates that the eyespots also function in later stages of development. The newly developing *r-opsin1*-expressing photoreceptor of the eyespot projects its axon to the apical nerve plexus rather than to the prototroch cell, suggesting that the eyespot develops more complex circuitry mediating aspects of photo-behavior other than phototaxis (for example, circadian entrainment).

A transgenic *Platynereis* line expressing enhanced green fluorescent protein (EGFP) under the control of the *cis*-regulatory elements of *r-opsin1* revealed the presence of pigment-associated eyelets (frontolateral eyelets) in juvenile and adult *Platynereis* (Backfisch et al. 2013). The continuous presence of *r-opsin1* in the eyespots throughout late larval stages (Fig. 2L–N), the presence of pigment, and the expression of *pax6* in the eyespot in early larval stages (Arendt et al. 2002) and in the frontolateral eyelets (Backfisch et al. 2013) argue that the frontolateral eyelets are equivalent to the eyespots.

Our phylogenetic tree suggests that the divergence of *r-opsin1* and *r-opsin3* predates the divergence of sedentary and errant annelids. We found that the two opsins are expressed in adjacent cells in the eyespots and co-express in the adult eyes. It would be interesting to test how common this is for annelids. Interestingly, the presence of two photoreceptors has been described in the eyespots of the sedentary annelids *Pectinaria koreni* and *Spirorbis spirorbis* (Bartolomaeus 1992a). Two-celled eyespots also occur in the Sipuncula (Blumer 1997), the likely sister group to the Errantia–Sedentaria clade (Struck et al. 2011). Further sampling of annelid opsins is needed to clarify the exact timing of duplication of *r-opsin1* and *r-opsin3*.

Some mollusk r-opsins form a clade (Clade II) with annelid *r-opsin1* and *r-opsin3*. Several mollusks have everse rhabdomeric eyes both in the larval and the adult stages. These eyes are morphologically similar to adult eyes of annelids (Gibson 1984). It will be interesting to test whether Clade II opsins are expressed in these molluskan eyes.

In the eyes of adult *Platynereis*, the presence of both r-opsins in the photoreceptor's rhabdomeres, in the vicinity of the pigment cups, is consistent with their roles in detecting the direction of incoming light. Several examples of opsin co-expression are known in animals and, provided that the spectral properties are different, can broaden the spectral sensitivity of photoreceptors (Arikawa et al. 2003). The co-expression of opsins in the eyes of adult *Platynereis* may serve a similar function.

Alternatively, photoreceptors may change the opsin they express during a developmental transition, as in *Drosophila* (Sprecher and Desplan 2008). We can exclude such a developmental switch in

Fig. 4 Continued
(white). (L) Close-up image of the eyespot, (M) close-up image of the adult eye. In (M), the fluorescent signal is overlaid with the DIC signal in the right panel to show the eye pigment. (N–P) Immunostaining for r-opsin1 (red) in 72-hpf and 5-dpf larvae counterstained for acetylated tubulin (white). (O) Close-up image of the eyespot, (P) close-up image of the adult eye. In (P), the fluorescent signal is overlaid with the DIC signal in the right panel to show the eye pigment. (Q) *In situ* hybridization for r-opsin1 (red) in a 5-dpf larva counterstained for acetylated tubulin (white) reveals the mRNA signal in the photoreceptor projections in the adult eye. (R) Immunostaining for r-opsin1 (red) in a 5-dpf larva counterstained for acetylated tubulin (white). (S) Close-up image of the right adult eye and the apical nerve plexus. In (B, C), arrowheads indicate the basal body of PRC2 and in (L, O), arrowheads indicate the photoreceptor's rhabdomeres. Asterisks show the pigment cups (in M, P), the immunostaining signal in the photoreceptor cell-body deeper in the tissue (in O), and the r-opsin1 signal in the apical nerve plexus in the area of the photoreceptor projections (in R, S). AAEN, anterior adult-eye nerve; AE, adult eye; CPC, ciliated prototroch cell; ES, eyespot; PAEN, posterior adult-eye nerve; PC, pigment cell; PRC, photoreceptor cell. Scale bars: (A, B, I) 2 µm, (C, G) 0.5 µm, (F, Q, S) 10 µm, (M) 15 µm, (K, N, R) 30 µm, (L, O, P) 5 µm.

Platynereis, given that the two opsins co-express in the adult eyes and are present throughout larval and adult stages.

Besides their canonical localization in the photoreceptor cell body and rhabdom, *r-opsin1* mRNA and protein are also present in the photoreceptor's axon terminals, indicative of mRNA localization and localized translation. The localization of mRNA is a widespread and important regulatory mechanism for the post-translational regulation of gene expression in neurons and other types of cells (Martin and Ephrussi 2009). The localization of the *r-opsin1* mRNA to the axons of the photoreceptors may have functional significance in the perception of light. Since the axon terminals are not shaded by pigment, the opsin molecules present there cannot have a function in directional sensitivity. The r-opsin1 in the axon terminals may play a more general regulatory role, for example in the detection of overall ambient light intensity.

Our results highlight an unexpected functional elaboration of the eyespots of *Platynereis* larvae, suggesting that the eyespots take on a function additional to phototaxis during larval development. Furthermore, molecular, behavioral, and ultrastructural work on *Platynereis* larvae will allow the functional analysis of the six larval eyes and their opsins within the context of simple photo-behaviors of larvae.

Acknowledgments

We thank Elizabeth Williams and Markus Conzelmann for their comments on the article and Albina Asadulina for help with image processing.

Funding

This work was supported by a Sequencing Grant from the Max Planck Society (M.IF.A.ENTW8050 to G.J.). The research leading to these results received funding from the European Research Council under the European Union's Seventh Framework Programme (FP7/2007-2013)/European Research Council Grant Agreement 260821.

Supplementary data

Supplementary Data available at *ICB* online.

References

Arendt D. 2003. Evolution of eyes and photoreceptor cell types. Int J Dev Biol 47:563–71.

Arendt D. 2004. Ciliary photoreceptors with a vertebrate-type opsin in an invertebrate brain. Science 306:869–71.

Arendt D, Tessmar K, de Campos-Baptista M-IM, Dorresteijn A, Wittbrodt J. 2002. Development of pigment-cup eyes in the polychaete *Platynereis dumerilii* and evolutionary conservation of larval eyes in Bilateria. Development 129:1143–54.

Arendt D, Wittbrodt J. 2001. Reconstructing the eyes of Urbilateria. Phil Trans Roy Soc B 356:1545–63.

Arikawa K, Mizuno S, Kinoshita M, Stavenga DG. 2003. Coexpression of two visual pigments in a photoreceptor causes an abnormally broad spectral sensitivity in the eye of the butterfly *Papilio xuthus*. J Neurosci 23:4527–32.

Backfisch B, Veedin Rajan VB, Fischer RM, Lohs C, Arboleda E, Tessmar-Raible K, Raible F. 2013. Stable transgenesis in the marine annelid *Platynereis dumerilii* sheds new light on photoreceptor evolution. Proc Natl Acad Sci USA 110:193–8.

Bartolomaeus T. 1992a. Ultrastructure of the photoreceptors in certain larvae of the Annelida. Microfauna Marina 7:191–214.

Bartolomaeus T. 1992b. Ultrastructure of the photoreceptors in the larvae of Lepidochiton cinereus (Mollusca, Polyplacophora) and Lacuna divaricata (Mollusca, Gastropoda). Microfauna Marina 7:215–36.

Blumer M. 1997. The larval ocelli of Golfingia misakiana (Sipuncula, Golfingiidae) and of a pelagosphera of another unidentified species. Zoomorphology 117:115–20.

Brandenburger J, Woolacott R, Eakin R. 1973. Fine structure of eyespots in tornarian larvae (Phylum: Hemichordata). Z Zellforsch 142:89–102.

Cardona A, Saalfeld S, Preibisch S, Schmid B, Cheng A, Pulokas J, Tomancak P, Hartenstein V. 2010. An integrated micro- and macroarchitectural analysis of the Drosophila brain by computer-assisted serial section electron microscopy. PLoS Biol 8:e1000502.

Conzelmann M, Jékely G. 2012. Antibodies against conserved amidated neuropeptide epitopes enrich the comparative neurobiology toolbox. EvoDevo 3:23.

Döhren von J, Bartolomaeus T. 2007. Ultrastructure and development of the rhabdomeric eyes in *Lineus viridis* (Heteronemertea, Nemertea). Zoology (Jena) 110:430–8.

Eakin RM, Brandenburger JL. 1981. Fine structure of the eyes of *Pseudoceros canadensis* (Turbellaria, Polycladida). Zoomorphology 98:1–16.

Edgar RC. 2004. MUSCLE: a multiple sequence alignment method with reduced time and space complexity. BMC Bioinformatics 5:113.

Fischer AH, Henrich T, Arendt D. 2010. The normal development of *Platynereis dumerilii* (Nereididae, Annelida). Front Zool 7:31.

Gibson BL. 1984. Cellular and ultrastructural features of the adult and the embryonic eye in the marine gastropod, Ilyanassa-Obsoleta. J Morphol. 181:205–20.

Guindon S, Dufayard JF, Lefort V, Anisimova M, Hordijk W, Gascuel O. 2010. New algorithms and methods to estimate maximum-likelihood phylogenies: assessing the performance of PhyML 3.0. Syst Biol 59:307–21.

Hattar S, Liao HW, Takao M, Berson DM, Yau KW. 2002. Melanopsin-containing retinal ganglion cells: architecture, projections, and intrinsic photosensitivity. Science 295: 1065–70.

Jékely G, Arendt D. 2007. Cellular resolution expression profiling using confocal detection of NBT/BCIP precipitate by reflection microscopy. BioTechniques 42:751–5.
Jékely G, Colombelli J, Hausen H, Guy K, Stelzer E, Nédélec F, Arendt D. 2008. Mechanism of phototaxis in marine zooplankton. Nature 456:395–9.
Lacalli TC. 1996. Frontal eye circuitry, rostral sensory pathways and brain organization in amphioxus larvae: evidence from 3D reconstructions. Phil Trans Roy Soc B 351:243–63.
Lacalli TC. 2009. Serial EM analysis of a copepod larval nervous system: Naupliar eye, optic circuitry, and prospects for full CNS reconstruction. Arthropod Struct Dev 38:361–75.
Leys SP, Degnan BM. 2001. Cytological basis of photoresponsive behavior in a sponge larva. Biol Bull 201:323–38.
Loytynoja A, Goldman N. 2008. Phylogeny-aware gap placement prevents errors in sequence alignment and evolutionary analysis. Science 320:1632.
Martin KC, Ephrussi A. 2009. mRNA localization: gene expression in the spatial dimension. Dev Cell 136:719–30.
Nordström K, Wallén R, Seymour J, Nilsson D. 2003. A simple visual system without neurons in jellyfish larvae. Proc Biol Sci 270:2349–54.
Nylander JAA, Wilgenbusch JC, Warren DL, Swofford DL. 2008. AWTY (are we there yet?): a system for graphical exploration of MCMC convergence in Bayesian phylogenetics. Bioinformatics 24:581–3.
Passamaneck YJ, Furchheim N, Hejnol A, Martindale MQ, Lüter C. 2011. Ciliary photoreceptors in the cerebral eyes of a protostome larva. EvoDevo 2:6.
Porter ML, Bok MJ, Robinson PR, Cronin TW. 2009. Molecular diversity of visual pigments in Stomatopoda (Crustacea). Vis Neurosci 26:255.
Rhode B. 1992. Development and differentiation on the eye in *Platynereis dumerilii* (Annelida, Polychaeta). J Morphol 212:71–85.
Ronquist F, Teslenko M, van der Mark P, Ayres DL, Darling A, Höhna S, Larget B, Liu L, Suchard MA, Huelsenbeck JP. 2012. MrBayes 3.2: efficient Bayesian phylogenetic inference and model choice across a large model space. Syst Biol 61:539–42.
Sprecher SG, Desplan C. 2008. Switch of rhodopsin expression in terminally differentiated Drosophila sensory neurons. Nature 454:533–7.
Struck TH, Paul C, Hill N, Hartmann S, Hösel C, Kube M, Lieb B, Meyer A, Tiedemann R, Purschke G, et al. 2011. Phylogenomic analyses unravel annelid evolution. Nature 471:95.
Terakita A. 2005. The opsins. Genome Biol 6:213.
Tessmar-Raible K, Steinmetz PRH, Snyman H, Hassel M, Arendt D. 2005. Fluorescent two-color whole mount in situ hybridization in *Platynereis dumerilii* (Polychaeta, Annelida), an emerging marine molecular model for evolution and development. BioTechniques 39:460, 462, 464.
Thorson G. 1964. Light as an ecological factor in the dispersal and settlement of larvae of marine bottom invertebrates. Ophelia 1:167–208.
Ullrich-Lüter EM, Dupont S, Arboleda E, Hausen H, Arnone MI. 2011. Unique system of photoreceptors in sea urchin tube feet. Proc Natl Acad Sci USA 108:8367–72.
Vopalensky P, Pergner J, Liegertova M, Benito-Gutierrez E, Arendt D, Kozmik Z. 2012. Molecular analysis of the amphioxus frontal eye unravels the evolutionary origin of the retina and pigment cells of the vertebrate eye. Proc Natl Acad Sci USA 109:15383–8.

Supplementary Figure 1.

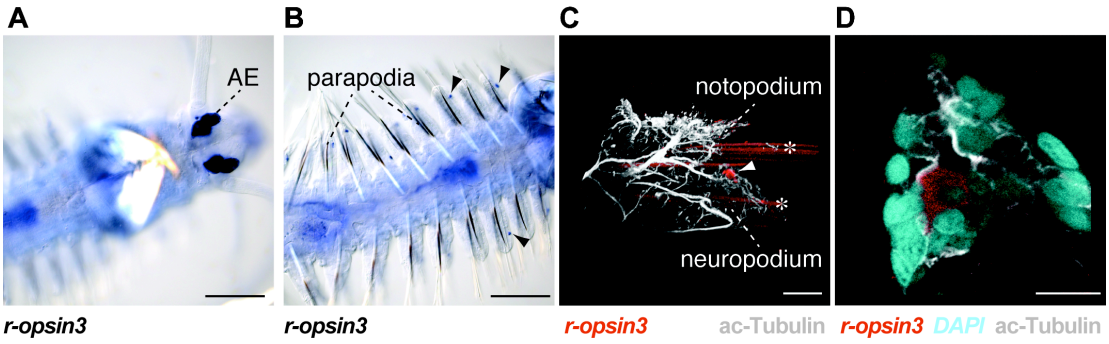

Expression of *r-opsin3* in the adult eyes and parapodia in an adult *Platynereis*. (A, B) Differential interference contrast (DIC) image of an adult *Platynereis* with *r-opsin3* expression in the adult eyes (A) and in the parapodia in the trunk (B). (C) *In situ* hybridization for *r-opsin3* (red) counterstained for acetylated tubulin (white) showing expression in a notopodium of an adult. (D) Close up image of the notopodium showing *r-opsin3* expression in a single cell (red), counterstained for acetylated tubulin (white) and DAPI (cyan). Asterisks in (C) show the chaetae, arrowheads in (B, C) indicate the *r-opsin3*-expressing cells in the notopodia. Scale bars: (A-D) 50 µm.